UNIVERSITY OF CALIFORNIA SAN DIEGO
SAN DIEGO STATE UNIVERSITY

Structural architecture of the Western and Central Transverse Ranges, California, USA

A dissertation submitted in partial satisfaction of the requirements for the degree Doctor of Philosophy

in

Geophysics

by

Yuval Levy

Committee in charge:

San Diego State University

Professor Thomas Rockwell, Chair
Professor Trent Biggs

University of California San Diego

Professor Neal Driscoll
Professor Yuri Fialko
Professor Tara Hutchinson

2019

The Dissertation of Yuval Levy is approved, and it is acceptable in quality and form for publication on microfilm and electronically:

_____

_____

_____

_____

_____
Chair

University of California San Diego

San Diego State University

2019

Table of contents

List of figures

List of tables

Acknowledgments

I would like to thank Professor Thomas Rockwell for taking me as a student and letting me work on the complex geological of the Western Transverse Ranges where he conducted his own research as a PhD student.

I would also like to acknowledge Scott Marshall for his invaluable expertise and work on testing my fault model, and the rest of my collaborators Neal Driscoll, Hector Perea, John H. Shaw and Andreas Plesch for their valuable time and advice. And last but not least I would like to thank my fellow students Elizabeth White and Drake Singleton for the time shared.

Chapter 2, in full, is a reprint of the material as it appears in Lithosphere 2019: Y. Levy, T.K. Rockwell1, J.H. Shaw, A. Plesch, N.W. Driscoll, and H. Perea, “Structural modeling of the Western Transverse Ranges: An imbricated thrust ramp architecture”. The dissertation author was the primary investigator and author of this paper.

Chapter 3, is currently being prepared for submission for publication of the material. Levy, Yuval; Scott Marshall; Rockwell, Thomas K. The dissertation/thesis author was the primary investigator and author of this material.

Chapter 4, is currently being prepared for submission for publication of the material. Levy, Yuval; Rockwell, Thomas K. The dissertation/thesis author was the primary investigator and author of this material.

Vita

2008-2011	Research Assistant, Geological Survey Israel
2011	Bechelor of science, The Hebrew University of Jerusalem
2011-2013	Teaching Assistant, The Hebrew University of Jerusalem
2013-2014	Geologist, Quantum Pacific Exploration
2014	Master's of Science, The Hebrew University of Jerusalem
2014-2019	Teaching Assistant, San Diego State University
2019	Doctor of Philosophy, University of California San Diego
	and San Diego State University

Publications

Y. Levy, T.K. Rockwell, J.H. Shaw, A. Plesch, N.W. Driscoll, H. Perea; Structural modeling of the Western Transverse Ranges: An imbricated thrust ramp architecture. Lithosphere doi: https://doi.org/10.1130/L1124.1

Singleton, D. M., Rockwell, T. K., Murbach, D., Murbach, M., Maloney, J. M., Freeman, T., & Levy, Y. (2019). Late-Holocene Rupture History of the Rose Canyon Fault in Old Town, San Diego: Implications for Cascading Earthquakes on the Newport–Inglewood–Rose Canyon Fault System. *Bulletin of the Seismological Society of America*, *109*(3), 855-874.

Hughes, A., Rood, D. H., Whittaker, A. C., Bell, R. E., Rockwell, T. K., Levy, Y., Wilcken, K.M., Corbett, L.B., Bierman, P.R., DeVecchio, D.E. and & Marshall, S. T. (2018). Geomorphic evidence for the geometry and slip rate of a young, low-angle thrust fault: Implications for hazard assessment and fault interaction in complex tectonic environments. *Earth and Planetary Science Letters*, *504*, 198-210.

ABSTRACT OF THE DISSERTATION

Structural architecture of the Western and Central

Transverse Ranges, California, USA

by

Yuval Levy

Doctor of Philosophy in Geophysics

University of California San Diego, 2019

San Diego State University, 2019

Professor Thomas K. Rockwell, Chair

The Transverse Ranges of California is an active fold-and-thrust belt and has produced some of the most destructive earthquakes in Southern California. Understanding the subsurface structure has both scientific and societal importance, in particular for earthquake hazard assessments. The diverse set of conflicting structural models, specifically in the Western Transverse Ranges, highlights the lack in understanding of the fault architecture in the subsurface. This Thesis presents a new structural model for the Western Transverse Ranges, a test of the model predictions

against GPS measurements, and an advancement of the understating of the subsurface structure, evolution and slip rates in the Central Transverse Ranges. After the full range of available observations was compiled we applied structural forward modeling using Trishear to match the observed structure and the interpreted evolution. The first chapter describes modeling of the Western Transverse Ranges since the Pliocene as a southward propagating imbricate thrust system. The second chapter presents a refinement of the model in chapter one, which was accomplished by comparing of a series of kinematic model predictions against GPS measurements in order to narrow the estimated range of dips for the deep part of the fault system. This is also the first time a structural model for the entire Western Transverse Ranges incorporates the full range of geological and geophysical data and observations. The third chapter presents the structural evolution of the Sylmar basin in the highly populated area of San Fernando Valley, northern Los Angeles county. The chapter presents an argument for lowering the estimated slip rate of the Santa Susana fault and distributing it to the faults that are located farther south. The structural understanding as developed by this thesis can help to improve the earthquake risk assessments in the Transverse Ranges.

Chapter 1 Introduction

The Transverse Ranges of California are a narrow east-trending strip of mountain ranges and valleys that trend diagonally transverse to the prevailing northwest structural grain of the Coast Ranges Province to the northwest, and the Peninsular Ranges Province to the southeast (Dibblee, 1982). The Transverse Ranges extends diagonally across the San Andreas plate boundary and rift zone, which is longitudinal through the Coast Ranges Province to the northwest and disappears in the Salton Trough to the southeast (Dibblee, 1982). The western and central Transverse Ranges have undergone compressional deformation since the Pliocene and continue to do so today (Atwater, 1998; Huftile and Yeats, 1996). The north-south tectonic compression is a result of the location of the Transverse Ranges relative to the big bend of the San Andreas fault (Rodgers, 1975), and to the strike slip faults west of the San Andreas and San Jacinto faults, including faults of the Continental Borderland to the south (Figure 1).

Two of the most devastating earthquakes in southern California occurred in this region, the 1971 Mw 6.7 San Fernando and 1994 Mw 6.7 Northridge earthquakes. Each of these events resulted in great cost in damaged infrastructure, along with 60 causalities and thousands more wounded. Both earthquakes exhibited a thrust type focal mechanism (Hauksson et al., 1995; Oakeshott, 1975; Whitcomb et al., 1973), and the Northridge earthquake originated on a fault that was unknown prior to the earthquake (Hauksson et al., 1995). In addition to these historical earthquakes, paleoseismic studies have revealed that very large and rapid uplift events have occurred in the western Transverse Ranges in pre-historic times (Rockwell et al., 2016; McAuliffe et al., 2015). These observed uplift events were estimated to be the result of Mw 7.5–8 earthquakes (Rockwell et al., 2016; McAuliffe et al., 2015). These events stress the need for accurate structural models of the

Transverse Ranges for the purpose of improving the earthquake risk assessment in the region.

Numerous structural models for the western and central Transverse Ranges have been advanced over the years (e.g.: Yeats et al., 1988; Namson and Davis, 1988; Shaw and Suppe, 1994; Hubbard et al., 2014; Davis and Namson 1998; Tsutsumi and Yeats, 1999). However, many of these models are incomplete or contradict some geological and geophysical observations that have accumulated over the years. The main focus of this dissertation is to improve the earthquake hazard assessment in the Transverse Ranges by improving structural models of the Transverse Ranges to be compatible with observations. The first two chapters include the development of a comprehensive structural model for the western Transverse Ranges fold and thrust belt since the Pliocene. In Chapter 2, I present the results of Trishear forward modeling for a number of cross sections that span the western Transverse Ranges. This forward model is constrained by geological observations of the ages of the different structures and by the vertical rates of subsidence and uplifted fluvial terraces.

The second chapter is a kinematic slip test of the predicted active thrust front in the western Transverse Ranges. The predicted uplift rate from the model is compared to data from Global Positioning Stations (GPS) in order to reduce the uncertainty of the estimated range of dips for the deep ramp in the structural models.

The third chapter is focused on the central Transverse Ranges, specifically on the Santa Susana fault system. The Santa Susana fault is located in northeastern San Fernando Valley and is typically assigned a high slip rate in the literature (Field et al.,

2014; Huftile and Yeats, 1996; Petersen and Wesnousky, 1994). In contrast to the assigned high slip rate, the fault does not currently produce the geomorphological features typically found in a region of high uplift rate despite the low erosion rates in the area (Scott and Williams, 1978). In fact, young alluvium is accumulated farther south along the Mission Hills and Northridge Hills faults. This observation, along with new paleoseismic trench observations presented in the chapter, suggests that a southward propagation of the thrust front has also occurred in the central Transverse Ranges. In the third chapter, I present a complex Trishear forward model that includes a Miocene extensional stage prior to the ongoing compressional stage in order to demonstrate how the system evolved in time. The structural model, combined with the geomorphic and paleoseismic observations, suggests that the published average slip rate estimates for the Santa Susana fault are too high and that slip is likely mostly now on faults to the south.

Figure

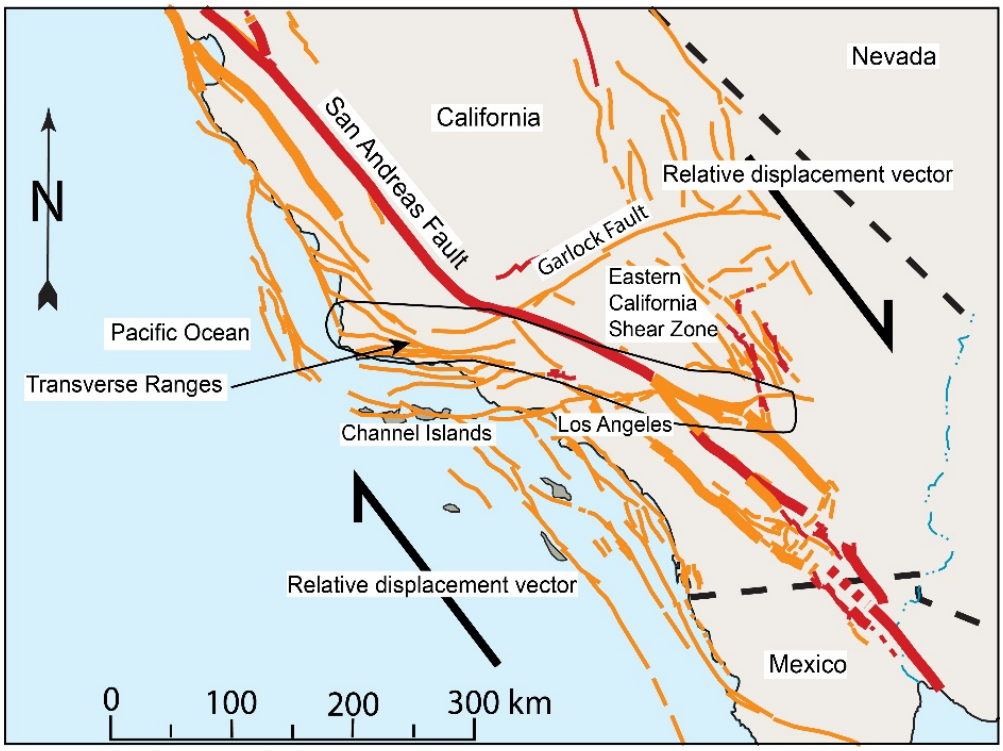

Figure 1.1. A regional fault map of southern California showing the location of the Transverse Ranges (black frame) and relative motion of the San Andreas plate boundary.

References

Atwater, T.M., 1998. Plate tectonic history of southern California with emphasis on the western Transverse Ranges and northern Channel Islands. Contrib. to Geol. North. Channel islands, South. Calif. Am. Assoc. Pet. Geol. Pacific Sect. 1–8. https://doi.org/10.1130/DNAG-GNA-N.21

Dibblee, T.W., 1982. Regional Geology of the Transverse Ranges Province of southern California, in: Fife, D.L., Minch, J.A. (Eds.), Geology and Mineral Wealth of the California Transverse Ranges. South Coast Geologcal Society, Inc., Santa Ana, pp. 7–26.

Field, E.H., Arrowsmith, R.J., Biasi, G.P., Bird, P., Dawson, T.E., Felzer, K.R., Jackson, D.D., Johnson, K.M., Jordan, T.H., Madden, C., 2014. Uniform California earthquake rupture forecast, version 3 (UCERF3)—The time-independent model. Bull. Seismol. Soc. Am. 104, 1122–1180.

Hauksson, E., Jones, L.M., Hutton, K., 1995. The 1994 Northridge earthquake sequence in California: seimological and tectonic aspects. J. Geophys. Res. 100, 12,335-12,355. https://doi.org/10.1029/95jb00865

Huftile, G.J., Yeats, R.S., 1996. Deformation rates across the Placerita (Northridge Mw = 6.7 Aftershock Zone) and Hopper Canyon segments of the western transverse ranges deformation belt. Bull. Seismol. Soc. Am. 86, s3–s18.

Levy, Y., Rockwell, T.K., Shaw, J.H., Plesch, A., Driscoll, N.W., Perea, H., 2019. Structural modeling of the Western Transverse Ranges: An imbricated thrust ramp architecture. Lithosphere 11, 868–883. https://doi.org/10.1130/L1124.1

Oakeshott, G.B. (Ed.), 1975. San Fernando, California, Earthquake of 9 February 1971. California Division of Mines and Geology.

Petersen, M.D., Wesnousky, S.G., 1994. Fault slip rates and earthquake histories for active faults in southern California. Bull. - Seismol. Soc. Am. 84, 1608–1649.

Rodgers, D.A., 1975. Deformation, Stress Accumulation, and Secondary Faulting in the Vicinity of the Transverse Ranges of Southern California. Brown University.

Scott, B.K.M., Williams, R.P., 1978. Erosion and Sediment Yields in the Transverse Ranges, Southern California, Geological Survey Professional Paper.

Whitcomb, J.H., Allen, C.R., Garmany, J.D., Hileman, J.A., 1973. San Fernando Earthquake series, 1971: Focal mechanisms and tectonics. Rev. Geophys. 11, 693–730. https://doi.org/10.1029/RG011i003p00693

Chapter 2 Structural modeling of the Western Transverse Ranges: An imbricated thrust ramp architecture

Levy, Y.[1, 2], Rockwell, T.K.[1], Shaw J.H.[3], Plesch A.[3], Driscoll N.W.[2], and Perea H.[2,4]

[1]Department of Geological Sciences, San Diego State University, 5500 Campanile Dr. San Diego, Ca 92182, USA

[2]Scipps Institution of Oceanography, University of California, San Diego, 9500 Gilman Drive, La Jolla, Ca 92037 USA

[3] Department of Earth and Planetary Sciences, Harvard University, 20 Oxford Street, Cambridge, Ma 02138, USA

[4] Institut de Ciencies del Mar, Consejo Superior de Investigaciones Cientificas, Psg. Maritim de la Barceloneta, 37-49, 08003 Barcelona, Spain

Abstract

Active fold-and-thrust belts can potentially accommodate large-magnitude earthquakes, so understanding the structure in such regions has both societal and scientific importance. Recent studies have provided evidence for large earthquakes in the Western Transverse Ranges of California, USA. However, the diverse set of conflicting structural models for this region highlights the lack of understanding of the subsurface geometry of faults. A more robust structural model is required to assess the seismic hazard of the Western Transverse Ranges. Toward this goal, we developed a forward structural model using Trishear in MOVE® to match the first-order structure of the Western Transverse Ranges, as inferred from surface geology, subsurface well control, and seismic stratigraphy. We incorporated the full range of geologic observations,

including vertical motions from uplifted fluvial and marine terraces, as constraints on our kinematic forward modeling. Using fault-related folding methods, we predicted the geometry and sense of slip of the major faults at depth, and we used these structures to model the evolution of the Western Transverse Ranges since the late Pliocene. The model predictions are in good agreement with the observed geology. Our results suggest that the Western Transverse Ranges comprises a southward-verging imbricate thrust system, with the dominant faults dipping as a ramp to the north and steepening as they shoal from ~16°–30° at depth to ~45°–60° near the surface. We estimate ~21 km of total shortening since the Pliocene in the eastern part of the region, and a decrease of total shortening west of Santa Barbara down to 7 km near Point Conception. The potential surface area of the inferred deep thrust ramp is up to 6000 km2, which is of sufficient size to host the large earthquakes inferred from paleoseismic studies in this region.

Introduction

Active fold-and-thrust belts produce destructive earthquakes, such as the M 7.9 Wenchuan earthquake in 2008 and the M 7.3 Gorkha earthquake in 2015 (Hayes et al., 2016). Estimating the geometry of faults at depth is important for risk assessment because the deep connectivity in thin-skinned fold-and-thrust belts determines the plausible sizes of earthquakes that a system can host (Wells and Coppersmith, 1994). Furthermore, many structural predictive models have been developed because this class of structures acts as potential hydrocarbon traps (e.g., Suppe, 1983; Suppe and Medwedeff, 1990; Erslev, 1991; Groshong, 1994; Poblet and McClay, 1996). The Western Transverse Ranges (Fig. 1) of southern California is an active fold-and-thrust belt (Namson and Davis, 1988; Shaw and Suppe, 1994) in a highly populated region, with 18 million people inhabiting the Los Angeles Basin along its southern margin. Recent studies

of coastal uplift and borehole transects across a fold scarp have revealed that very large and rapid uplift events have occurred along the Pitas Point/Ventura fault system (Fig. 1B, localities a and b; Hubbard et al., 2014), the offshore part of which is referred to as the Pitas Point fault and the onshore part of which is referred to as the Ventura fault. The observed uplift events were estimated to be the result of Mw 7.5–8 earthquakes (Rockwell et al., 2016; McAuliffe et al., 2015). For instance, Holocene coastal marine terraces near Punta Gorda between Ventura and Santa Barbara, California, record four uplift events in the past 6.7 k.y., with an average of 10 m per uplift event (Rockwell et al., 2016), Punta Gorda (Fig. 1B, locality a) is situated on the axis of the Pitas Point/Ventura Avenue anticline along a section where the Pitas Point fault is mostly or completely blind, so much or all of the fault slip is translated into uplift through folding and back-thrusting. Similarly, the onshore Ventura fault has produced up to 6 m of vertical deformation per event (McAuliffe et al., 2015). These uplift events are comparable to the magnitude of uplift observed in the 1999 M 7.6 Chi-Chi earthquake in Taiwan (Ma et al., 1999), and scaling relations (Wells and Coppersmith, 1994) suggest that these are the result of large earthquakes. Considering the complex structural geology in the upper several kilometers of the Western Transverse Ranges, the observed uplifts were suggested to be the result of multisegment thrust fault ruptures (Hubbard et al., 2014). However, this explanation has been questioned based on arguments of fault complexity (Sorlien and Nicholson, 2015).

Various structural models (e.g., Yeats et al., 1988; Namson and Davis, 1988; Shaw and Suppe, 1994; Hubbard et al., 2014; Sorlien and Nicholson, 2015) have been advanced over the years to describe the complex fault architecture in the Western Transverse Ranges. Nevertheless, there are ongoing debates regarding these proposed models, mainly centered on the direction of dip of the primary structures and their senses

of slip. As a result, series of competing, alternative models for these structures are represented in the Southern California Earthquake Center's (SCEC) Community Fault Model (CFM; Nicholson et al., 2017; Plesch et al., 2007) and used in regional hazards assessments.

In this work, we incorporated published geological observations, including late Quaternary geologic vertical motions, to be used as interpretive constraints on a kinematic forward model for the Western Transverse Ranges. We started with the detailed regional mapping by Dibblee (2002) and incorporated subsurface data from the numerous oil wells in the region, as well as offshore seismic reflection profiles and their interpretations (Sorlien and Nicholson, 2015) and published geological observations (Davis and Namson, 1998; Hubbard et al., 2014; Jackson, 1981; Namson and Davis, 1988; SarnaWojcicki and Yerkes, 1982; Schlueter, 1976; Yeats, 1983). From these sources, we constructed seven geologic cross sections of the upper few kilometers, with sections across the eastern Ventura Basin westward to near Point Conception (Fig. 2). We then applied forward modeling using the Trishear module in Move® (https://www.mve.com/) to replicate or match the primary structural elements of the Western Transverse Ranges, as shown in the geologic cross section, with the intent of developing a crustal-scale model of the entire seismogenic portion of the crust. Incorporated into this modeling was information on the local and regional vertical motions, which aided in constraining the fault dip at depth. The final result is a retrodeformable, area-balanced kinematic model that matches and accounts for the surficial and shallow subsurface geology, the local and regional structural relief, and late Quaternary vertical motions as determined from geologic studies of uplifted and deformed marine and fluvial terrace sequences. We applied this model to test the

possibility that the Western Transverse Ranges hosts a fault system that may be capable of generating earthquakes responsible for the large uplift events observed in the region.

Geological background

The Western Transverse Ranges are composed of continental plutonic and metamorphic basement in the east and juxtaposed or accreted oceanic ophiolitic–Franciscan basement complex in the west, both overlain by a ~13-km-thick section of Cretaceous and Cenozoic sedimentary and volcanic deposits (Fig. 3; Dibblee, 1982a). In the Mesozoic and early Cenozoic, the Transverse Ranges block, or blocks, occupied the forearc region of a subduction zone collecting continental shelf sediments (Atwater, 1998). During the Oligocene, the Pacific plate made contact with North America (Atwater, 1998), and the tectonic regime in the Western Transverse Ranges changed as the San Andreas transform plate boundary (Fig. 1A) evolved over time (Crowell, 1979). In the middle Miocene, the configuration had a transtensional geometry that was responsible for localized extension, rotation, and left-lateral shearing (Atwater, 1998). Later, beginning in the Pliocene, the region began to undergo shortening (Atwater, 1998; Dibblee, 1982b; Rockwell, 1983); this shortening regime continues to the present (Rockwell, 1988; Rockwell et al., 1988; Marshall et al., 2013).

The sedimentary series is almost entirely marine, except for the Oligocene Sespe and late Quaternary Saugus Formations, implying that the region has mostly experienced continuous subsidence. Bird and Rosenstock (1984) presented a case to explain the regional subsidence with a model of mantle downwelling and incipient subduction, which might explain the mechanism required to accommodate such a thick stratigraphic sequence. While the deposition of the terrestrial Oligocene Sespe sediments might imply

uplift, global sea level changed during that period due to the formation of the large ice sheets in Antarctica (Miller et al., 2005).

Deposition in the Santa Barbara/Ventura Basin, south of the range (Figs. 2, 3, and 4), has been nearly continuous since the Eocene, and it accelerated in the Pliocene (Dibblee, 1982b; Yeats and Rockwell, 1991). Northward from the Santa Ynez fault system, the Eocene sequence thins rapidly, as do the Oligocene Sespe Formation and the Rincon and Vaqueros Formations (Dibblee, 1982b). An angular unconformity is locally present between the middle Miocene (Mohnian) Monterey Formation and older strata (Figs. 2, 3, and 4), which suggests a pre– late Miocene period of erosion that may have resulted from local uplift during Miocene extension. There are two models that describe the Miocene period of rotation and local extension, as indicated by paleomagnetic measurements (e.g., Hornafius, 1985; Hornafius et al., 1986, 1982; Nicholson et al., 1994; Schwartz 2018). One model suggests that the Western Transverse Ranges rotated clockwise by 110° as a large coherent block (Hornafius et al., 1982; Nicholson et al., 1994). Dibblee (1982b), referring to this earlier work (Hornafius et al., 1982), stated that so much rotation and the space problem with large adjacent blocks would be difficult if not impossible to account for from the geology. Alternatively, Schwartz (2018) suggested that the Miocene rotation more likely occurred as rotation of microplates. In either case, the paleomagnetic measurements show that most of the rotation accrued between 12 and 8 Ma (Hornafius et al., 1986; Schwartz, 2018), and therefore the rotation observed in the Western Transverse Ranges predated the current shortening regime, which began during the Pliocene.

Figure 2 presents a compilation of a large number of geologic maps of the Western Transverse Ranges (Dibblee, 2002). A first-order observation is that topography

is being built to the north, and the structural relief from north to south is ~11 km with the north side up, as Cretaceous rocks are exposed along the Santa Ynez anticlinorium and Quaternary rocks are exposed to the south in the Ventura anticline and in the Ventura Basin (Figs. 2, 3, and 4).

The most obvious feature along the Santa Ynez mountain range is the ~160-km-long, E-W–trending Santa Ynez anticlinorium. This anticlinorium has a mostly overturned south limb, with a 5-km-thick section of overturned Eocene marine and Oligocene strata. East of Ojai Valley (Fig. 1B), the south limb is cut by the south-verging San Cayetano fault, which is interpreted as the emergent portion of the associated thrust underneath this fold (Namson and Davis, 1988). Where the San Cayetano fault is emergent, the fault displaces early Eocene rocks in the hanging wall against Quaternary rocks in the footwall with as much as 9 km of stratigraphic separation at the surface (Rockwell, 1988), although additional shortening by folding may require a larger basement offset.

The nomenclature in the Western Transverse Ranges is a source for confusion, so it is important to clarify that the Santa Ynez fault, in many locations, is too far north from the anticlinorium to be interpreted as the fault that produced this large fold (Fig. 2). Furthermore, the Santa Ynez fault currently exhibits mainly left-lateral strikeslip motion (Darrow and Sylvester, 1983), and it has a very steep dip that varies from dipping to the north to dipping to the south along its strike. Although its late Quaternary slip history is strikeslip motion, the Santa Ynez fault has sustained as much as 1–3 km of dip slip, which presumably occurred prior to its current role partitioning the majority of the strike slip accommodated within the Western Transverse Ranges.

There are a variety of structural interpretations for this region (Fig. 5). Yeats et al. (1988) presented balanced cross sections with a dominant north-verging structure, the

Sisar décollement, at 8 km depth, south of the Red Mountain and San Cayetano faults. In their model (Fig. 5A), both the Ventura Avenue anticline and the Sulphur Mountain anticline, the latter of which is located between the Lion and South Sulphur Mountain faults (Fig. 1A), were formed by a south-dipping thrust system that roots to a décollement ~8 km under the surface.

Namson and Davis (1988) presented their model (Fig. 5B) based on fault-propagation fold and fault-bend fold methods (Suppe,1983). They proposed the presence of a detachment at 12–15 km depth and associated the San Cayetano thrust with the Santa Ynez anticlinorium. From seismological observations, a northdipping low-angle fault was interpreted that might also relate to Namson and Davis' (1988) décollement at depths of ~12 km (Corbett and Johnson, 1982; Hauksson et al., 2016; Huang et al., 1996). South of the anticlinorium, the main thrust in the Namson and Davis (1988) model dips south, in what seems to be a structure that is comparable to the Sisar décollement presented by Yeats et al. (1988). Namson and Davis (1988) interpreted the South Sulphur Mountain anticline to result from the south-dipping Lion fault, and the Ventura Avenue anticline has a number of small layer-parallel faults, dipping alternately south and north, associated with it in their model.

Hubbard et al. (2014) applied fault-related folding theories (Shaw et al., 2005; Suppe, 1983; Suppe and Medwedeff, 1990) and used well and seismic reflection data in the Ventura Basin to construct a model of the Ventura Avenue anticline. They incorporated the Ventura fault as the structure producing the Ventura Avenue anticline, and they connected this fault with the Red Mountain, Lion, and San Cayetano faults, with a flat thrust within the Rincon shale at ~7 km depth. The linkage between the detachment and San Cayetano fault yields a ramp-flat-ramp geometry for the Pitas Point/Ventura fault.

In this model, the structure forming Sulphur Mountain is also interpreted as a south-dipping fault. This model is represented as one version in the SCEC CFM5.2 (Fig. 5C; Plesch et al., 2007; Nicholson et al., 2017).

Sorlien and Nicholson (2015) presented several interpreted seismic cross sections in the offshore Ventura–Santa Barbara Basin but did not extend or interpret faults below the depth of imagery, i.e., ~6–7 km. Their sections demonstrate that the offshore Pitas Point fault system is aligned with the onshore Ventura fault and anticline. One of the versions of the SCEC CFM presents high-angle reverse oblique faults as the dominant structures producing the Western Transverse Ranges (Fig. 5D; Nicholson et al., 2017). Faults are connected as a regional flower structure in this version, and there is no blind San Cayetano fault west of Ojai Valley. This version appears to attribute the formation of the Santa Ynez anticlinorium to a south-dipping Santa Ynez fault, but this cannot be correct because the anticlinorium is overturned (verges) to the south, and the fault is far to the north.

Timing and style of deformation

The formation of the Santa Ynez anticlinorium probably initiated during the late Pliocene or early Quaternary (Dibblee, 1982a), and folding ceased before 200 ka (Rockwell, 1988). The age of initiation of the San Cayetano fault is not directly constrained. Rockwell (1983) documented that uplift to the north initiated by ca. 3.2 Ma, based on analysis of microfauna in the Lower Pliocene Pico Formation, which also contained clasts of the Miocene Monterey Formation that were derived from the north. These may have been shed from folding and uplift north of the Santa Ynez range, or from the anticlinorium itself. The south-verging, overturned Red Mountain anticline and north-dipping Red Mountain fault began motion by at least 1 Ma (Yerkes and Lee, 1987). The

current dip on the Red Mountain fault is anomalous in that it dips steeply (70°) to the north, which is unfavorable for accommodation of shortening.

Folding of the onshore Ventura Avenue anticline is estimated to have begun around ca. 300–200 ka (Rockwell et al., 1984) and continues to the present (Hubbard et al., 2014; McAuliffe et al., 2015; Rockwell et al., 2016). In the offshore to the west, the same fold trend initiated motion earlier in the Quaternary and appears to be progressively older toward the west (Sorlien and Nicholson, 2015). This makes sense if the primary cause of folding in the Western Transverse Ranges is associated with the continued development of the Big Bend in the San Andreas fault (Crowell, 1979), as the westernmost Transverse Ranges toward Point Conception are now translated west of the Big Bend such that the shortening should have been earlier, and the current rate should be much lower. We discuss this further later in this paper.

The late Quaternary vertical motions are an important consideration in the development of a defendable structural model. North of the Arroyo Parida fault, terraces of the Ventura River (Fig. 1B, locality c) indicate regional uplift (without folding) at ~1 mm/yr across the southern flank of the Santa Ynez anticlinorium for at least the past 200 k.y. (Rockwell et al., 1984). Similarly, the Santa Ynez Valley north of the anticlinorium is rising at a similar rate of ~1 mm/yr (Fig. 1B, locality d; Farris, 2017). These observations argue for a regional uplift rate north of the Arroyo Parida fault of ~1 mm/ yr, which must be accounted for in any viable structural model. Farther west in the Santa Barbara region (Fig. 1B), current contractional deformation is also localized south of the Arroyo Parida–Mission Ridge fault, although the main topographic relief is to the north in the Santa Ynez Mountains (Gurrola et al., 2014). Southward, active deformation extends offshore into Santa Barbara Basin, with active folding of the Pitas Point/ Ventura Avenue, Red

Mountain, Oak Ridge, and Mid-Channel anticlinal trends (Perea et al., 2017; Shaw and Suppe, 1994; Sorlien and Nicholson, 2015). The ca. 57 ka marine terraces demonstrate an uplift rate of ~1 mm/yr at Isla Vista (Fig. 1B, locality e; Gurrola et al., 2014) and at least 0.3 mm/yr farther west (Fig. 1B, locality f) between Gaviota and Point Conception (Rockwell et al., 1992). The apparent decrease in rate to the west is consistent with observed lower rates of shortening based on global positioning system (GPS) data (Marshall et al., 2013).

The most rapid rates of uplift in the entire region are associated with the Ventura–San Miguelito anticline at Punta Gorda (Fig. 1B, locality a), where the long-term rate is estimated at 6–7 mm/yr (Rockwell et al., 2016). This is also where four Holocene marine terraces have been identified, with each terrace interpreted to correspond to an abandoned abrasion surface due to uplift produced by an earthquake (Rockwell et al., 2016). The highest Holocene terrace is preserved at ~38 m above modern sea level near the fold crest and is interpreted to represent the cumulative uplift from four large earthquakes (Rockwell et al., 2016). In addition, analysis of GPS data showed that this region has the highest rate of shortening (fig. 5 in Marshall et al., 2013). Finally, results from a geodetic study showed an uplift signal north of the Santa Ynez range, which is consistent with interseismic strain accumulation on active thrusts in the Western Transverse Ranges (Hammond et al., 2018).

Cross sections

We constructed seven geological cross sections over a 140 km length of the Western Transverse Ranges, from near Fillmore westward to near Point Conception (Figs. 2 and 4), using surface geology and dip data (Dibblee, 2002), subsurface well control (see Appendix), and seismic and previous geologic sections (Davis and Namson,

1998; Hubbard et al., 2014; Jackson, 1981; Namson and Davis, 1988; SarnaWojcicki and Yerkes, 1982; Schlueter, 1976; Sorlien and Nicholson, 2015; Yeats, 1983). Each cross section (Fig. 4) presents near-surface observations, and interpretations where surface data were projected downward to a small extent. Interpretations of thickness are based on calculations of true thickness from the geological maps (Dibblee, 2002) and from the stratigraphic columns presented in Dibblee (1982a). The overturned south limb of the anticlinorium is apparent in sections 1–5. To the west, in cross sections 6 and 7, the south limb is not overturned, but the anticlinorium still appears to be the largest structure.

The first-order observations of uplift in the north and subsidence in the south point to a southward-directed motion for the main faults at depth. These southward-verging faults are interpreted to accommodate the observed shortening and uplift. The models that consider the south-dipping faults as the dominant structures, such as the inferred Sisar detachment, which has been interpreted primarily as a tool to balance cross sections (Yeats et al., 1988), are thus inconsistent with the well-documented vertical motions of the region. Observationally, the Ventura–Santa Barbara Basin is subsiding at a high rate of 2–3 mm/yr, whereas onshore north of the basin, there are observations that argue for relatively high rates of uplift.

One aspect of our geological interpretation that is significantly different from previous interpretations (Fig. 5) relates to the fault that produces the South Sulphur Mountain anticline; the subsurface is poorly constrained by well control because most of the oil production has been from shallow strata. The regional orientation and alignment of the structures (Fig. 2), along with the overturned south flank (verges south) and stratigraphic relief, suggest that this anticline was produced by a north-dipping fault. In cross section 2 (Fig. 4), we interpret it as a south-verging structure, with the South

Sulphur Mountain fault as the main thrust and the Lion fault as a back thrust, rather than the previously suggested interpretation of a dominant southdipping fault (Hubbard et al., 2014; Namson and Davis, 1988; Yeats et al., 1988), which did not include the observed overturned south flank (Fig. 2; Dibblee, 2002).

Finally, our model seeks to explain the southward younging or serial development of the first-order structures, from early development of the Santa Ynez anticlinorium to the late Quaternary evolution of the onshore Ventura Avenue anticline, as described in the next section.

Evolution of the fold-and-thrust system since the Pliocene

When considering all of the observations referred to above on the timing and location of folding, it is apparent that the Western Transverse Ranges are a southward-propagating fold-and-thrust belt, as first suggested by Rockwell (1983), and that it is evolving in a fashion similar to other forward-propagating fold-and-thrust belts (Boyer and Elliott, 1982; Butler, 1987; DeCelles et al., 2001; Jordan et al., 1993; Morley, 1988; Wiltschko and Dorr, 1983), as also demonstrated in laboratory experiments (e.g., Storti et al., 1997; Smit et al., 2003). Onshore near Ventura, current deformation is localized between the Arroyo Parida fault (Rockwell et al., 1984) and the Ventura fault (Hubbard et al., 2014; McAuliffe et al., 2015), with the majority of shortening taken up by the Ventura Avenue anticline and associated Ventura fault. Offshore, east of Santa Barbara, the pattern is a little more complex based on new seismic reflection (CHIRP) data (Perea et al., 2017). The interpretation of these data suggests that the deformation has jumped from east to west and from south to north, from the Pitas Point/Ventura Avenue anticline and Pitas Point fault to the Red Mountain anticline and then to the Mesa–Rincon Creek fold system (located in Fig. 1B between locality e and Santa Barbara). Close to Ventura, the

most active structures are the Pitas Point/Ventura Avenue anticline and Pitas Point fault, whereas the Mesa–Rincon Creek fold system is the most active structure close to Santa Barbara (Perea et al., 2017).

We conclude that a blind extension of the San Cayetano fault west of Ojai Valley produced the mostly overturned Santa Ynez anticlinorium as the first location of the thrust front, as first suggested by Namson and Davis (1988). North of the Santa Ynez range, the Pine Mountain fault might predate the San Cayetano fault, but the lack of age data or associated stratigraphic observations does not allow us to resolve this question at this time, and total shortening from this structure is minor compared to that of the anticlinorium to the south. The observation that folding had ceased prior to 200 ka implies that the blind San Cayetano fault west of Ojai Valley (Fig. 1B) is no longer active. By at least 1 Ma (Yerkes and Lee, 1987), the thrust front propagated south, first to the Red Mountain and South Sulphur Mountain faults, and then, in the late Quaternary, to the currently active but mostly blind Pitas Point/Ventura fault, with the Pitas Point/Ventura Avenue and related anticlines developing in the hanging wall. The Red Mountain fault continues to play a role in the offshore Santa Barbara Basin, but onshore, we interpret the late Quaternary deformation and steep dip of the fault to be the result of passive flexural slip due to folding in the back limb of the Ventura Avenue anticline, similar to the schematic development of the imbricate thrust system presented by Poblet and Lisle (2011). This sequence of events for the onshore Ventura Basin is consistent with other well-documented fold-and-thrust belts worldwide, where propagation of the thrust front develops “in sequence” with the direction of vergence of the primary structures. Figure 6 illustrates our proposed model for the evolution of the first-order Pliocene structure of the Western Transverse Ranges fold-and-thrust belt.

Model assumptions

We made a number of assumptions to model the geometry and evolution of faults at depth. The stratigraphy in the model is simplified, and the thicknesses of the units are fixed, although in the real world, there are local changes due to the Miocene period of rotation and extension. Considering that our goal was to model the overall first-order, Pliocene and younger contractional deformation of the Western Transverse Ranges, we suggest that the resulting mismatches from not incorporating these stratigraphic details are minor.

The second assumption is that out-of-plane motion can be neglected. Some faults in the Western Transverse Ranges have accommodated some strike-slip motion during the late Quaternary, and the larger earthquakes in the Central Transverse Ranges, to the east of the study area, have exhibited up to 30% left-lateral strike-slip motion (cf. the 1971 San Fernando earthquake). However, the orientation of shortening relative to the stress field generated by the Big Bend of the San Andreas fault argues that the maximum compressive stress is N-S (Rodgers, 1975), and this is borne out by modern geodetic observations that demonstrate primarily NNW-SSE shortening across the Western Transverse Ranges (Marshall et al., 2013), which, if anything, should produce a very minor rightlateral component of motion on E-W–striking faults. Thus, the amount of strike-slip relative to the rate of shortening is expected to be small, but we address it further here to avoid the common criticism of two-dimensional (2-D) modeling where there is a potential component of strikeslip motion.

The three high-angle strike-slip faults that may impact our forward modeling are the Big Pine, Santa Ynez, and Arroyo Parida faults (Fig. 1B). There are few data on the recent activity of the Big Pine fault, although it is sufficiently north of the main structures

that any strike-slip motion will have negligible effect. The Santa Ynez fault has been studied to some degree with paleoseismic trenches; Darrow and Sylvester (1983, 1984) excavated a “box trench” (two perpendicular and two parallel trenches across a fault) to estimate 5–10 m of left-lateral displacement of basal terrace gravels, which are overlain by several meters of sediment and capped by a middle Holocene soil, which in turn provides a minimum age of displacement of ca. 5 ka. The next higher terrace (Qt2) has an estimated soil age of ca. 16 ka, placing a maximum age on the basal gravels. Thus, the maximum late Quaternary slip rate range for the Santa Ynez fault is estimated to be 0.3–2 mm/yr.

The Arroyo Parida fault displays no evidence of lateral slip in late Pleistocene terraces of the Ventura River (Fig. 1B, locality g; Rockwell et al., 1984), although a minor component could have been missed at the scale of mapping (1:20,000). Near Carpinteria (Fig. 1B, locality h), fluvial channels incised into bedrock in the Santa Ynez range display left deflections where the channels cross the Arroyo Parida fault. However, the bedrock channels must predate the last interglacial marine terraces, which cut across rock downstream from the fault crossings and are likely considerably older. Based on these observations, it does not appear that the Arroyo Parida fault has sustained much, if any, late Quaternary lateral slip at the Ventura River, and it likely has a low rate of well less than 1 mm/yr near Carpinteria and Santa Barbara. We consider both the Santa Ynez and Arroyo Parida faults as the structures that accommodate the partitioned strike-slip motion in the Western Transverse Ranges.

Seismological data also argue for a component of lateral slip, as most of the larger Transverse Ranges earthquakes exhibited oblique slip, based on observations from surface ruptures (Keller and DeVecchio, 2013) or focal mechanism solutions (Corbett and

Johnson, 1982), although many of these observations are far to the east. In summary, there is a lateral component of shear in the Western Transverse Ranges, but considering a rate that is most likely less than 2 mm/yr, versus a contraction rate of that is close to 10 mm/yr, the lateral slip is considerably subordinate to the rate of shortening. Considering that the shortening of the Western Transverse Ranges initiated at ca. 3–2 Ma, there has been only a few kilometers of lateral shear during the period of contraction. In contrast, the Paleogene sedimentary rocks show lateral continuities on the scale of tens of kilometers with gradual thinning to the north in the direction of contraction. Therefore, the lateral component of strains should have only a minor effect on forward modeling that assumes pure contraction, especially for the pre-Miocene strata, which record the major shortening associated with the Santa Ynez anticlinorium.

Similarly, the thicknesses of most of the Neogene rocks to the top of Miocene are relatively constant, although there are exceptions due to extensional faulting during the Miocene, which are accounted for in the model. This is evident from the relatively constant thickness of marine units that form the Santa Ynez range from Point Conception to at least the Ventura River, with local areas of complexity. Based on the above discussion, we assume that the effects of out-of-plane motion are negligible for our forward modeling, as presented below.

Estimate of dip for the fault at depth

There is a considerable debate as to whether the structures in the Western Transverse Ranges are controlled solely by high-angle reverse oblique faults (Nicholson et al., 2017) or whether there is a regional detachment or gently dipping thrust ramp that underlies the region (e.g., Namson and Davis, 1988; Shaw and Suppe, 1994). As mentioned in the geological background section, Namson and Davis (1988) presented

evidence for placing a décollement at a depth of 12–15 km depth, and seismological observations support this interpretation (Corbett and Johnson, 1982; Hauksson et al., 2016; Huang et al., 1996). Hubbard et al. (2014) proposed the existence of a flat at ~7 km, in contrast to previous models with a south-dipping detachment under the basin (Namson and Davis, 1988; Yeats et al., 1988). Hubbard et al.'s (2014) flat was interpreted to connect a high-angle deep ramp of the San Cayetano fault to the Pitas Point/ Ventura fault system via the "southern San Cayetano fault." Recent work has established that the southern branch of the San Cayetano exists, and it is the likely surface linkage between the San Cayetano and Ventura faults (Hughes et al., 2018). The geometry presented by Hubbard et al. (2014), which includes an ~30°N-dipping thrust ramp that extends downward from the flat, was favored over the high-angle reverse faults model by mechanical modeling (Marshall et al., 2017). The north-dipping thrust ramp proposed by Hubbard et al. (2014) provides a reasonable mechanism to explain uplift in the Western Transverse Ranges. However, it has yet to be tested against the observed regional uplift of ~1 mm/yr north of the Arroyo Parida fault (Rockwell et al., 1984) and in Santa Ynez Valley (Farris, 2017), or the lack of late Quaternary folding of the Santa Ynez range. Therefore, we explored this further, and we suggest that this deeper ramp must be more gently dipping to the north to account for the regionally observed uplift.

We estimated the plausible dip range by accounting for the rates of vertical and horizontal motion using a simplistic kinematic model (Fig. 7A) that assumed that the observed uplift north of the zone of active folding is a result of slip on the underlying, deep low-angle thrust. Regional subsidence due to mantle downwelling (Bird and Rosenstock, 1984) is also accounted for in the model. The subsidence rate was evaluated assuming that the Upper Quaternary coarse clastic sediments in Ventura Basin were originally at or

close to the surface and that their current depth is the result of subsidence. Their ages have been previously defined by the presence of tephras and fossil extinction horizons (Yeats, 1983), so a subsidence rate could be calculated. Using the top of the Repetto member of the Pico Formation onshore between the Ventura and Oak Ridge faults results in a subsidence rate of ~2.6 mm/yr for the onshore central trough of Ventura Basin. For the offshore, the depth to the top of the Repetto member resolves a rate of ~2.5 mm/yr. The 2.5 mm/yr rate was used in our model as an estimate of the regional subsidence rate, although this rate might be considered as a maximum rate, in case subsidence is faster in the basin due to sediment loading, which is likely the case. In such a case, the calculated dip angle that we used may also be a maximum dip angle.

We employed shortening rates of 6.5–10 mm/ yr determined from previous geologic and geodetic studies (Marshall et al., 2013; Rockwell et al., 1988) and our estimate of the change in line length of a horizon at the top of the Pico Formation in the Ventura area, south of the Red Mountain fault (Fig. 4, cross-section 3). The required dip of the lower fault ramp based on our model is shown by the intersection of each line and the 1 mm/yr uplift rate (Fig. 7B). The range of plausible dips is 16°–30° when accounting for the uncertainties in the shortening and uplift rates. In our models, we used a dip of 20° for the deep ramp, which is similar to the dip inferred for the fault that produced the Fillmore earthquake swarm based on microseismicity (Hauksson et al., 2016), as well as the dip of the fault that produced the 1978 M 6 Santa Barbara earthquake (Corbett and Johnson, 1982).

Forward modeling

In order to test the interpretation of a southward-propagating fault system and estimate the first-order geometry of the deep faults of the fold-and-thrust belt, we applied

fault-bend folding (Suppe, 1983) and Trishear (Erslev, 1991) forward modeling. The results of the models were compared with and tested against the geologic cross sections presented in Figure 4. This comparison allowed us to assess whether a large deep thrust ramp may plausibly represent a continuous fault surface along strike that is capable of hosting large earthquakes. We generated a series of kinematic forward models using the Trishear (Erslev, 1991) module in MOVE® by Midland Valley Exploration Ltd. (https://www.mve.com/) to match the surface and near-surface geology. We modeled a southward-propagating fault system by iterative steps. That is, we first produced slip on a fault to the north of the Santa Ynez anticlinorium to match some of the deformation in the hanging wall of the San Cayetano fault. We then "propagated" the deformation southward by initiating slip on a new fault to represent the San Cayetano fault, followed by the Red Mountain–South Sulphur Mountain fault, and finally the Pitas Point/ Ventura fault system. We iterated this with various fault configurations until we matched the surface geology as interpreted in our geologic cross sections. The order of faulting has an important impact on the patterns of resulting deformation, so representation of the regional evolution of structures in our models, as described above, provided an important constraint. Earlier stages of our models represent initial conditions that were then modified by subsequent faulting and folding. After each modeling step, we made an adjustment to the fault geometry and displacement parameters until we reached a satisfying result under the different constraints of age, geometry, and amount of shortening; hence, this was an iterative process. In Figure 6, we present the steps we applied for cross section 2 (Fig. 4); a similar procedure was performed for each of the other cross sections. We used the same parameters for the different modeled sections except for fault spacing and fault displacement. The extent to which the thrust front propagated toward the south through

time is apparent in Figure 2, as the distance between the San Cayetano, Red Mountain/ South Sulphur Mountain, and Pitas Point/Ventura faults changes along strike. The amount of slip, or contraction, used in the models varied as overall shortening decreased to the west, so slip was reduced for cross sections 5, 6, and 7 to match the amount of deformation represented in the surface and near-subsurface geology. The parameters we used for the final model are: For the San Cayetano fault, we used a propagation to slip ratio of 1, we used 20 Trishear zones, and we did not apply an offset for the Trishear angle. For the Red Mountain/South Sulphur Mountain fault, we used a propagation to slip ratio of 0.8 with 8 Trishear zones, and an offset of 0.6 for the Trishear angle. For the Pitas Point/Ventura fault, we used propagation to slip ratio of 0.3, 1 Trishear zone, and an offset of 0.9 for the Trishear angle. The propagation to slip ratio for each fault was selected to match the shape of the fold as best we could through trial and error; we did not thoroughly explore the sensitivity of this parameter. Figure 8 presents additional models using different dips than our preferred model for the lower ramp in order to demonstrate the sensitivity of relief and fold shape on the geometry of the lower ramp.

Results

The model (Fig. 6) illustrates the concept of southward thrust propagation over time, attendant fault dip, and expected patterns of uplift and folding, with uplift of the hanging wall and the locus of folding migrating southward through time. The comparison of the model predictions with the geological cross sections shows a good first-order match and demonstrates that the models capture the first-order patterns of folding and structural relief (Figs. 9 and 10). Despite having a rather large spacing between cross sections, the similar fault geometry inferred at depth, along with the interpreted structural evolution through time, reproduces the surface dips of the anticlinorium and the younger anticlines

to the south as the thrust front progressed south along the 140 km length of the range covered by the cross sections. Furthermore, the structural relief and stratigraphy in the forward models match well with the geologic cross sections constructed using classical techniques.

In our modeling, we included the sequence of events and ages of structures, as presented or determined in previous studies. There is some shortening represented by folding north of the San Ynez range, mostly associated with the Pine Mountain fault (Fig. 2), but the first major thrust front along the length of the Santa Ynez anticlinorium resulted from initiation of motion on the San Cayetano fault. This was followed by propagation of the thrust fault southward to the Red Mountain–South Sulphur Mountain fold and later to the Pitas Point/Ventura fault, all of which formed the imbricated thrust and ramp architecture as depicted in Figure 9. In cross sections 2 through 5 (Figs. 9 and 10), there is a flat between the emergent Red Mountain and Ventura frontal faults, as modeled and interpreted by others (Hubbard et al., 2014; Namson and Davis, 1988; Shaw and Suppe, 1994; Yeats et al., 1988,) and we reproduced the low-angle flat in our modeling. In fact, we tried to eliminate this midcrustal flat and found that it was required in order to retain connectivity and simultaneously reproduce the surface geometry. The presence of the flat is also favored by mechanical models that analyzed geodetic data for the presence or absence of a midcrustal flat (Marshall et al., 2017).

Cross-section 1 (Fig. 10) required a simple geometry, compared to the other cross sections, without a ramp-flat-ramp structure. This was expected because there is no major fold south of the San Cayetano fault near Fillmore (Fig. 1B); a simpler structural configuration required a simpler structural evolution and model. It might be expected that the marginal cross section would exhibit a different geometry close to the lateral

boundaries of the system. That said, a young fold emerges out of the late Quaternary alluvium west of Fillmore and south of the San Cayetano fault (Rockwell, 1988; Hughes et al., 2018) that was too small to model at the scale of the model, but it does represent the very recent southward propagation of the San Cayetano fault, as demonstrated by Hughes et al. (2018).

Based on these models, we estimated that ~21 km of total shortening has accrued since contraction began in the Pliocene in the eastern part of the Ventura Basin (cross-sections 1–4). The required shortening decreases to ~13 km in cross-section 5, ~11 km in cross-section 6, and ~7 km at the westernmost cross-section 7 near Point Conception. The average shortening rate implied by this amount of shortening, considering the age uncertainty, is 6.5–9.1 mm/yr for cross sections 1–4, in close agreement with geodetic estimates, which suggest an average current shortening rate of 7 mm/yr (Marshall et al., 2013), and geologic estimates of 8–10 mm/ yr (Rockwell et al., 1988). Another factor of note is that the geodetic estimates of shortening in the westernmost Western Transverse Ranges (area of cross-section 7) are much lower than near Ventura (Marshall et al., 2013), consistent with our estimate that only a third of the shortening is required to produce the observed structures for the area of cross-section 7.

This reduction in shortening westward is consistent with the observation that the anticlinorium is not overturned west of cross-section 5 (Figs. 2 and 4), which also argues for a lesser amount of total shortening. The alternative is to place the main fault deeper, but the observation that the depth of microseismicity in the Western Transverse Ranges seems to shallow from east to west indicates that the seismogenic depth also shallows from east to west (Nazareth and Hauksson, 2004). This contradicts deepening the

location of the main lower ramp and thus supports our decision to match the observed folding patterns with a westward decrease in slip.

The westward decrease in the amount of shortening is likely the result, in part, of the position of the westernmost Transverse Ranges relative to the Big Bend of the San Andreas fault, which has evolved over time. Early in the history of contraction (late Pliocene?), the region around Point Conception would have been far to the east of its current position because of less total slip on the San Andreas fault. Therefore, the contraction in the west may be older, resulting from the previous location of this region directly south of the Big Bend in the San Andreas fault. Furthermore, the Big Bend of the San Andreas, which is inferred to be a major factor in contraction in the Western Transverse Ranges, has evolved over time as slip accrued on the Garlock fault (Fig. 1A) from extension in the Great Basin (Davis and Burchfiel, 1973).

Full agreement between model prediction and geologic observations is unrealistic for a number of reasons. First, changes in thickness are observed as units thin to the north, and it is difficult to model this aspect accurately in Trishear. In addition, secondary structures and additional deformation resulting from minor back thrusts and from out-of-plane strike-slip faulting are difficult to quantify, although the amount of strike-slip motion is minor compared to dip slip, and the initial geometry of the Paleogene section was relatively simple. Finally, the superposition of the present compressional deformation regime on the Miocene extensional regime is another factor that introduces additional complications. For example, the Miocene growth strata and sections that were eroded make it difficult to compare the observed geology to a simple layered model. The simplifications we made, mainly using a layer cake model, might affect the amount of total shortening we used in the model. In the case that the Lower Eocene or Cretaceous units

already had some relief from north to south, a lower dip or slip on the modeled faults would have been required, and vice versa. Because we have no way to constrain the paleorelief of these units, we cannot quantify this uncertainty, although there are no clastic deposits eroded from the Eocene strata in the Miocene units, which argues against subaerial exposure of the Eocene strata to the north. Considering those issues, and accepting the limitations of our inherent assumptions, we suggest that our structural models reproduce the geometry and kinematics of the major thrust sheets, and they are consistent with all large-scale observations along the transects (Figs. 9 and 10).

Three-dimensional fault surface

Considering that the depth of the brittle-ductile transition in the Western Transverse Ranges is as deep as 18–20 km, based on depth distribution of the seismic moment release (Nazareth and Hauksson, 2004), we can estimate the fault surface area for the underlying thrust. Figure 11 presents an interpolated fault surface (using the spline curve method) for that portion of the crust that lies in the seismogenic zone. In this threedimensional (3-D) model, we connected the various fault lines with the assumption that the active deep fault connects to the frontal foldand-thrust zone as one continuous thrust surface. Based on this model, we estimated that the surface area of the fault is ~6000 km2 . If the entire ~140 km length of the fault system fails in a single event, an earthquake in the Mw 7.8 range is possible, based on scaling relations (Leonard, 2010). As the slip rate, and therefore expected slip per event, decrease to the west, this is likely a maximum estimate of the plausible earthquake magnitude. This magnitude of potential earthquake, or at least a magnitude in the Mw 7.5–7.8 range, is supported by the aforementioned recent studies of coastal uplift, borehole excavations, and structural analysis (Hubbard et al., 2014; McAuliffe et al., 2015; Rockwell et al., 2016). The

Holocene coastal marine terraces near Punta Gorda between Ventura and Santa Barbara record Holocene uplift events that average 10 m (Rockwell et al., 2016). Similarly, the onshore Ventura fault has produced up to 6 m of vertical deformation per event (McAuliffe et al., 2015). These amounts of uplift in a single event are only known worldwide from large earthquakes. The evidence for large displacements or uplift led Hubbard et al. (2014) to propose that some ruptures must involve multiple segments to accommodate the expected surface area of such uplifts. They argued that rupture of just the emergent portion of the San Cayetano and Ventura faults was too small to explain such large events, and thus proposed multisegment ruptures that extended east and/or west. Our interpretation for the surface area of the thrust is about twice that of Hubbard et al. (2014) due to the shallower dip of the lower ramp down to 18–20 km depth and extension of the fault system to the west. Thus, our fault representation is of sufficient size to host the class of earthquakes that independent paleoseismic data indicate have occurred within the system. One other aspect is worth noting. The low dip that we infer for the underlying thrust ramp in our model predicts that a geodetic uplift signal should be observable to the north of the Santa Ynez range, contrary to that from the steeper dips inferred for other models (Sorlien and Nicholson, 2015; Nicholson et al., 2017). Our model is consistent with the geodetic uplift signal north of the Santa Ynez range (Hammond et al., 2018), which indicates that the deep thrust related to the shortening at the brittleductile transition zone is in the same area as we predict.

Conclusions

Based on our new kinematic forward modeling effort, we propose that the primary structures of the Western Transverse Ranges result from a southward-verging system of folds and thrust faults that have evolved through time. In our model, the lower ramp dips

~20° (with possible range of 16°–30°) to the north, to explain the regional uplift of 1 mm/yr, and the upper ramp dips ~45°–60° to the north, based on well data. Based on seven forward models (Figs. 9 and 10) that explain well the observed surface geology and interpreted cross sections, we infer that the deep structure is best represented by a large, continuous thrust sheet that connects the various geological structures observed at the surface. The presence of this large, interpreted fault can explain the large deformations that have been documented for the Pitas Point/ Ventura fault system at the coast. The potential surface area of a rupture in the seismogenic zone may be as large as ~6000 km2; such a scenario could yield an earthquake as large as M 7.8 (Hubbard et al., 2014; McAuliffe et al., 2015; Rockwell et al., 2016). Further, we predict that the rate of shortening drops significantly in the offshore from east to west, which implies that displacement per event also likely falls off to the west.

Finally, our approach of accounting for observations that constrain the model but do not serve as inputs might be applied in other fold-and-thrust belts worldwide. Independent information on fault slip rates, uplift and shortening rates, relative timing of structures, geodetic data, and other independent information help to guide the development and restrict the degrees of freedom for structural models of the entire seismogenic crust, as in our models for the Western Transverse Ranges.

Acknowledgments

Chapter 2, in full, is a reprint of the material as it appears in: Y. Levy, T.K. Rockwell, J.H. Shaw, A. Plesch, N.W. Driscoll, and H. Perea, 2019, “Structural modeling of the Western Transverse Ranges: An imbricated thrust ramp architecture” *Lithosphere*; 11 (6): 868-883. The dissertation author was the primary investigator and author of this paper.

This research was supported by the Southern California Earthquake Center (SCEC), Contribution 8054. SCEC is funded by National Science Foundation Cooperative Agreement EAR1033462 and U.S. Geological Survey Cooperative Agreement G12AC20038. H. Perea was supported by the European Union's Horizon 2020 research and innovation program under grant H2020-MSCA-IF-2014 657769. We thank Alex Hughes, Dylan Rood, Scott Marshall, and Nate Onderdonk for interesting and helpful discussions, and we thank Edward Keller and Vikash Tripathy for excellent reviews of an early version of this manuscript.

Figures

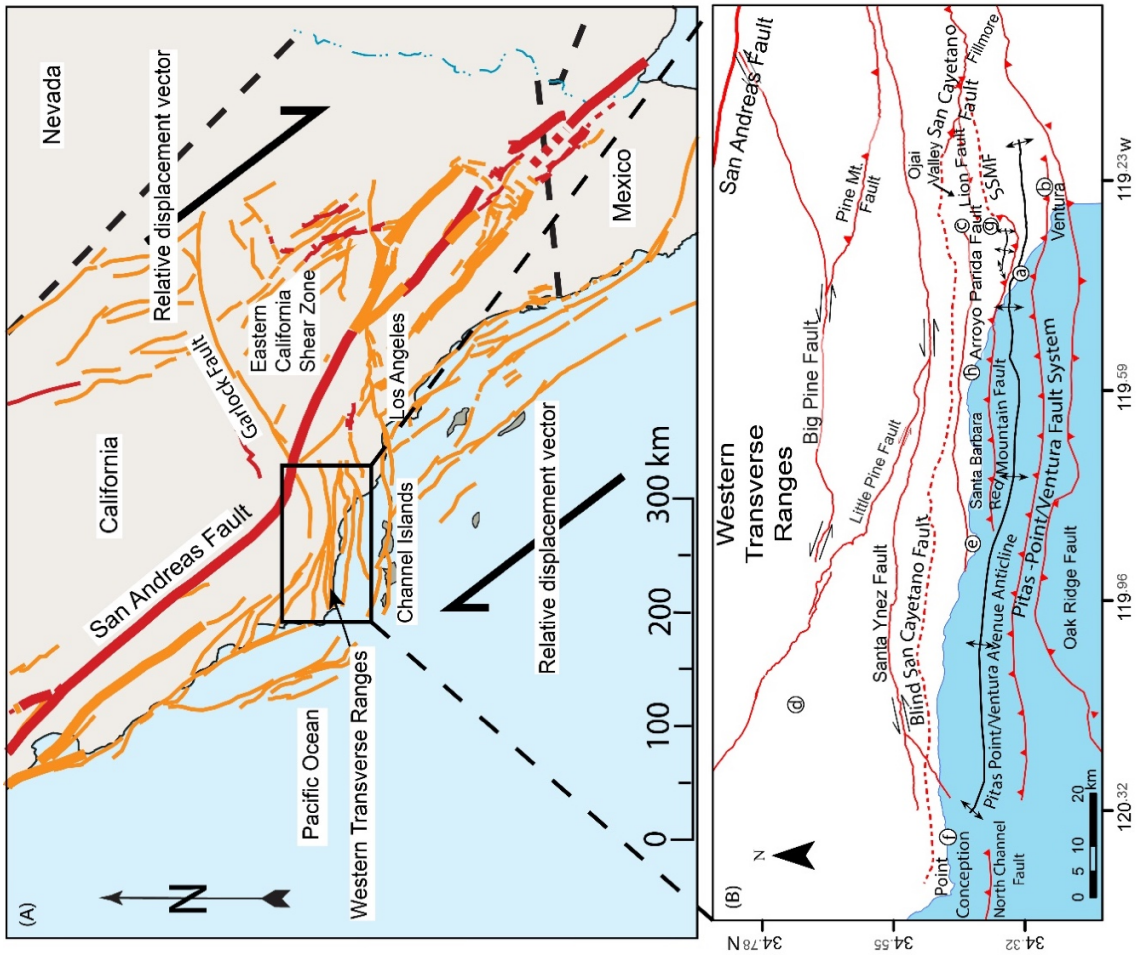

Figure 2.1. (A) Regional fault map of California. The relative motion of the Pacific and North American plates is right lateral and is on the order of 45 mm/yr. The Western Transverse Ranges, located within the black box located south of the Big Bend of the San Andreas fault, accommodate the shortening resulting from the geometry of the Big Bend of the San Andreas fault and the right-lateral strikeslip faults southeast of the channel islands. (B) Main faults in the Western Transverse Ranges and location of geomorphic studies in the region: a (Punta Gorda)—uplifted and tilted marine terraces (Rockwell et al., 2016), b—location of the sections from McAuliffe et al. (2015), c—uplifted fluvial terraces with no tilting (Rockwell et al., 1984), d—uplifted fluvial terraces with some tilting (Farris, 2017), e—marine oxygen isotope stage (MIS) 3 marine terraces demonstrating an uplift rate of ~1 mm/yr at Isla Vista (Gurrola et al., 2014), f—MIS 5 marine terraces demonstrating an uplift rate of at least 0.3 mm/yr between Gaviota and Point Conception (Rockwell et al., 1992), g—tilted and uplifted fluvial terraces with no horizontal deflection (Rockwell et al., 1984, 1988), h—Carpenteria. SSMF—South Sulphur Mountain fault.

Figure 2.2. Geological map of the Western Transverse Ranges compiled from Dibblee (2002). The Santa Ynez anticlinorium and general east-west trend of the structures are apparent. Stratigraphic column is given in Figure 3. The stratigraphic column in this figure does not represent thickness, and it is missing some units that are outside the area of the cross sections; coloring of the geological units in the map is consistent with the column. Dip data are presented only as type and direction. Locations of the different cross sections are marked with black lines. Locations of previous model as presented in Figure 5 are marked with dotted lines and indicated by letters. The model presented by line b exceeds the limits of the figure to the south as marked by an arrow in the bottom right corner. SCF—San Cayetano fault; BSCF—blind San Cayetano fault; SYF—Santa Ynez fault; SSMF—South Sulphur Mountain fault; VF—Ventura fault; PMF—Pine Mountain fault; PPF—Pitas Point fault; RMF—Red Mountain fault.

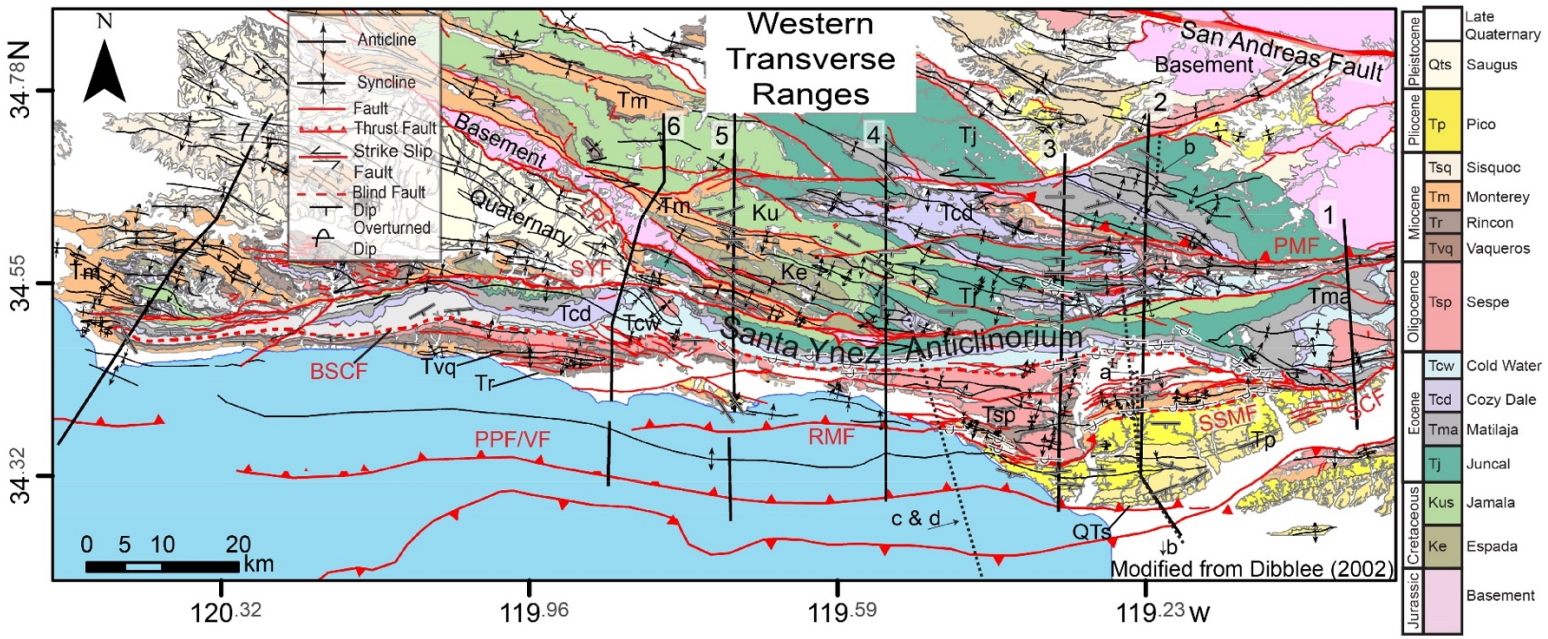
Western Transverse Ranges
Santa Ynez Anticlinorium
San Andreas Fault
Basement
Quaternary
Anticline
Syncline
Fault
Thrust Fault
Strike Slip Fault
Blind Fault
Dip
Overturned Dip
BSCF
SYF
PPF/VF
RMF
PMF
SSMF
SCF
Tm
Tvq
Tr
Tcd
Tcw
Ku
Ke
Tj
Tma
Tsp
Tp
QTs
c & d
0 5 10 20 km
34.78N
34.55
34.32
120.32
119.96
119.59
119.23 W
Modified from Dibblee (2002)
Late Quaternary
Qts Saugus
Tp Pico
Tsq Sisquoc
Tm Monterey
Tr Rincon
Tvq Vaqueros
Tsp Sespe
Tcw Cold Water
Tcd Cozy Dale
Tma Matilaja
Tj Juncal
Kus Jamala
Ke Espada
Basement
Pleistocene
Pliocene
Miocene
Oligocene
Eocene
Cretaceous
Jurassic

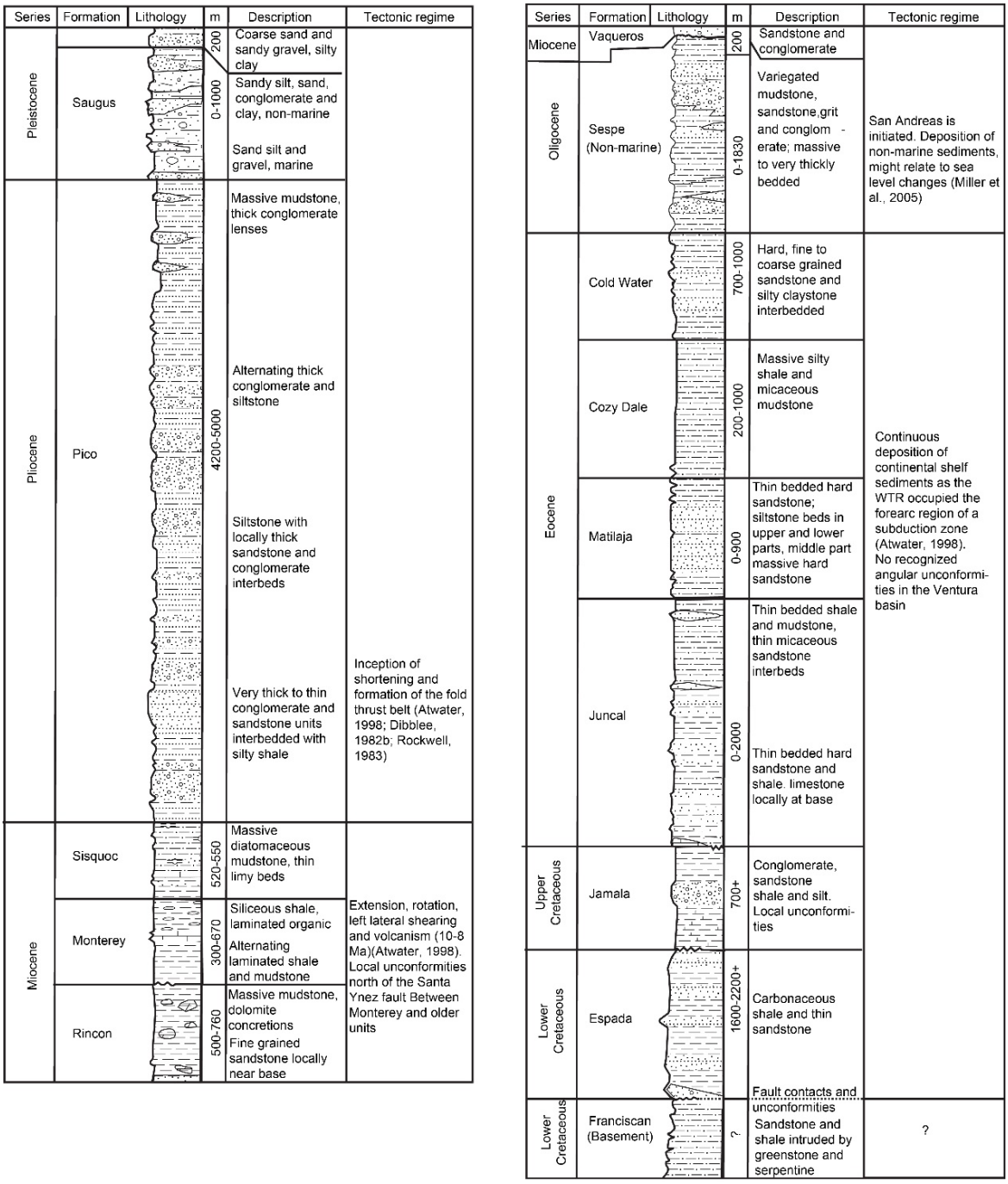

Figure 2.3. Stratigraphic column of the Western Transverse Ranges (WTR) modified from Dibblee (1982b). Thickness is presented in meters in the numerical column. This is a generalized stratigraphy, and some units have fault contacts as can be seen in Figure 2. For stratigraphic columns in different localities, we refer to Dibblee (1982b). We added a column that describes the tectonic regime.

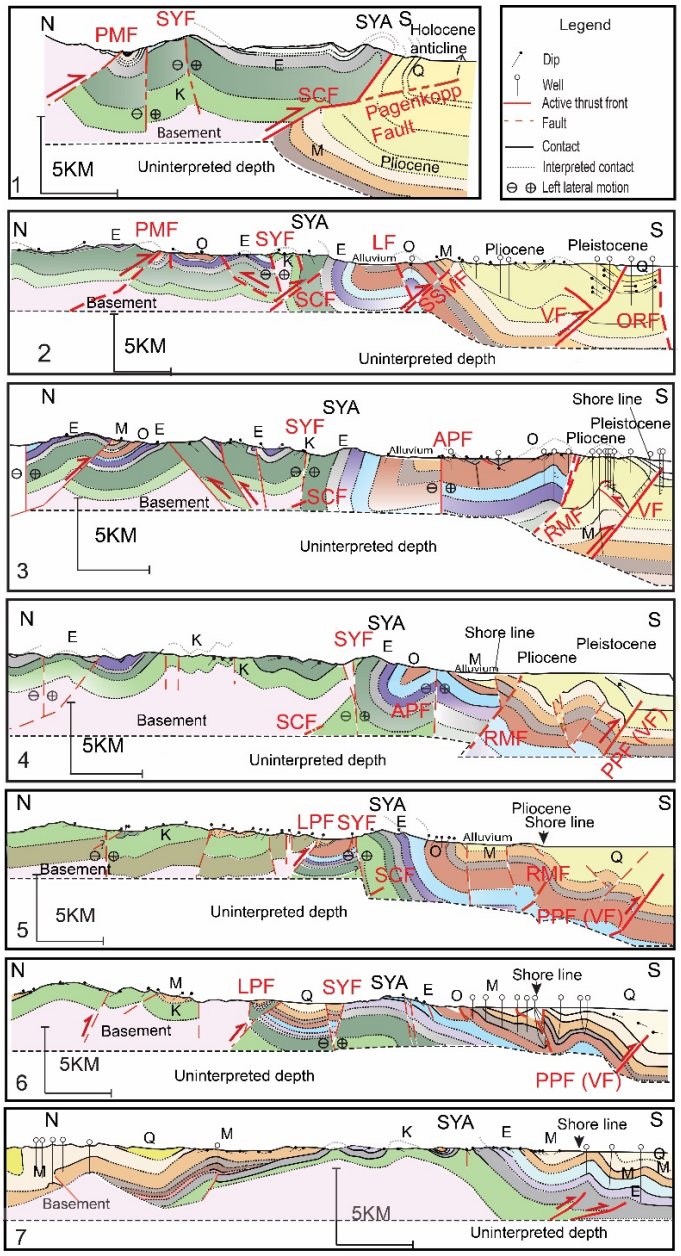

Figure 2.4. Geological cross sections (locations in Fig. 2). The sections present mainly observations and some interpretation based on stratigraphic thickness from maps and Dibblee (1982a). The blind San Cayetano fault, as we interpret it, is not included in all the sections, as there are no direct observations of the fault west of Ojai Valley, and we did not interpret the full depth of the seismogenic zone. SYA—Santa Ynez anticlinorium. Geological units: K—Cretaceous; E—Eocene; O—Oligocene; M—Miocene; Q—Quaternary. Faults (red letter): SCF—San Cayetano fault; SYF—Santa Ynez fault; SSMF—South Sulphur Mountain fault; VF—Ventura fault; PPF—Pitas Point fault; LF—Lion fault; ORF—Oak Ridge fault; PMF—Pine Mountain fault; LPF—Little Pine fault; RMF—Red Mountain fault; APF—Arroyo Parida fault.

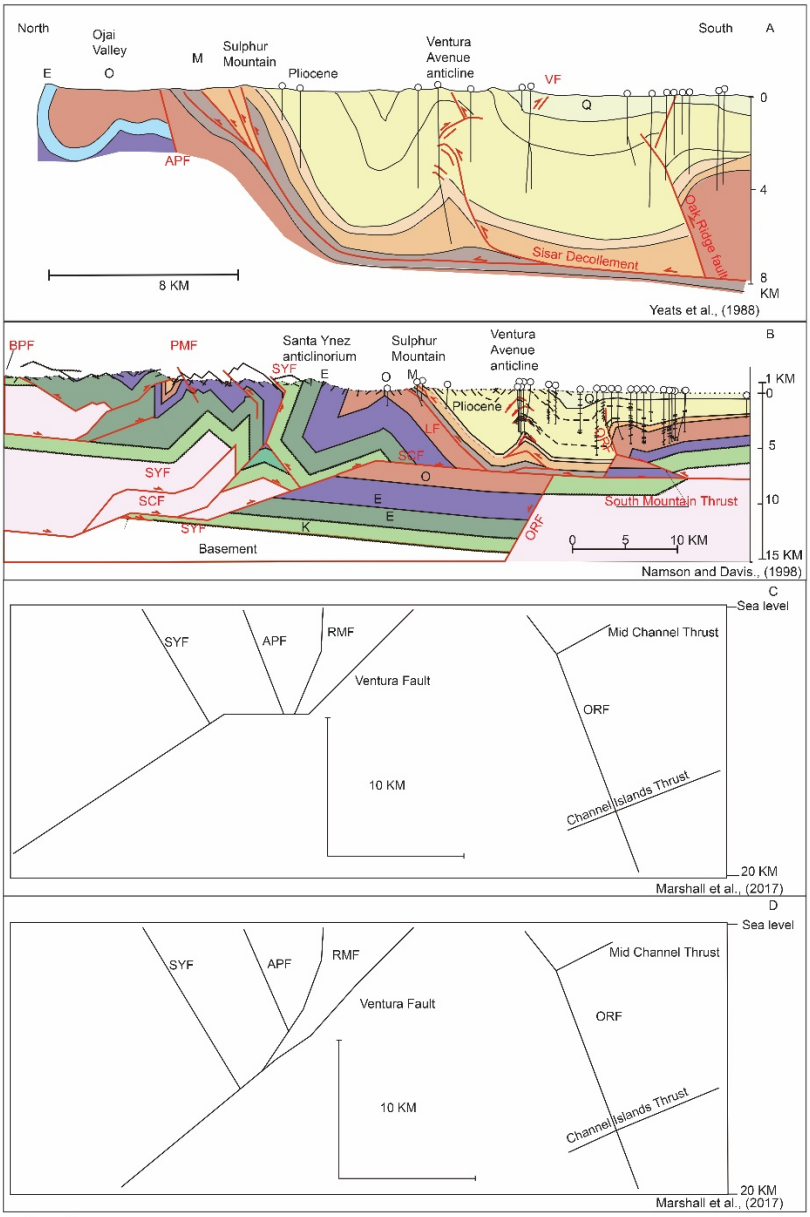

Figure 2.5. Previous structural and fault models for the region (locations in Fig. 2). (A) Cross section B-B′ of Yeats et al. (1988). (B) Cross section from (Davis and Namson, 1998), where Eocene is presented as one unit in purple. (C–D) Two versions of the Community Fault Model of the Southern California Earthquake Center (Nicholson et al., 2017; Plesch et al., 2007) for this region: the Hubbard model (C) and the flower structure model (D) as presented in Marshall et al. (2017). Cross sections and models were edited to match the color coding and abbreviations used in this paper. Geological units: K—Cretaceous; E—Eocene; O—Oligocene; M—Miocene; Q—Quaternary. Faults (red letter): SCF—San Cayetano fault; SYF—Santa Ynez fault; VF—Ventura fault; PPF—Pitas Point fault; LF—Lion fault; ORF—Oak Ridge fault; PMF—Pine Mountain fault; BPF—Big Pine fault; RMF—Red Mountain fault; APF—Arroyo Parida fault.

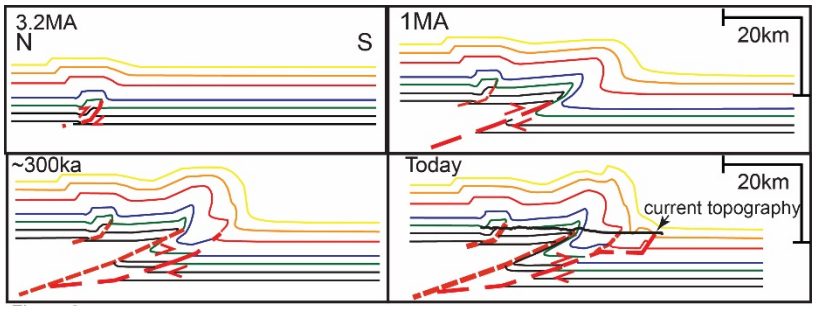

Figure 2.6. Trishear forward model showing the evolution of the fold-and-thrust belt system in the Western Transverse Ranges since late Pliocene time for cross section 2 (Fig. 4) as the thrust front has migrated south in the direction of vergence. Dashed red lines mark faults; thin colored lines represent rough approximation for contacts of footwall stratigraphy; thick black line in the last plot (present) represents the current topography. Colored lines demonstrate the resulting modeled deformation across the section and can be compared to the observed folds and dips. We did not model out-of-sequence thrusting; therefore, faults in the model are no longer active once a new thrust is superposed. Preexisting deformation was modeled in first panel (3.2 Ma), while secondary or outof-plane deformation was mostly neglected. The result after cutting the lines with topography is presented in Figure 9; similar steps were performed for the other cross sections, and the final result was compared to surface and near-surface observations (Fig. 10).

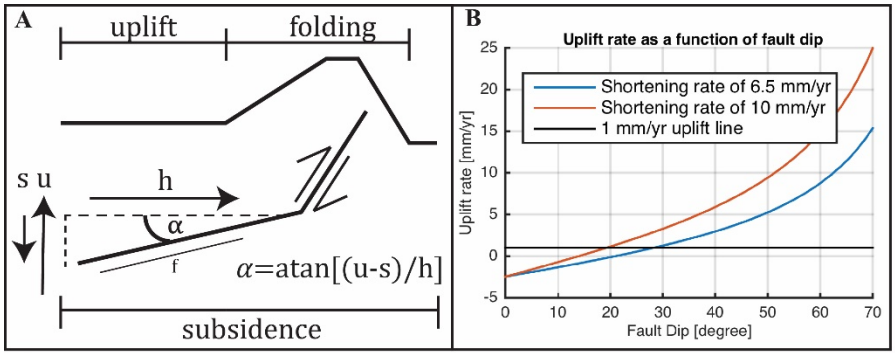

Figure 2.7. (A) Model used to calculate the fault dip for the lower ramp. Parameters: α—fault dip; h—horizontal shortening rate; u—uplift rate; s—subsidence rate. We assumed that competing rates of uplift and regional subsidence will equal the observed rate of uplift where there is no folding. (B) Plot of dip vs. observed uplift rate for different shortening rates and a subsidence rate of 2.5 mm/yr. The prediction for fault dip is at the intersection of the results (red and blue curves) with the 1 mm uplift line (black), which is the reported regional uplift. See text for further information.

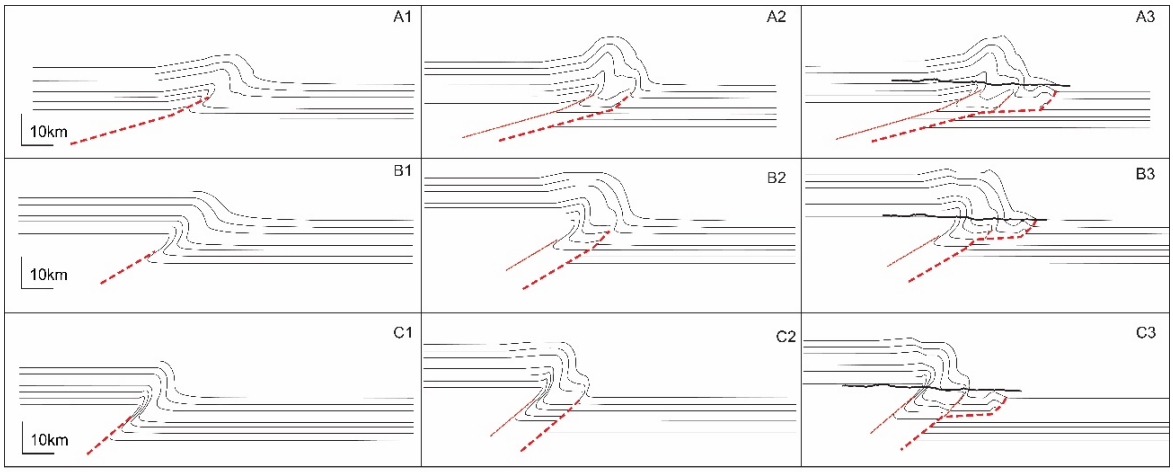

Figure 2.8. Models that present different dips for the lower ramp. Thick dashed red line is the fault that slipped most recently, whereas the thinner red line is an older inactive thrust, the thin black lines represent hypothetical contacts, and the thick black lines in A3, B3, and C3 represent the current topography. For these models, we used the same parameters as described in the text for the model presented in Figure 6. Model A1–A3 presents a deep ramp dipping 15° degrees north. Model B1–B3 presents a deep ramp dipping 30° degrees north. Model C1–C3 presents a deep ramp dipping 40° degrees north. The 40° dip is beyond our estimated range of likely dips as it does not well represent the known geology.

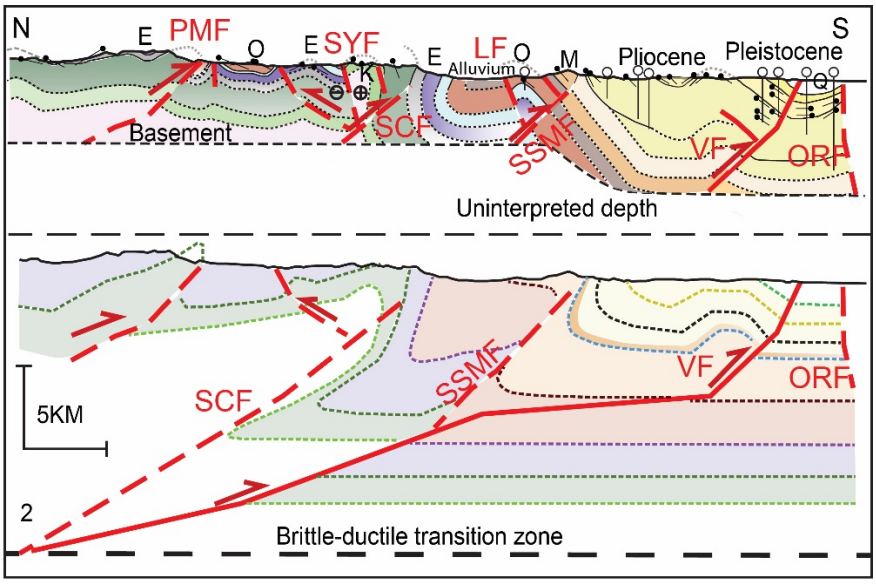

Figure 2.9. Comparison between geological cross section 2 (upper cross section) and the Trishear forward model (lower cross section) showing a good first-order match between the two. See Figure 2 for location of the cross section. Stratigraphy was simplified in the model. For abbreviations, see Figure 4. In the model, the thin colored lines represent rough simplified approximation for contacts of footwall stratigraphy.

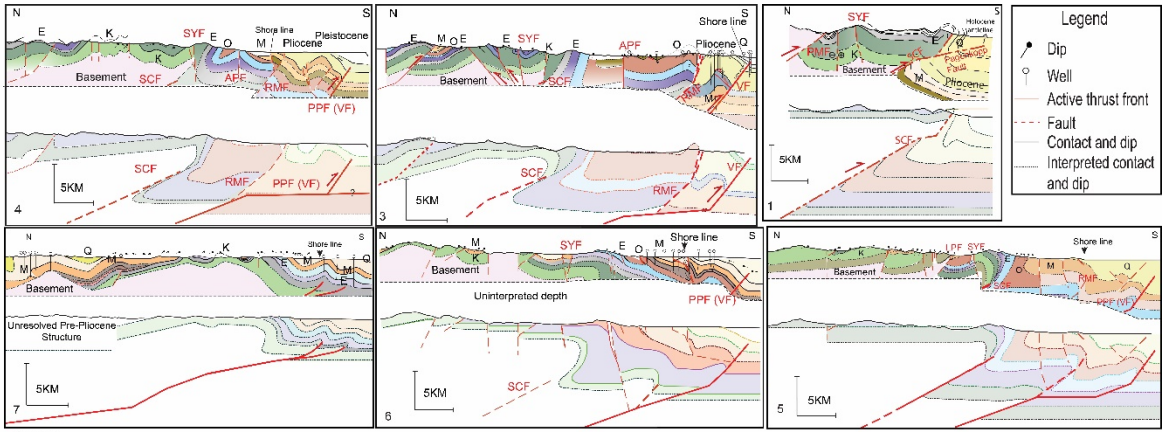

Figure 2.10. Comparison between the geological cross sections (upper cross section) and the Trishear forward model (lower cross section) for cross sections 1 and 3–7 showing a good first-order match between the two. See Figure 2 for locations of the cross sections and Figure 9 for deeper structure of sections 3–6. For abbreviations, see Figure 4. In the model, the thin colored lines represent rough simplified approximation for contacts of footwall stratigraphy.

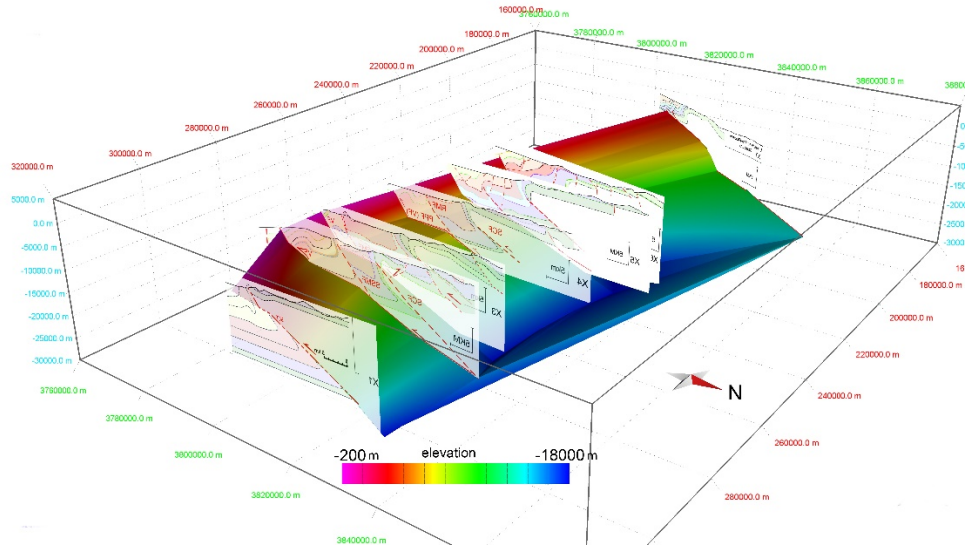

Figure 2.11. Interpolation of the predicted active fault surface. Surface was interpolated from the modeled fault lines using spline curve method down to the seismogenic depth (18 km; Nazareth and Hauksson, 2004). The surface area of the fault is estimated at ~6000 km2, which can potentially host a high 7 magnitude earthquake according to scaling relations (Leonard, 2010).

Appendix: well data

In Appendix Table A2, we include the API numbers and coordinates for the wells we incorporated into our cross sections. Some of the wells were interpreted by the studies cited in our work, while others had a well log available through the Department of Conservation, California, website (https://maps.conservation.ca.gov/doggr/wellfinder/#close).

Table A2.1. Well data.

API	Longitude	Latitude
11105289	-119.297089	34.31761
11120851	-119.226167	34.31161
11103876	-119.297111	34.309279
11105923	-119.229634	34.295784
11105917	-119.218798	34.292384
11104005	-119.268814	34.28971
11105919	-119.190851	34.290011
11104006	-119.269424	34.28689
11105811	-119.306094	34.285428
11106169	-119.316914	34.283682
11120500	-119.207144	34.281811

Table A2.2. Well data.

API	Longitude	Latitude
11105928	-119.332858	34.348772
11100922	-119.322307	34.38954
11102077	-119.33852	34.319543
11120458	-119.317652	34.321161
11105164	-119.297092	34.325153
11100511	-119.234496	34.382496
11105939	-119.251238	34.360451
11100511	-119.234496	34.382496
11105939	-119.251238	34.360451
11105935	-119.25202	34.370525
11101115	-119.233681	34.432549
11121257	-119.2338	34.433422
11101102	-119.231976	34.432883
11121031	-119.222902	34.402922
11120161	-119.218663	34.542139
8303609	-119.727188	34.400926

Table A2.3. Well data.

API	Longitude	Latitude
8303632	-119.714455	34.40124
8303653	-119.715492	34.402276
8303976	-119.848383	34.434992
8304148	-119.747003	34.899036
8304278	-119.747152	34.928694
8304525	-119.729351	34.876494
28303775	-119.855967	34.40898
28304047	-119.779482	34.365094
28304050	-119.705845	34.34834
28304052	-119.813845	34.367982
28304053	-119.82462	34.363392
28304605	-119.919105	34.393514
28304697	-119.882622	34.389519
28304698	-119.882484	34.3898
8303609	-119.727188	34.400926
8303632	-119.714455	34.40124

Table A2.4. Well data.

API	Longitude	Latitude
8303653	-119.715492	34.402276
8303976	-119.848383	34.434992
8304148	-119.747003	34.899036
8304278	-119.747152	34.928694
8304525	-119.729351	34.876494
28303775	-119.855967	34.40898
28304047	-119.779482	34.365094
28303820	-120.45	34.426468
28300100	-120.46	34.411772
28303823	-120.44	34.438653
11105798	-119.197698	34.268451
11106171	-119.317652	34.28989
11106129	-119.352373	34.58016
11106170	-119.334111	34.313489

References cited

Atwater, T.M., 1998, Plate tectonic history of southern California with emphasis on the western Transverse Ranges and northern Channel Islands, in Weigand, P.W., ed., Contributions to the Geology of the Northern Channel Islands, Southern California: American Association of Petroleum Geologists, Pacific Section, Miscellaneous Publication 45, p. 1–8, https://doi.org/10.32375/1998-MP45.1.

Bird, P., and Rosenstock, R.W., 1984, Kinematics of present crust and mantle flow in southern California: Geological Society of America Bulletin, v. 95, p. 946–957, https://doi .org/10.1130/0016-7606(1984)952.0.CO;2.

Boyer, S.E., and Elliott, D., 1982, Thrust systems: American Association of Petroleum Geologists Bulletin, v. 66, p. 1196–1230.

Butler, R.W.H., 1987, Thrust sequences: Journal of the Geological Society [London], v. 144, p. 619–634, https://doi .org/10.1144/gsjgs.144.4.0619.

Corbett, E.J., and Johnson, C.E., 1982, The Santa Barbara, California, earthquake of 13 August 1978: Bulletin of the Seismological Society of America, v. 72, p. 2201–2226.

Crowell, J.C., 1979, The San Andreas fault system through time: Journal of the Geological Society [London], v. 136, p. 293–302, https://doi.org/10.1144/gsjgs.136.3.0293.

Darrow, A.C., and Sylvester, A.G., 1983, Activity of the Central Reach of the Santa Ynez Fault: Menlo Park, California, U.S. Geologic Survey Technical Report, 28 p.

Darrow, A.C., and Sylvester, A.G., 1984, Activity of the Central Reach of the Santa Ynez Fault: Continuation of Investigations: U.S. Geologic Survey Technical Report, Contract 21367, 18 p.

Davis, G.A., Burchfiel, B.C., 1973, Garlock fault: An intracontinental transform structure, Southern California Garlock fault: Geological Society of America Bulletin, v. 84, p. 1407–1422, https://doi.org/10.1130/0016-7606(1973)842.3.CO;2.

Davis, T.L., and Namson, J.S., 1998, USGS Cross Sections 3–8: http://davisnamson.com/index.htm (accessed 12 January 2018).

DeCelles, P.G., Robinson, D.M., Quade, J., Ojha, T.P., Garzione, C.N., Copeland, P., and Upreti, B.N., 2001, Stratigraphy, structure, and tectonic evolution of the Himalayan foldthrust belt in western Nepal: Tectonics, v. 20, p. 487–509, https://doi.org/10.1029/2000TC001226.

Dibblee, T.W., 1982a, Regional geology of the Transverse Ranges Province of southern California, in Fife, D.L., and Minch, J.A., eds., Geology and Mineral Wealth of the California Transverse Ranges: Santa Ana, California, South Coast Geological Society, Inc., p. 7–26.

Dibblee, T.W., 1982b, Geology of the Santa Ynez–Topatopa Mountains, Southern California, in Fife, D.L., and Minch, J.H., eds., Geology and Mineral Wealth of the

California Transverse Ranges: Santa Ana, California, South Coast Geological Society, Inc., p. 41–56.

Dibblee, T.W., 2002, Dibblee Geological Foundation: Geological Map Catalog (1–21, 24, 26, 27, 40–46, 53–55, 60, 186–189, 199–201, 254–259): https://www.sbnature.org/ dibblee/ (accessed 20 July 2015).

Erslev, E.A., 1991, Trishear fault-propagation folding: Geology, v. 19, p. 617–620, https://doi.org/10.1130/0091-7613 (1991)0192.3.CO;2.

Farris, A.C., 2017, Quantifying Late Quaternary Deformation in the Santa Ynez Valley, Santa Barbara County, California [Master's thesis]: Long Beach, California, California State University, 150 p. Groshong, R.H.J., 1994, Area balance, depth to detachment, and strain in extension: Tectonics, v. 13, p. 1488–1497, https://doi.org/10.1029/94TC02020.

Gurrola, L.D., Keller, E.A., Chen, J.H., Owen, L., and, Spencer, J.Q., 2014, Tectonic geomorphology of marine terraces; Santa Barbara fold belt, California: Geological Society of America Bulletin, v. 126, p. 219–233, https://doi.org /10.1130/B30211.1.

Hammond, W.C., Burgette, R.J., Johnson, K.M., and Blewitt, G., 2018, Uplift of the Western Transverse Ranges and Ventura area of Southern California: A four-technique geodetic study combining GPS, InSAR, leveling, and tide gauges: Journal of Geophysical Research–Solid Earth, v. 123, p. 836–858, https://doi.org/10.1002/2017JB014499.

Hauksson, E., Andrews, J., Plesch, A., Shaw, J.H., and Shelly, D.R., 2016, The 2015 Fillmore earthquake swarm and possible crustal deformation mechanisms near the bottom of the eastern Ventura Basin, California: Seismological Research Letters, v. 87, no. 4, p. 807–815, https://doi.org /10.1785/0220160020.

Hayes, G.P., Meyers, E.K., Dewey, J.W., Briggs, R.W., Earle, P.S., Benz, H.M., Smoczyk, G.M., Flamme, H.E., Barnhart, W.D., Gold, R.D., and Furlong, K.P., 2016, Tectonic Summaries of Magnitude 7 and Greater Earthquakes from 2000 to 2015: U.S. Geological Survey Open-File Report 2016–1192, 148 p., https://doi.org/10.3133/ofr20161192.

Hornafius, J.S., 1985, Neogene tectonic rotation of the Santa Ynez Range, Western Transverse Ranges, California, suggested by paleomagnetic investigation of the Monterey Formation: Journal of Geophysical Research, v. 90, p. 12503, https://doi.org/10.1029/JB090iB14p12503.

Hornafius, J.S., Kamerling, M., Terres, R., and Luyendyk, B., 1982, Differential tectonic rotation within the western Transverse Ranges: Geological Society of America Abstracts with Programs, v. 14, no. 4, p. 173–174.

Hornafius, J.S., Luyendyk, B.P., Terres, R.R., and Kamerling, M.J., 1986, Timing and extent of Neogene tectonic rotation in the western Transverse Ranges, California (USA): Geological Society of America Bulletin, v. 97, p. 1476– 1487, https://doi.org/10.1130/0016-7606(1986)972.0.CO;2.

Huang, W., Silver, L.T., and Kanamori, H., 1996, Evidence for possible horizontal faulting in southern California from earthquake mechanisms: Geology, v. 24, p. 123– 126, https://doi.org/10.1130/0091-7613(1996)0242.3.CO;2.

Hubbard, J., Shaw, J.H., Dolan, J.F., Pratt, T.L., McAuliffe, L.J., and Rockwell, T.K., 2014, Structure and seismic hazard of the Ventura Avenue anticline and Ventura fault, California: Prospect for large, multisegment ruptures in the Western Transverse Ranges: Bulletin of the Seismological Society of America, v. 104, p. 1070–1087, https://doi .org/10.1785/0120130125.

Hughes, A., Rood, D.H., Whittaker, A.C., Bell, R.E., Rockwell, T.K., Levy, Y., Wilcken, K.M., Corbett, L.B., Bierman, P.R., DeVecchio, D.E., Marshall, S.T., Gurrola, L.D., and Nicholson, C., 2018, Geomorphic evidence for the geometry and slip rate of a young, low-angle thrust fault: Implications for hazard assessment and fault interaction in complex tectonic environments: Earth and Planetary Science Letters, v. 504, p. 198–210, https://doi.org/10.1016/j .epsl.2018.10.003.

Jackson, P.A., 1981, Structural Evolution of the Carpinteria Basin, Western Transverse Ranges, California [Master's thesis]: Corvallis, Oregon, Oregon State University, 106 p.

Jordan, T.E., Allmendinger, R.W., Damanti, J.F., and Drake, R.E., 1993, Chronology of motion in a complete thrust belt: The Precordillera, 30–31°S: Andes Mountains: Journal of Geology, v. 101, p. 135–156.

Keller, E.A., and DeVecchio, D.E., 2013, Tectonic geomorphology of active folding and development of transverse drainages, in Shroder, J., ed., Treatise on Geomorphology: San Diego, California, Academic Press, p. 129–147, https://doi.org/10.1016/B978-0-12-374739-6.00088-9.

Leonard, M., 2010, Earthquake fault scaling: Self-consistent relating of rupture length, width, average displacement, and moment release: Bulletin of the Seismological Society of America, v. 100, p. 1971–1988, https://doi.org/10 .1785/0120090189.

Ma, K.-F., Lee, C.-T., Tsai, Y.-B., Shin, T.-C., and Mori, J., 1999, The Chi-Chi, Taiwan, earthquake: Large surface displacements on an inland thrust fault: Eos (Washington, D.C.), v. 80, p. 605–611, https://doi.org/10.1029/99EO00405.

Marshall, S.T., Funning, G.J., and Owen, S.E., 2013, Fault slip rates and interseismic deformation in the Western Transverse Ranges, California: Journal of Geophysical Research–Solid Earth, v. 118, p. 4511–4534, https://doi .org/10.1002/jgrb.50312.

Marshall, S.T., Funning, G.J., Krueger, H.E., Owen, S.E., and Loveless, J.P., 2017, Mechanical models favor a ramp geometry for the Ventura–Pitas Point fault, California: Geophysical Research Letters, v. 44, no. 3, p. 1311–1319, https://doi.org/10.1002/2016GL072289.

McAuliffe, L.J., Dolan, J.F., Rhodes, E.J., Hubbard, J., Shaw, J.H., and Pratt, T.L., 2015, Paleoseismologic evidence for large-magnitude (Mw 7.5–8.0) earthquakes on the Ventura blind thrust fault: Implications for multifault ruptures in the Transverse Ranges of

southern California: Geosphere, v. 11, p. 1629–1650, https://doi.org/10.1130 /GES01123.1.

Miller, K.G., Kominz, A., Browning, J. V, Wright, J.D., and Mountain, G.S., 2005, The Phanerozoic record of sea level change: Science, v. 310, no. 5752, p. 1293–1298, https://doi.org/10.1126/science.1116412. Morley, C.K., 1988, Out-of-sequence thrusts: Tectonics, v. 7, p. 539–561, https://doi.org/10.1029/TC007i003p00539.

Namson, J.S., and Davis, T., 1988, Structural transect of the western Transverse Ranges, California: Implications for lithospheric kinematics and seismic risk evaluation: Geology, v. 16, p. 675–679, https://doi.org/10.1130/0091-7613 (1988)0162.3.CO;2.

Nazareth, J.J., and Hauksson, E., 2004, The seismogenic thickness of the southern California crust: Bulletin of the Seismological Society of America, v. 94, p. 940–960, https:// doi.org/10.1785/0120020129.

Nicholson, C., Sorlien, C.C., Atwater, T., Crowell, J.C., and Luyendyk, B.P., 1994, Microplate capture, rotation of the Western Transverse Ranges, and initiation of the San Andreas transform as a low-angle fault system: Geology, v. 22, p. 491–495, https://doi.org/10.1130/0091-7613 (1994)0222.3.CO;2.

Nicholson, C., Plesch, A., and Shaw, J.H., 2017, Community Fault Model Version 5.2: Updating and expanding the CFM 3D fault set and its associated fault database: 2017 Southern California Earthquake Center (SCEC) Annual Meeting, 10–13 September, 2017, poster 234.

Perea, H., Ucarkus, G., Driscoll, N.W., Kent, G.M., Levy, Y., and Rockwell, T.K., 2017, Holocene deformation events in the offshore Transverse Ranges (California, USA) constrained by new high-resolution geophysical data: Expanded abstract for the 8th International Union for Quaternary Research (INQUA) Meeting on Paleoseismology, Active Tectonics and Archeoseismology (PATA), New Zealand, 13–16 November 2017, p. 4.

Plesch, A., Shaw, J.H., Benson, C., Bryant, W.A., Carena, S., Cooke, M., Dolan, J., Fuis, G., Gath, E., Grant, L., Hauksson, E., Jordan, T., Kamerling, M., Legg, M., Lindvall, S., Magistrale, H., Nicholson, C., Niemi, N., Oskin, M., Perry, S., Planansky, G., Rockwell, T.K., Shearer, P., Sorlien, C., Süss, M.P., Suppe, J., Treiman, J., and Yeats, R.S., 2007, Community Fault Model (CFM) for southern California: Bulletin of the Seismological Society of America, v. 97, p. 1793–1802, https://doi.org/10.1785/0120050211.

Poblet, J., and Lisle, R.J., 2011, Kinematic evolution and structural styles of fold-and-thrust belts, in Poblet, J., and Lisle, R.J., eds., Kinematic Evolution and Structural Styles of Fold-and-Thrust Belts: Geological Society [London] Special Publication 349, p. 1–24, https://doi.org/10.1144/SP349.1.

Poblet, J., and McClay, K.R., 1996, Geometry and kinematics of single-layer detachment folds: American Association of Petroleum Geologists Bulletin, v. 80, p. 1085–1109, https:// doi.org/10.1306/64ED8CA0-1724-11D7-8645000102C1865D.

Rockwell, T.K., 1983, Soil Chronology, Geology, and Neotectonics of the North Central Ventura Basin, California [Ph.D. thesis]: Santa Barbara, California, University of

California, 424 p. Rockwell, T.K., 1988, Neotectonics of the San Cayetano fault, Transverse Ranges, California: Geological Society of America Bulletin, v. 100, p. 500–513, https://doi.org/10 .1130/0016-7606(1988)1002.3.CO;2.

Rockwell, T.K., Keller, E.A., Clark, M.N., and Johnson D.L., 1984, Chronology and rates of faulting of Ventura River terraces, California: Geological Society of America Bulletin, v. 95, p. 1466–1474, https://doi.org/10.1130/0016-7606 (1984)952.0.CO;2.

Rockwell, T.K., Keller, E.A., and Dembroff, G.R., 1988, Quaternary rate of folding of the Ventura Avenue anticline, Western Transverse Ranges, southern California: Geological Society of America Bulletin, v. 100, p. 850–858, https://doi .org/10.1130/0016-7606(1988)1002.3.CO;2.

Rockwell, T.K., Nolan, J., Johnson, D.L., Patherson, R.H., 1992, Ages and deformation of marine terraces between Point Conception and Gaviota, Western Transverse Ranges California, in Fletcher, C.H., and Wehmiller, J.F., eds., Quaternary Coasts of the United States: Marine and Lacustrine Systems: Society for Sedimentary Geology (SEPM) Special Publication 48, p. 333–341.

Rockwell, T.K., Clark, K., Gamble, L., Oskin, M.E., Haaker, E.C., and Kennedy, G.L., 2016, Large Transverse Range earthquakes cause coastal upheaval near Ventura, Southern California: Bulletin of the Seismological Society of America, v. 106, p. 2706–2720, https://doi.org/10.1785/0120150378.

Rodgers, D.A., 1975, Deformation, Stress Accumulation, and Secondary Faulting in the Vicinity of the Transverse Ranges of Southern California [Ph.D. thesis]: Providence, Rhode Island, Brown University, 181 p.

Sarna-Wojcicki, A.M., and Yerkes, R.F., 1982, Comment on article by R.S. Yeats on “Low-shake faults of the Ventura Basin, California,” in Cooper, J.D., compiler, Neotectonics in Southern California, 78th Annual Meeting Guidebook: Anaheim, California, Cordilleran Section, Geological Society of America, p. 17–19.

Schlueter, J.C., 1976, Geology of the Upper Ojai–Timber Canyon Area, Ventura County, California [M.S. thesis]: Athens, Ohio University, 76 p.

Schwartz, D., 2018, Large coherent block versus microplate rotation of the Western Transverse Ranges: A fresh look at paleomagnetic constraints [M.S. thesis]: San Diego, California, University of California–San Diego, 37 p.

Shaw, J.H., and Suppe, J., 1994, Active faulting and growth folding in the eastern Santa Barbara Channel, California: Geological Society of America Bulletin, v. 106, p. 607–626, https://doi.org/10.1130/0016-7606(1994)1062.3.CO;2.

Shaw, J.H., Connors, C.D., and Suppe, J., 2005, Seismic Interpretation of Contractional Fault-Related Folds: An AAPG Seismic Atlas: American Association of Petroleum Geologists Studies in Geology 53, 156 p.

Smit, J.H.W., Brun, J.P., and Sokoutis, D., 2003, Deformation of brittle-ductile thrust wedges in experiments and nature: Journal of Geophysical Research, v. 108, p. 2480, https://doi.org/10.1029/2002JB002190.

Sorlien, C.C., and Nicholson, C., 2015, Post–1 Ma Deformation History of the Pitas Point–North Channel–Red Mountain Fault System and Associated Folds in Santa Barbara Channel, California: U.S. Geological Survey National Earthquake Hazards Reduction Program Final Report, Award G14AP00012, 24 p.

Storti, F., Salvini, F., and McClay, K.R., 1997, Fault-related folding in sandbox analogue models of thrust wedges: Journal of Structural Geology, v. 19, p. 583–602, https://doi .org/10.1016/S0191-8141(97)83029-5.

Suppe, J., 1983, Geometry and kinematics of fault- bend folding: American Journal of Science, v. 283, p. 684–721, https://doi.org/10.2475/ajs.283.7.684. Suppe, J., and Medwedeff, D.A., 1990, Geometry and kinematics of fault-propagation folding: Eclogae Geologicae Helvetiae, v. 454, p. 409–454, https://doi.org/10.5169 /seals-166595.

Wells, D.L., and Coppersmith, K.J., 1994, New empirical relationships among magnitude, rupture length, rupture area and surface displacement: Bulletin of the Seismological Society of America, v. 84, p. 974–1002.

Wiltschko, D.V., and Dorr, J.A., 1983, Timing of deformation in Overthrust belt and foreland of Idaho, Wyoming, and Utah: American Association of Petroleum Geologists Bulletin, v. 67, p. 1304–1322, https://doi.org/10.1306/03B5B740 -16D1-11D7-8645000102C1865D.

Yeats, R.S., 1983, Large-scale Quaternary detachments in Ventura Basin, southern California: Journal of Geophysical Research, v. 88, p. 569–583, https://doi.org/10.1029 /JB088iB01p00569.

Yeats, R.S., and Rockwell, T.K., 1991, Quaternary geology of the Ventura and Los Angeles Basins, California, in Morrison, R.B., ed., Quaternary Nonglacial Geology: Conterminous U.S.: Boulder, Colorado, Geological Society of America, The Geology of North America, v. K-2, p. 185–189.

Yeats, R.S., Huftile, G.J., and Grigsby, F.B., 1988, Oak Ridge fault, Ventura fold belt, and the Sisar décollement, Ventura basin: California Geology, v. 16, p. 1112–1116, https:// doi.org/10.1130/0091-7613(1988)0162.3 .CO;2.

Yerkes, R.F., and Lee, W.H.K., 1987, Late Quaternary deformation in the Western Transverse Ranges, in Recent Reverse Faulting in the Transverse Ranges, California: U.S. Geological Survey Professional Paper 1339, p. 71–82.

Chapter 3 Testing Structural Model Predictions against Geodetic Data in the Western Transverse Ranges, Southern California

Levy, Y.[1, 2], Marshall, S. T. [3], Rockwell, T.K.[1]

[1]Department of Geological Sciences, San Diego State University, 5500 Campanile Dr. San Diego, CA 92182, USA

[2]Scripps Institution of Oceanography, University of California, San Diego, 9500 Gilman Drive, La Jolla, CA 92037 USA

[3] Department of Geology, Appalachian State University, 287 Rivers St, Boone NC 28608, USA

Abstract

In the western Transverse Ranges of southern California, USA, several conflicting structural models have been presented for this region over the years. Despite this, none of these models incorporated the full range of available geological observations and geophysical data. In this work, we test a recently published structural model for this region against vertical velocities measured by continuous GPS stations, and compare the results to previous structural models. While well data and structural modeling constrain the shallow fault structure, GPS data can be used to constrain the dip angle of a proposed deep ramp proposed for this region whereas the shallow structure is constrained by well data and structural modeling. We reduce the range of plausible dips from 16-30 to 25-30 degrees, and for the first time, present a structural model for this region that is consistent with the full range of data and observations. We suggest that a similar interdisciplinary approach could be applied in order to improve earthquake hazard assessments.

Introduction

The western Transverse Ranges of Southern California (Figures 1 and 2) is an active fold and thrust belt (Namson and Davis, 1988; Shaw and Suppe, 1994; Levy et al., 2019) in a highly populated region. Recent studies of coastal uplift and borehole transects across a fold scarp have revealed that very large and rapid uplift events have occurred along the Pitas-Point/Ventura fault system (Rockwell et al. 2016; McAuliffe et al. 2015), which is interpreted as the thrust front of the western Transverse Ranges fold and thrust belt (Levy et al., 2019; Hubbard et al., 2014). The observed uplift events were estimated to be the result of M_w 7.5-7.8 earthquakes (Rockwell et al. 2016; McAuliffe et al. 2015). These estimates for large magnitude Holocene earthquakes stress the importance of correctly assessing the regional structural architecture of the thrust system for hazard assessment, as none of the previous structural models had the surface area to accommodate events at this scale, as inferred from scaling relations (Leonard, 2010). Therefore, advancing the structural understanding of the western Transverse Ranges has major societal importance.

Understanding of the fault structure of the western Transverse Ranges (Figure 1 and 2) has progressed over the years as new observations and data have accumulated (e.g.: Rockwell, 1983; Namson and Davis, 1988; Yeats et al., 1988; Shaw and Suppe, 1994; Hubbard et al., 2014). However, due to the ongoing debate at the Southern California Earthquake Center regarding the subsurface architecture, and the number of competing models, we conducted a comprehensive structural analysis in order to refine our understanding of the subsurface architecture (Levy et al., 2019). Levy et al.'s (2019) structural model was developed from a series of cross sections that span 140 km of the range, with the purpose of capturing the lateral variability in total shortening, fault

geometry and shortening rate. This model incorporated existing structural models (Schlueter, 1976; Jackson, 1981; Sarna-wojcicki and Yerkes, 1982; Yeats, 1983; Davis and Namson, 1998; Namson and Davis, 1988; Hubbard et al., 2014), surface data from maps (Dibblee, 2002), well data, seismic surveys (Sorlien and Nicholson, 2015), and was constrained by the observed geological vertical rates (Rockwell et al., 1984; Rockwell et al., 1992; Farris, 2017), ages of structures (Dibblee, 1982b; Rockwell, 1988; Yerkes and Lee, 1987) and the southward migration of folding in time (Rockwell, 1983). This comprehensive model details the evolution of an imbricate thrust fault system that has evolved since the Pliocene. The model was constructed using structural methods (Erslev, 1991; Suppe, 1983) in conjunction with the geological constraints mentioned above. Levy et al's (2019) model demonstrated the southward migration of the locus of deformation in the Western Transverse Ranges through time, with the dominant faults dipping to the north as they shoal from ~16-30˚ degrees at depth to ~45-60˚ near the surface. While the range of dips assigned to the upper ramp is based on observations, the plausible range of dips for the lower ramp was estimated using Trishear (Erslev, 1991) forward modeling in MOVE (Petroleum Experts Ltd., 2018) and by balancing the observed geological vertical rates, as described in Levy et al. (2019).

Marshall et al., (2017) compared predictions of two structural models against Global Positioning System (GPS) observations of vertical motion in the western Transverse Ranges. The tested models that were compared are two alternative fault representations for the Western Transverse Ranges in the Southern California Earthquake Center's Community Fault Model (Nicholson et al., 2017; Plesch et al., 2007). The results of this comparison favored the representation which was developed by Hubbard et al. (2014), with a ramp-flat-ramp geometry, over the alternative representation

of steeply dipping faults, known among structural geologists who work in the region as the “flower structure model”. The model that was presented in Levy et al. (2019) is somewhat similar to the ramp-flat-ramp model (Hubbard et al., 2014), perhaps because of the use of fault-fold related methods. Aside from fold-fault related structural models being more consistent with the observed geology, Marshall et al. (2017) showed that they are also more consistent with the observed interseismic motion rate measured by Global Positioning System (GPS) stations. In the particular case of the western Transverse Ranges, the transition from up to down motion occurs north of the Santa Ynez mountain range (Hammond et al., 2018; Marshall et al., 2017), which requires that the fault goes through the brittle-ductile transition zone north of the range, because above that depth the fault is locked during the interseismic period and and no deformation is expected. The structural models that applied fold-fault related methods (Namson and Davis, 1988; Hubbard et al., 2014; Levy et al., 2019) all predicted shallower dip or/and a mid-crustal flat which pushed the fault’s brittle-ductile transition zone farther north.

In that predictions of interseismic motion can help distinguish between competing fault models (Marshall et al. 2017), we applied a similar approach to the Levy et al. (2019) structural model in order to better constrain the geometry of the deep thrust ramp. Our goal in the current work is to reduce the range of plausible dips for the lower ramp by comparing the regional vertical motions measured by GPS to a series of kinematic models with a range of locking depths and lower ramp dips.

Methods

The fault representation we test is the active thrust front configuration from Levy et al. (2019) (Figure 3). The fault surface was interpolated using a spline-based interpolation between cross section lines in the model, and was corrected for the position of the surface

trace. In order to test the entire range of plausible lower ramp dips, we ran a suite of kinematic dislocation models, each with different lower ramp dips of 16, 20, 25, 30, and 35˚. For each of these assigned lower ramp dips, we tested locking depths of 10, 15 and 20 km. The kinematic dislocation model simulates the interseismic deformation by applying slip on fault surface elements below the given locking depth.

Here, we use GPS data from 56 continuous stations in the Plate Boundary Observatory network provided by the MEaSUREs project (ftp://sopac-ftp.ucsd.edu/pub/timeseries/measures/ats/ WesternNorthAmerica/). The processing methodology is described in Marshall et al. (2017).

Results

Figure 4 presents an interpolated map of vertical velocities from the GPS stations. The GPS data in the western region of the Western Transverse Ranges is spatially sparse and exhibits spatially incoherent uplift patterns. Farther west, the spacing of the GPS stations is very large, and in fact, there is no station in the Santa Maria basin (Figure 2). Due to these issues, we focus our efforts on matching the deformation in the eastern sections of the system where observations are spatially denser.

Figure 5 shows a comparison of the 1D profiles through the GPS and the predicted vertical motion for different lower ramp dips along the three profile locations in figure 4. Our results suggest that the geodetic data in the eastern portion of the Ventura-Pitas Point fault is best fit by models with dips of 25-30˚, a locking depth of 10 to15 km, and a reverse slip rate of 5 mm/yr. While a 15 km locking depth is shallower than the ~18 km seismologic observations suggest (Nazareth and Hauksson, 2004), models using deeper locking depths produce uplift that is too far north compared to the GPS observations

(Appendix). The 5 mm/yr modeled slip rate is close to the lower end of slip rate estimates that are based on geology (Yeats, 1988; Hubbard et al., 2014; Levy et al., 2019).

Discussion

Until now, all of the preceding structural models for the Western Transverse Ranges, whether they focused on parts of the region (e.g.: Yeats, 1988; Hubbard et al., 2014) or the entire range (Davis and Namson, 1998a) did not include the full range of geological and geophysical data and observations. Specifically, existing studies did not include the long-term vertical geologic rates which place significant constraints on the viability of various model parameters such as fault dip or dip direction. The multidisciplinary approach used by Levy et al. (2019) in developing the structural model we test here makes for a more defendable model. While the Hubbard et al. (2014) model progressed the structural understanding of the region, the model focused on the Ventura River area and was not constrained by the vertical rates observed in geomorphological studies (Rockwell et al., 1984; 1988; Farris, 2017), nor did it use geodetic data. Hubbard et al. (2014) estimated a dip of 35-40˚ degrees for the lower ramp, and while a dip of 35˚ degrees will fit the GPS data reasonably well (Appendix), it is inconsistent with the location and magnitude of observed vertical rates north of the locus of active folding (Farris, 2017; Rockwell et al., 1984). Furthermore, it is clear that applying a structural method to resolve fault geometry by using only the observed surface fold geometry is not adequate in the case of a deep blind thrust that was not observed by seismological methods. In the Western Transverse Ranges, there have been no historical large magnitude, well-documented earthquakes, so seismological observations provide very limited insight on the deep geometry and architecture of the range. The geodetic data, in combination with the forward modeling approach applied in Levy et al. (2019), further

constrain the deep fault geometry, resulting in the reduction of the plausible range of dips from 16-30 ˚ to 25-30 ˚.

The available structural models in the Southern California Earthquake Center's Community Fault Model for the Western Transverse Ranges were tested mechanically by Marshall et al. (2017). The test favored a model with a ramp flat ramp fault geometry (Similar to our model) over a model with steeply dipping faults. The steeply dipping fault model clearly contradicts both geologic and geodetic data and observations of the location and magnitude of vertical motions (Marshall et al. 2017). Further, the flower structure model, which is based on the observation that there is up to 30% lateral slip in the WTR, requires more shortening at the surface than at depth as the lateral variation in the pre-middle Miocene strata is insufficient to account for the lack of apparent shortening (vertical separation) in the Paleogene section. For these reasons, the flower structure and other models that predict steep fault dips at depth are not viable.

The relatively shallow predicted locking depth of 15 km that arises from our results under-predicts the inferred depth of ~18 km from seismological observations (Nazareth and Hauksson, 2004). A comparison of estimated locking depths from geodesy and seismology along the San Andreas fault system (Smith-Konter et al., 2011) suggested that shallower geodetic locking depth estimate are the result of creep or temporal variations in strain release throughout the earthquake cycle. Earthquake swarms that were identified in the western Ventura basin (Hauksson et al., 2016; Shearer, 1998) might help explain the seismic verses geodetic depth disagreement, especially the 2015 Fillmore swarm at 11.8 to 13.8 km depth (Hauksson et al., 2016) which occurred on a low-angle thrust and included both seismic and aseismic slip. Recent studies show that the depth of seismicity increases abruptly with large earthquakes in southern California (Cheng and Ben-Zion,

2019 in press), implying that slip during such events extends as much as 5 km deeper into the top of the ductile zone because of a transient change from unstable to stable frictional response. Thus, during large Transverse Ranges earthquakes, seismic slip may well extend as deep as 18 km, consistent with estimates by Hauksson et al. (2016).

Conclusions

By comparing the predictions from forward kinematic dislocation models of the deep structure of the Western Transverse Ranges to GPS data, the range of plausible or most likely lower ramp dips was narrowed from 16-30˚ to 25-30˚. The Western part of the model is not well constrained because of the lack of good geodetic data, so additional GPS station placement and data collection in the western part of the Western Transverse Ranges may help to further improve the model.

This work demonstrates that by adding the constraints provided by GPS vertical motions to a wide range of geological and geophysical data and resultant models, we can better constrain fault geometry at depth, and produce an overall better constrained fault model.

Acknowledgments

Chapter 3, is currently being prepared for submission for publication of the material. Levy, Yuval; Scott Marshall; Rockwell, Thomas K. The dissertation/thesis author was the primary investigator and author of this material.

Figures

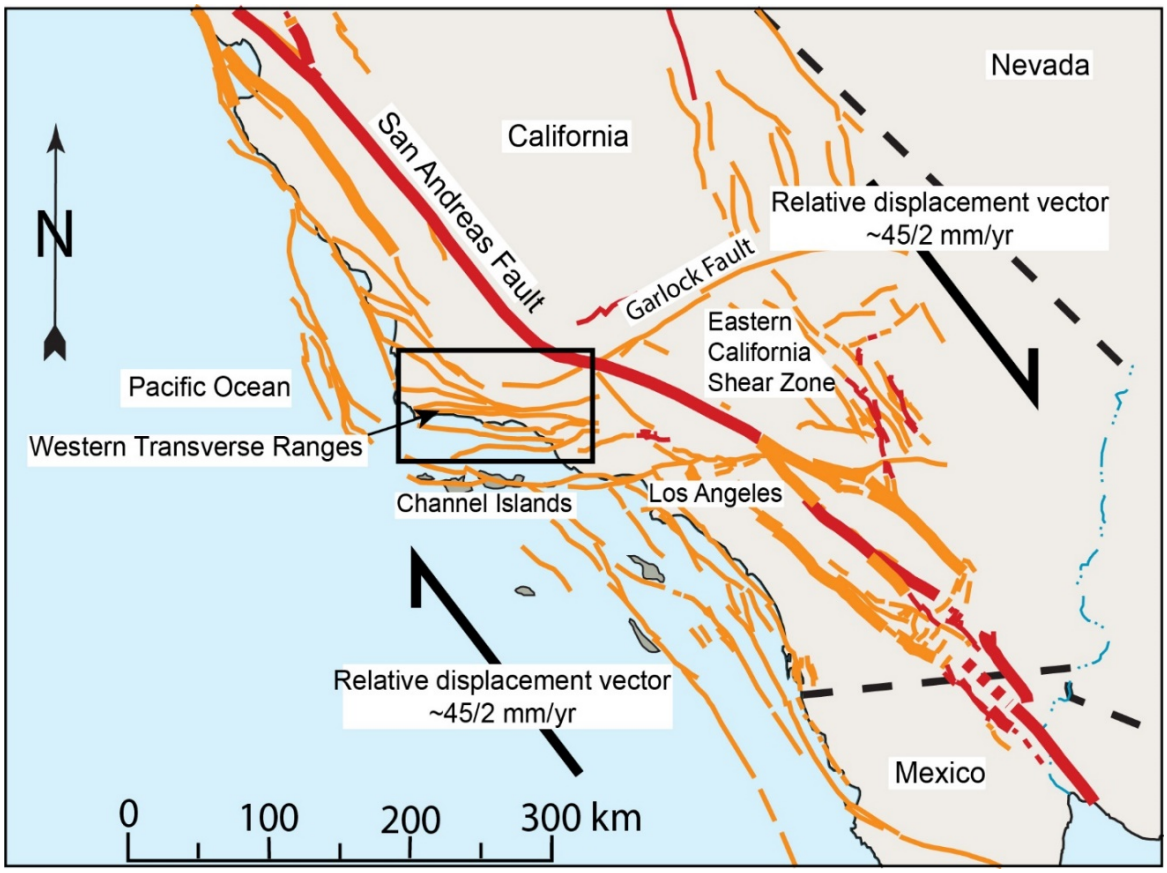

Figure 3.1. A regional fault map of California, USA. The relative motion of the Pacific and North American plates is right lateral and is 49.1-53.3 mm/yr (DeMets et al., 2010). The Western Transverse Ranges, located within the black box south of the big bend of the San Andreas Fault (SAF), accommodates the shortening resulting from the geometry of the big bend of the SAF, as well as translation from strike-slip faults west of the SAF.

Figure 3.2. Geological map of the Western Transverse Ranges compiled from Dibblee (2002) and presented in Levy et al. (2019). The Santa Ynez anticlinorium and general east-west trend of the structures are apparent. The stratigraphic column does not represent thickness; coloring of the geological units in the map is consistent with the column. Dip data is presented only as type and direction. Location of the different cross sections is marked with black lines. SCF: San Cayetano fault; BSCF: blind San Cayetano fault; SYF: Santa Ynez fault; SSMF: South Sulphur Mountain fault; VF: Ventura fault; PPF: Pitas Point fault; RMF: Red Mountain fault.

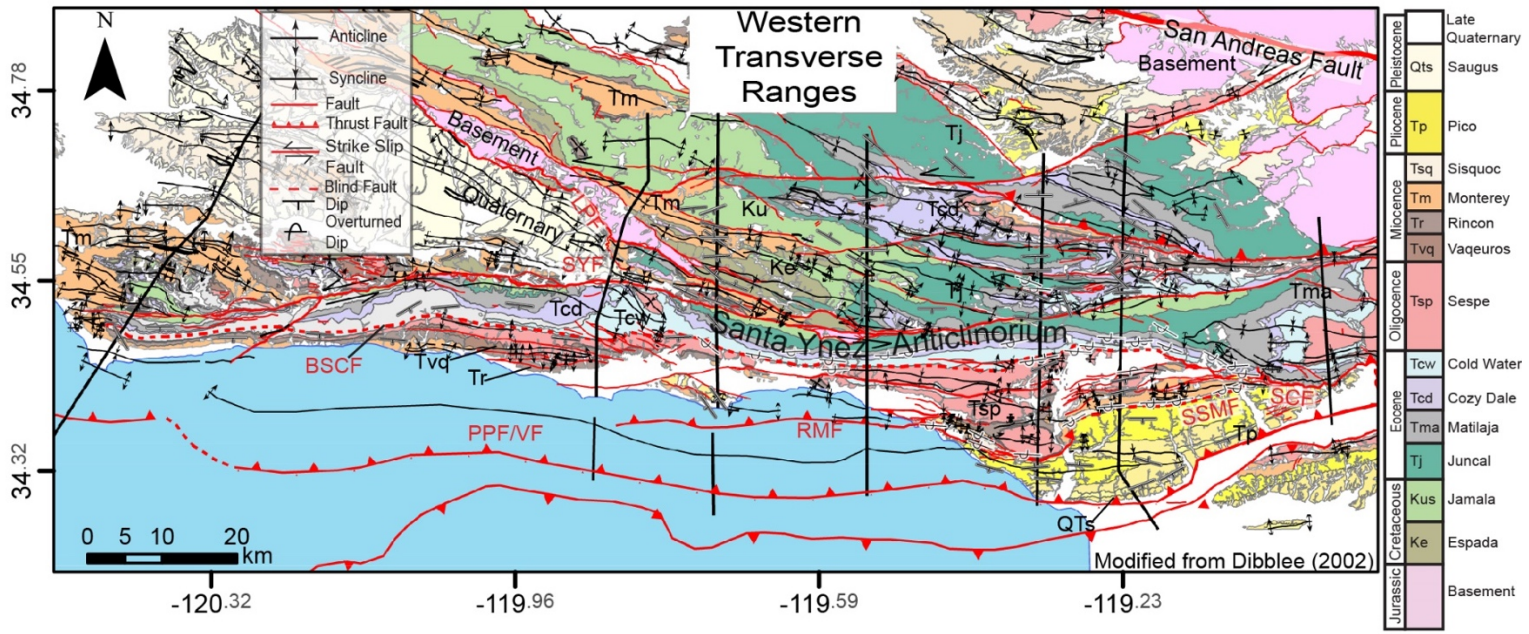
Western Transverse Ranges
N
Anticline
Syncline
Fault
Thrust Fault
Strike Slip Fault
Blind Fault
Dip
Overturned Dip
San Andreas Fault
Basement
Quaternary
Tm
Tj
Ku
Tcd
Ke
Tsp
Tma
Tcw
Tvq
Tr
Tp
QTs
SYF
BSCF
PPF/VF
RMF
SSMF
SCF
Santa Ynez Anticlinorium
0 5 10 20 km
Modified from Dibblee (2002)
34.78
34.55
34.32
-120.32
-119.96
-119.59
-119.23
Pleistocene
Pliocene
Miocene
Oligocene
Eocene
Cretaceous
Jurassic
Late Quaternary
Qts Saugus
Tp Pico
Tsq Sisquoc
Tm Monterey
Tr Rincon
Tvq Vaqueros
Tsp Sespe
Tcw Cold Water
Tcd Cozy Dale
Tma Matilaja
Tj Juncal
Kus Jamala
Ke Espada
Basement

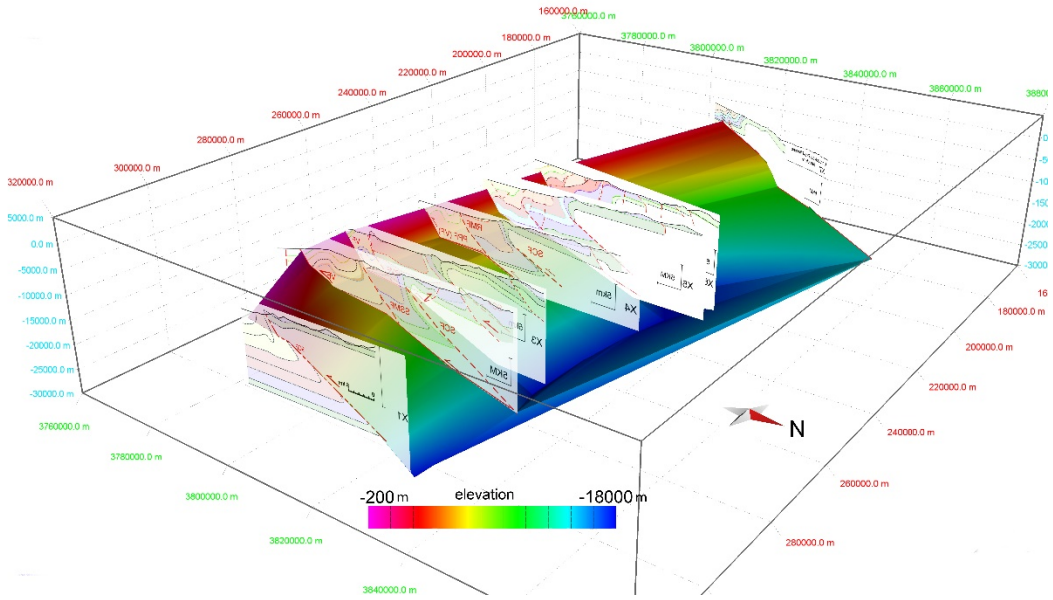

Figure 3.3. Interpolation of the predicted active fault surface from seven Trishear modeled cross sections that were compared to the observed geology. This figure presents the lower ramp dipping at 20˚ degrees, whereas Levy et al. (2019) predicted a plausible range of lower ramp dips of 16-30˚ degrees which is the tested range of dips in this paper. Locations of the cross sections are presented in figure 2.

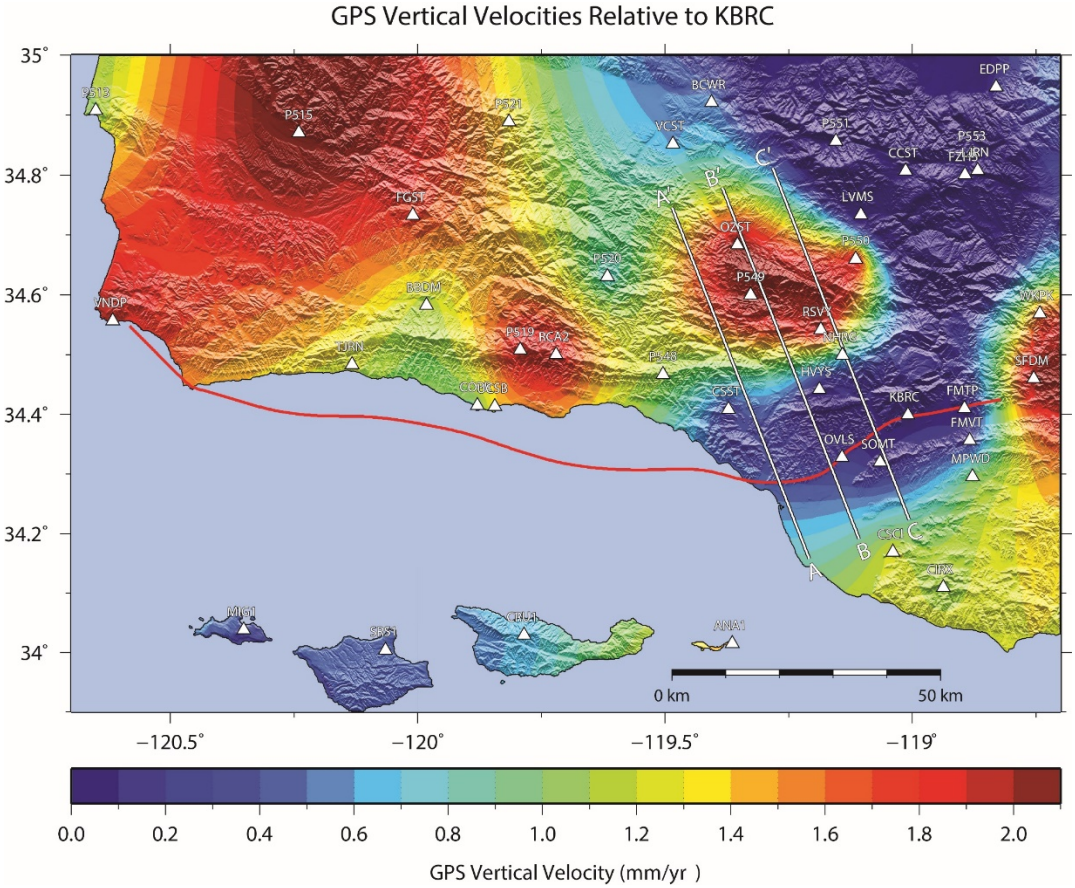

Figure 3.4. Interpolated vertical velocities (colors) from continuous GPS stations (triangles) in the western Transverse Ranges region relative to station KBRC. The red line represents the surface trace (or the upper tipline where blind) the PPF/VF thrust fault. White lines mark the locations of the cross sections presented in figure 5. Because the uplift signal is not coherent and thus unlikely to be due to faulting west of ~-119.5 longitude (Marshall et al., 2017), we therefore focus our efforts in matching the uplift signal near the cross section lines (white lines).

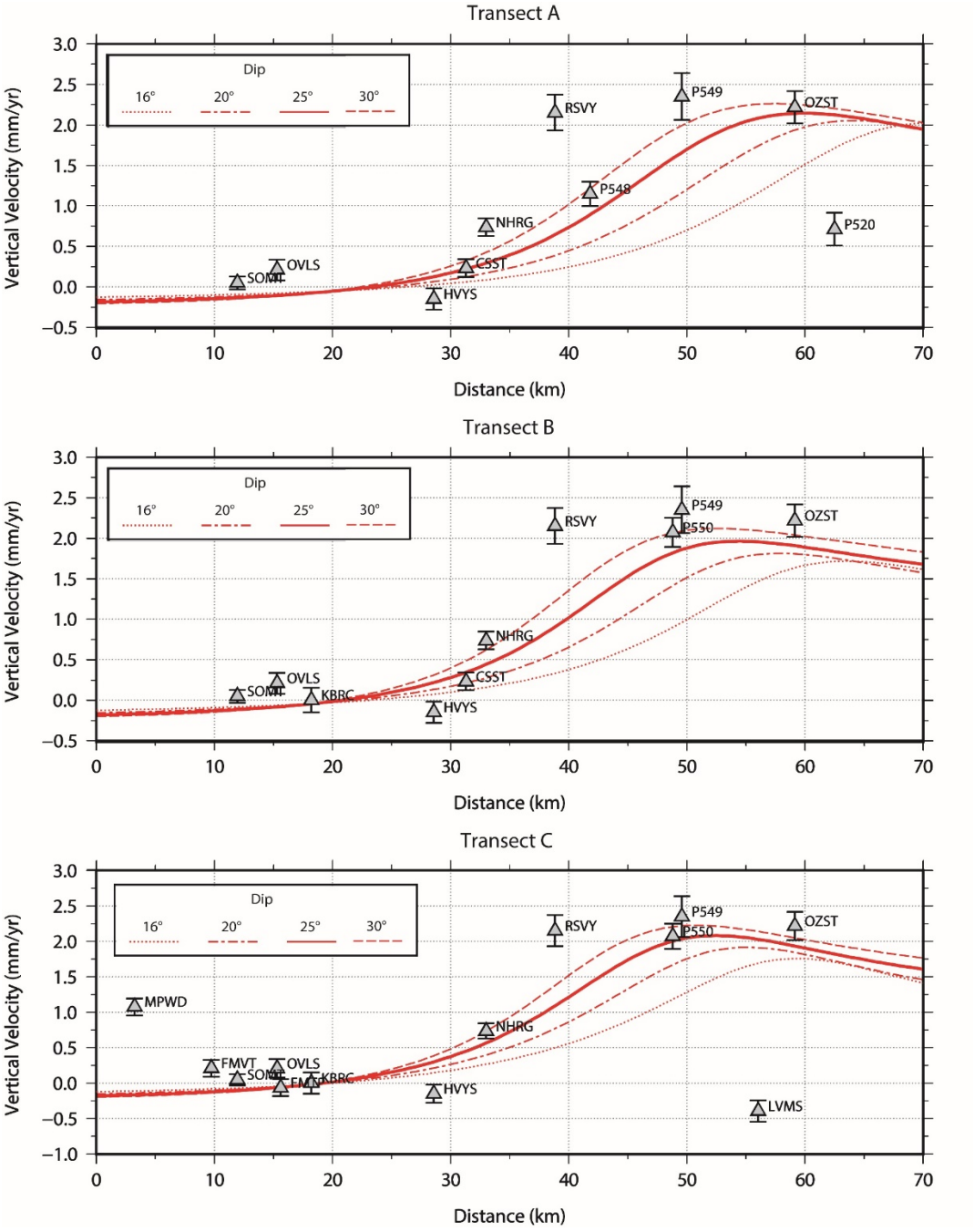

Figure 3.5. A cross section comparison between the GPS and model predictions with lower ramp dip of: 16, 20, 25 and 30 ˚ and locking depth of 15 kilometers. The locations of the cross sections are presented in Figure 4. For different locking depth we refer the reader to the Appendix.

Appendix

Results of the kinematic model with different deep ramp dip and locking depths for the three cross sections in Figure 4.4 in the text.

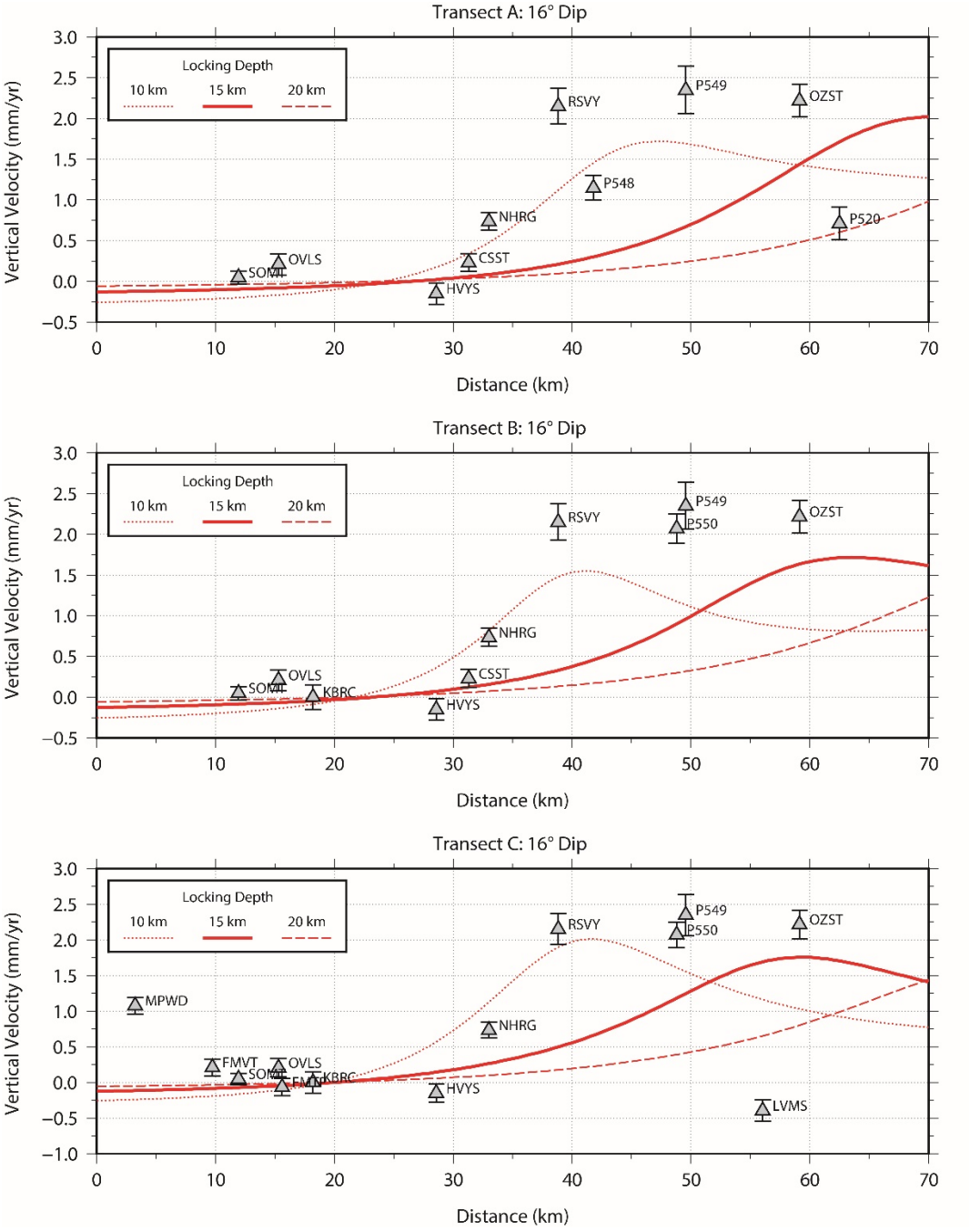

Figure 3.6. Results of model predictions using 16 degrees dip for the lower ramp and different locking depths (different lines) compared to GPS data (triangles) across the three transects in Figure 4.4.

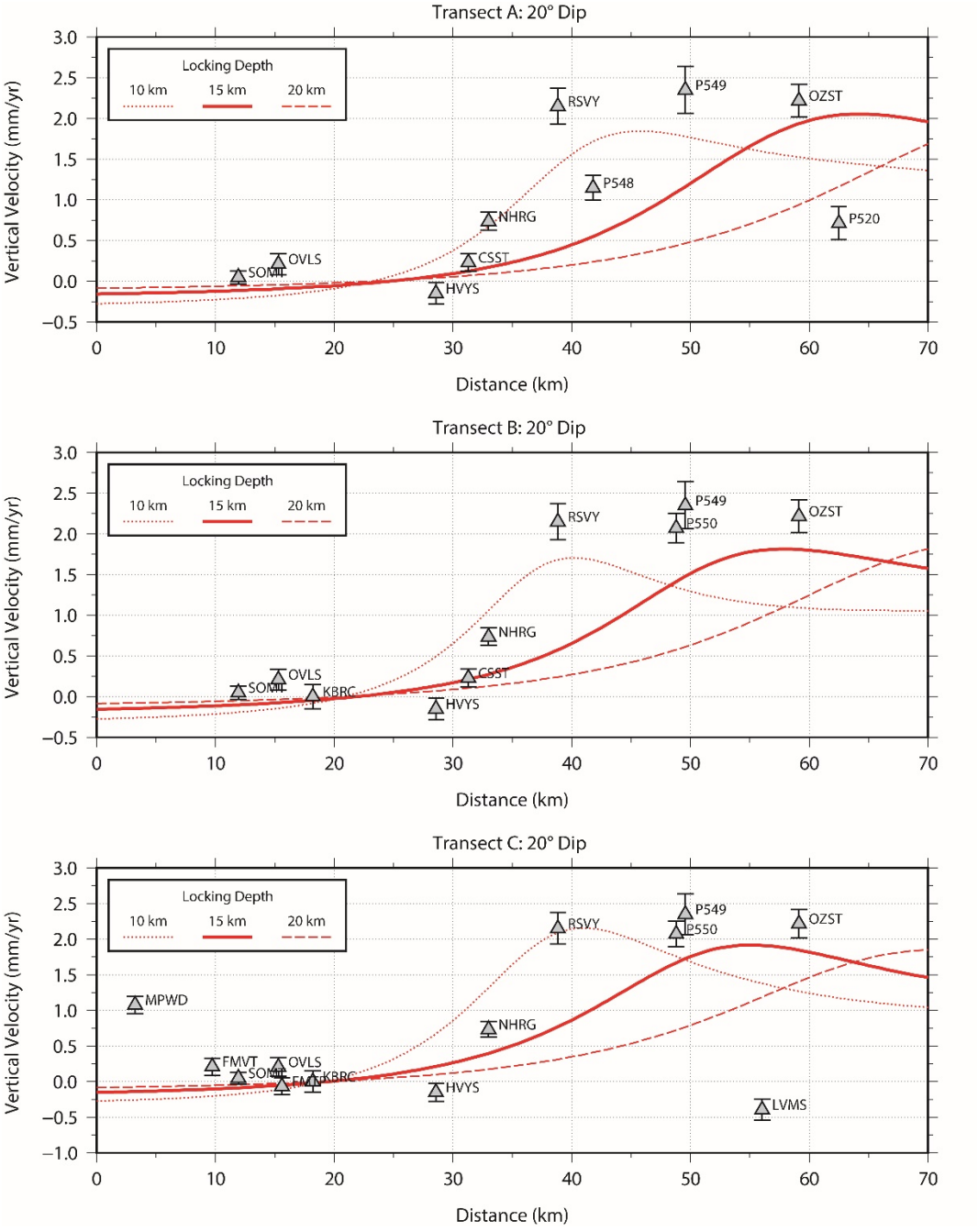

Figure 3.7. Results of model predictions using 20 degrees dip for the lower ramp and different locking depths (different lines) compared to GPS data (triangles) across the three transects in Figure 4.4.

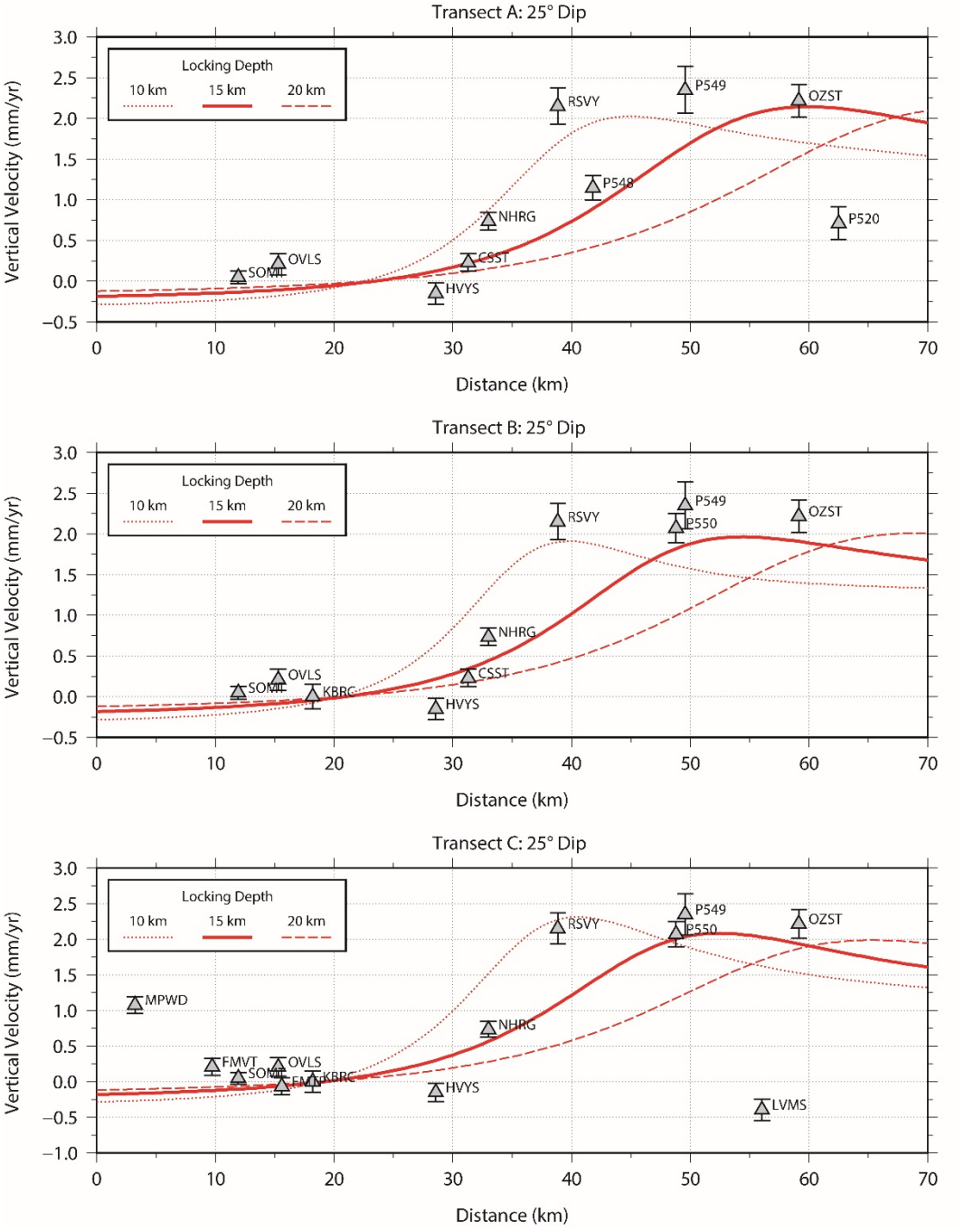

Figure 3.8. Results of model predictions using 25 degrees dip for the lower ramp and different locking depths (different lines) compared to GPS data (triangles) across the three transects in Figure 4.4.

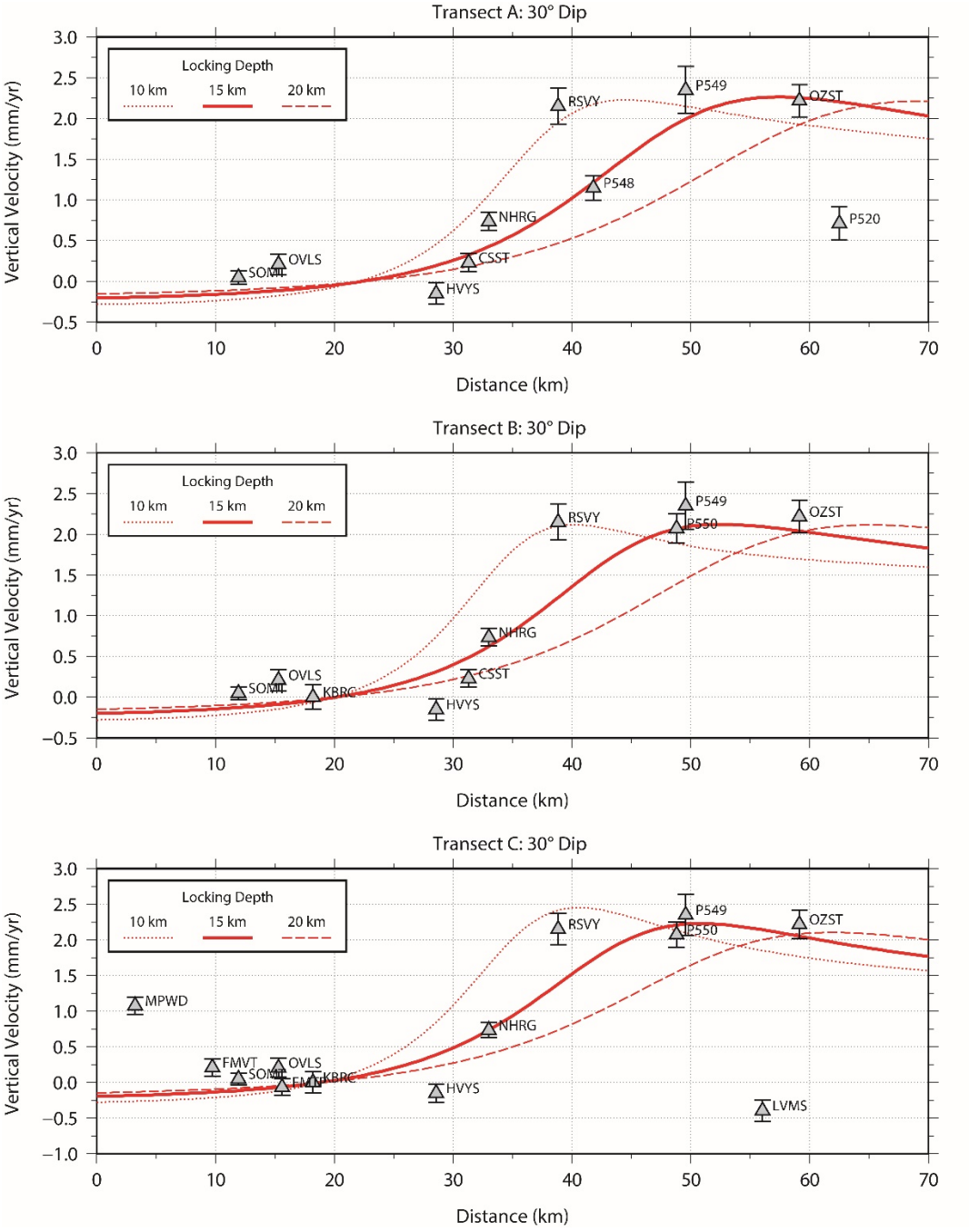

Figure 3.9. Results of model predictions using 30 degrees dip for the lower ramp and different locking depths (different lines) compared to GPS data (triangles) across the three transects in Figure 4.4.

References

Cheng, Y. and Y. Ben-Zion, 2019. Transient brittle-ductile transition depth induced by moderate-large earthquakes in southern and Baja California, *Geophys.*, *Res.*, *Lett.*, doi: 10.1029/2019GL084315.

Atwater, T.M., 1998. Plate tectonic history of southern California with emphasis on the western Transverse Ranges and northern Channel Islands. Contrib. to Geol. North. Channel islands, South. Calif. Am. Assoc. Pet. Geol. Pacific Sect. 1–8. https://doi.org/10.1130/DNAG-GNA-N.21

Baldwin, J.N., Kelson, K.I., Randolph, C.E., 2000. Late Quaternary fold deformation along the Northridge Hills fault, Northridge, California: Deformation coincident with past Northridge Blind-Thrust Earthquakes and other nearby structures? Bull. Seismol. Soc. Am. 90, 629–642. https://doi.org/10.1785/0119990056

Boellstroff, J.D., Steineck, P.L., 1975. Stratigraphic significance of fission-track ages on volcanic ashes in the marine late Cenozoic of Southern California. Earth Planet. Sci. Lett. 27(2), 143–154.

Burgette, R.J., Hanson, A.M., Scharer, K.M., Rittenour, T.M., Mcphillips, D., 2019. Late Quaternary slip rate of the Central Sierra Madre fault , southern California : Implications for slip partitioning and earthquake hazard. Earth Planet. Sci. Lett. 1, 1–12.

Campbell, R.H., Wills, C.J., Irvine, P.J., Swanson, B.J., 2014. Preliminary geologic map of the Los Angeles 30'x 60'quadrangle. Calif. Version 2.

Crowell, J.C., 1979. The San Andreas fault system through time. J. Geol. Soc. London. 136, 293–302.

Davis, T.L., Namson, J.S., 1998a. USGS Cross Sections 3-8 [WWW Document]. URL http://davisnamson.com/index.htm (accessed 1.12.18).

Davis, T.L., Namson, J.S., 1998b. USGS Cross Section 10 [WWW Document]. URL http://www.davisnamson.com/downloads/USGS Cross Section 10.pdf

DeMets, C., Gordon, R.G., Argus, D.F., 2010. Geologically current plate motions. Geophys. J. Int. 181, 1–80. https://doi.org/10.1111/j.1365-246X.2009.04491.x

Dibblee, T.W., 2002. Dibblee Geological Foundation: Geological Map Catalog (1-21, 24, 26, 27, 40-46, 53-55, 60, 186-189, 199-201, 254-259) [WWW Document]. URL https://www.sbnature.org/dibblee/ (accessed 7.20.15).

Dibblee, T.W., 1982a. Regional Geology of the Transverse Ranges Province of southern California, in: Fife, D.L., Minch, J.A. (Eds.), Geology and Mineral Wealth of the California Transverse Ranges. South Coast Geologcal Society, Inc., Santa Ana, pp. 7–26.

Dibblee, T.W., 1982b. Geology of the Santa Ynez-Topatopa Mountains, Southern California, in: Fife, D.L., Minch, J.H. (Eds.), Geology and Mineral Wealth of the California Transverse Ranges. South Coast Geologcal Society, Inc., Santa Ana, pp. 41–56.

Dibblee, T.W.J., 1991. Geologic map of the San Fernando and Van Nuys (north half quadrangles, Los Angeles County, California). Dibblee Geol. Found. Map DF-33, Scale 1:24,000.

Erslev, E.A., 1991. Trishear fault-propagation folding. Geology 19, 617–620.

Farris, A.C., 2017. Quantifying Late Quaternary Deformation in the Santa Ynez Valley, Santa Barbara County, California [Master thesis]. California State University, Long Beach.

Field, E.H., Arrowsmith, R.J., Biasi, G.P., Bird, P., Dawson, T.E., Felzer, K.R., Jackson, D.D., Johnson, K.M., Jordan, T.H., Madden, C., 2014. Uniform California earthquake rupture forecast, version 3 (UCERF3)—The time-independent model. Bull. Seismol. Soc. Am. 104, 1122–1180.

Fuis, G.S., Clayton, R.W., Davis, P.M., Ryberg, T., Lutter, W.J., Okaya, D.A., Hauksson, E., Prodehl, C., Murphy, J.M., Benthien, M.L., Baher, S.A., Kohler, M.D., Thygesen, K., Simila, G., Keller, G.R., 2003. Fault systems of the 1971 San Fernando and 1994 Northridge earthquakes, southern California: Relocated aftershocks and seismic images from LARSE II. Geology 31, 171–174. https://doi.org/10.1130/0091-7613(2003)031<0171:FSOTSF>2.0.CO;2

Furlong, K.P., Schwartz, S.Y., 2004. Influence of the Mendocino Triple Junction on the Tectonics of Coastal California. Annu. Rev. Earth Planet. Sci. 32, 403–433. https://doi.org/10.1146/annurev.earth.32.101802.120252

Hammond, W.C., Burgette, R.J., Johnson, K.M., Blewitt, G., 2018. Uplift of the Western Transverse Ranges and Ventura Area of Southern California: A Four-Technique Geodetic Study Combining GPS, InSAR, Leveling, and Tide Gauges. J. Geophys. Res. Solid Earth 1–23. https://doi.org/10.1002/2017JB014499

Hauksson, E., Andrews, J., Plesch, A., Shaw, J.H., Shelly, D.R., 2016. The 2015 Fillmore Earthquake Swarm and Possible Crustal Deformation Mechanisms near the Bottom of the Eastern Ventura Basin , California. Seismol. Res. Lett. 87. https://doi.org/10.1785/0220160020

Hauksson, E., Jones, L.M., Hutton, K., 1995. The 1994 Northridge earthquake sequence in California: seimological and tectonic aspects. J. Geophys. Res. 100, 12,335-12,355. https://doi.org/10.1029/95jb00865

Hubbard, J., Shaw, J.H., Dolan, J.F., Pratt, T.L., McAuliffe, L.J., Rockwell, T.K., 2014. Structure and Seismic Hazard of the Ventura Avenue Anticline and Ventura Fault, California: Prospect for Large, Multisegment Ruptures in the Western Transverse Ranges. Bull. Seismol. Soc. Am. 104, 1070–1087. https://doi.org/10.1785/0120130125

Huftile, G.J., Yeats, R.S., 1996. Deformation rates across the Placerita (Northridge Mw = 6.7 Aftershock Zone) and Hopper Canyon segments of the western transverse ranges deformation belt. Bull. Seismol. Soc. Am. 86, s3–s18.

Huftile, G.J., Yeats, R.S., 1995. Convergence rates across a displacement transfer zone in the western Transverse Ranges, Ventura basin, California. J. Geophys. Res. 100, 2043–2067.

Hughes, A., 2019. Quaternary structural evolution and seismic hazards of the onshore Ventura basin, southern Calicornia, USA. Imperial College London.

Ingersoll, R. V, 2001a. Tectonostratigraphy of the Santa Monica Mountains, Southern California. AAPG Pacific Sect. Geology an, 63–70.

Ingersoll, R. V, 2001b. Tectonostratigraphy of the Santa Monica Mountains, Southern California. AAPG Pacific Sect. Geology an, 63–70.

Jackson, P.A., 1981. Structural evolution of the Carpinteria Basin, Western Transverse Ranges, California. Oregon State University.

Langenheim, V.E., Wright, T.L., Okaya, D.A., Yeats, R.S., Fuis, G.S., Thygesen, K., Thybo, H., 2011. Structure of the San Fernando Valley region, California: Implications for seismic hazard and tectonic history. Geosphere 7, 528–572. https://doi.org/10.1130/GES00597.1

Leonard, M., 2010. Earthquake Fault Scaling: Self-Consistent Relating of Rupture Length, Width, Average Displacement, and Moment Release. Bull. Seismol. Soc. Am. 100, 1971–1988. https://doi.org/10.1785/0120090189

Levi, S., Yeats, R.S., 1993. Paleomagnetic Constraints on Santa Susana fault , Western Transverse Ranges , California. Tectonics 12, 688–702.

Levy, Y., Rockwell, T.K., Shaw, J.H., Plesch, A., Driscoll, N.W., Perea, H., 2019. Structural modeling of the Western Transverse Ranges: An imbricated thrust ramp architecture. Lithosphere 11, 868–883. https://doi.org/10.1130/L1124.1

Lindvall, S.C., Rubin, C.M., 2008. Slip Rate Studies along the Sierra Madre–Cucamonga Fault System Using Geomorphic and Cosmogenic Surface Exposure Age Constraints: Collaborative Research with Central Washington University and William Lettis & Associates, Inc.

Liu, L., Spasojević, S., Gurnis, M., 2008. Reconstructing Farallon plate subduction beneath North America back to the Late Cretaceous. Science (80-.). 322, 934–938.

LLC, N.S., 2019. Aliso Canyon Gas Storage Facility Geologic and Geomechanical Study.

Lung, R., Weick, R.J., 1987. Exploratory trenching of the Santa Susana fault in Los Angeles and Ventura counties: US Geol. Surv. Prof. Pap. 1339, 65–70.

Marshall, S.T., Funning, G.J., Krueger, H.E., Owen, S.E., Loveless, J.P., 2017. Mechanical models favor a ramp geometry for the Ventura-pitas point fault, California. Geophys. Res. Lett. 44. https://doi.org/10.1002/2016GL072289

Marshall, S.T., Funning, G.J., Owen, S.E., 2013. Fault slip rates and interseismic deformation in the western Transverse Ranges, California. J. Geophys. Res. Solid Earth 118, 4511–4534. https://doi.org/10.1002/jgrb.50312

McAuliffe, L.J., Dolan, J.F., Rhodes, E.J., Hubbard, J., Shaw, J.H., Pratt, T.L., 2015. Paleoseismologic evidence for large-magnitude (Mw 7.5-8.0) earthquakes on the Ventura blind thrust fault : Implications for multifault ruptures in the Transverse Ranges of southern California. Geosphere 11, 1–22. https://doi.org/10.1130/GES01123.1

Miller, K.G., Kominz, A., Browning, J. V, Wright, J.D., Mountain, G.S., 2005. The Phanerozoic record of sea level change. Science (80-.). 310, 1293–1298.

Namson, J.S., Davis, T., 1988. Structural transect of the western Transverse Ranges, California: Implications for lithospheric kinematics and seismic risk evaluation. Geology 16, 675–679. https://doi.org/10.1130/0091-7613(1988)016<0675:STOTWT>2.3.CO;2

Nazareth, J.J., Hauksson, E., 2004. The seismogenic thickness of the southern California crust. Bull. Seismol. Soc. Am. 94, 940–960. https://doi.org/10.1785/0120020129

Nicholson, C., Plesch, A., Shaw, J.H., 2017. Community Fault Model Version 5.2: Updating & expanding the CFM 3D fault set and its associated fault database., in: Poster Presentation at 2017 SCEC Annual Meeting. p. #234.

Nicholson, C., Sorlien, C.C., Tanya, A., C., C.J., Luyendyk, B.P., 1994. Microplate capture, rotation of the western Transverse Ranges, and initiation of the San Andreas transform as a low-angle fault system. Geology 22, 491–495.

Nilsen, T.H., 1984. Oligocene Tectonics and Sedimentation, California. Sediment. Geol. 38, 305–336.

Oakeshott, G.B. (Ed.), 1975. San Fernando, California, Earthquake of 9 February 1971. California Division of Mines and Geology.

Petersen, M.D., Wesnousky, S.G., 1994. Fault slip rates and earthquake histories for active faults in southern California. Bull. - Seismol. Soc. Am. 84, 1608–1649.

Petroleum Experts Ltd. (MVE Ltd.), 2018. MOVE https://www.mve.com/.

Plesch, A., Shaw, J.H., Benson, C., Bryant, W.A., Carena, S., Cooke, M., Dolan, J., Fuis, G., Gath, E., Grant, L., Hauksson, E., Jordan, T., Kamerling, M., Legg, M., Lindvall, S., Magistrale, H., Nicholson, C., Niemi, N., Oskin, M., Perry, S., Planansky, G., Rockwell, T.K., Shearer, P., Sorlien, C., Süss, M.P., Suppe, J., Treiman, J., Yeats, R.S., 2007. Community Fault Model (CFM) for southern California. Bull. Seismol. Soc. Am. 97, 1793–1802. https://doi.org/10.1785/0120050211

Rockwell, T.K., 1988. Neotectonics of the San Cayetano fault, Transverse Ranges, California. Geol. Soc. Am. Bull. 100, 500–513.

Rockwell, T.K., 1983. Soil Chronology, Geology, and Neotectonics of the North Central Ventura Basin, California [P.hD Thesis]. University of California, Santa Barbara.

Rockwell, T.K., Clark, K., Gamble, L., Oskin, M.E., Haaker, E.C., Kennedy, G.L., 2016. Large Transverse Range Earthquakes Cause Coastal Upheaval near Ventura, Southern California. Bull. Seismol. Soc. Am. 106, 2706–2720. https://doi.org/10.1785/0120150378

Rockwell, T.K., Keller, E.A., Clark M. N., Johnson Donald L., 1984. Chronology and rates of faulting of Ventura River terraces, California. Geol. Soc. Am. Bull. 95, 1466–1474.

Rodgers, D.A., 1975. Deformation, Stress Accumulation, and Secondary Faulting in the Vicinity of the Transverse Ranges of Southern California. Brown University.

Rumelhart, P.E., Ingersoll, R. V., 1997. Provenance of the upper Miocene Modelo Formation and subsidence analysis of the Los Angeles basin, southern California: Implications for paleotectonic and paleogeographic reconstructions. Bull. Geol. Soc. Am. 109, 885–899. https://doi.org/10.1130/0016-7606(1997)109<0885:POTUMM>2.3.CO;2

Sarna-wojcicki, A.M., Yerkes, R.F., 1982. Comment on article by R. S. Yeats on "low-shake Faults of the Ventura Basin, California," in: Neotectonic in Southern California, Guidebook. pp. 17–19.

Schlueter, J.C., 1976. Geology of the Upper Ojai - Timber Canyon area, Ventura County, California. Ohio University.

Schwartz, D., 2018. Large coherent block versus microplate rotaion of the Western Transverse Ranges: A fresh look at paleomagnetic constraints. University of California, San Diego.

Scott, B.K.M., Williams, R.P., 1978. Erosion and Sediment Yields in the Transverse Ranges, Southern California, Geological Survey Professional Paper.

Shaw, J.H., Suppe, J., 1994. Active faulting and growth folding in the eastern Santa Barbara Channel, California. Geol. Soc. Am. Bull. 106, 607–626. https://doi.org/10.1130/0016-7606(1994)106<0607:AFAGFI>2.3.CO;2

Shearer, P.M., 1998. Evidence from a cluster of small earthquakes for a fault at 18 km depth beneath Oak Ridge, Southern California. Bull. Seismol. Soc. Am. 88, 1327–1336.

Shields, K.E., 1977. Structure of the Northeastern Margin of the San Fernanado Valley, Los Angeles County, California. Ohio University.

Smith-Konter, B.R., Sandwell, D.T., Shearer, P., 2011. Locking depths estimated from geodesy and seismology along the San Andreas Fault System: Implications for seismic moment release. J. Geophys. Res. 116, 12. https://doi.org/10.1029/2010JB008117

Sorlien, C.C., Nicholson, C., 2015. Post-1 Ma Deformation History of the Pitas Point-North Channel-Red Mountain Fault System and Associated Folds in Santa Barbara Channel, California: U.S. Geological Survey National Earthquake Hazards Reduction Program final report, Award G14AP00012, 24 p.

Suppe, J., 1983. Geometry and Kinematics of Fault- bend Folding. Am. J. Sci. 283, 684–721. https://doi.org/10.5169/seals-166595

Tennyson, M.E., 1989. Pre-transform early Miocene extension in western California. Geology 17, 792–796. https://doi.org/10.1130/0091-7613(1989)017<0792:PTEMEI>2.3.CO;2

Tsutsumi, H., Yeats, R.S., 1999. Tectonic setting of the 1971 Sylmar and 1994 Northridge earthquakes in the San Fernando Valley, California. Bull. Seismol. Soc. Am. 89, 1232–1249.

Whitcomb, J.H., Allen, C.R., Garmany, J.D., Hileman, J.A., 1973. San Fernando Earthquake series, 1971: Focal mechanisms and tectonics. Rev. Geophys. 11, 693–730. https://doi.org/10.1029/RG011i003p00693

Woods, M.C., Seiple, W.R., 1995. The Northridge, California, Earthquake of 17 January 1994. California Department of Conservation, Division of Mines and Geology.

Wright, T.L., 1991. Structural geology and tectonic evolution of the Los Angeles Basin, California, in: Biddle, K.T. (Ed.), M 52: Active Margin Basins. AAPG Special Volumes, pp. 35–134.

Yeats, R.S., 1987. Late Cenozoic structure of the Santa Susana fault zone. US Geol. Surv. Profess. Pap 1339, 137–160.

Yeats, R.S., 1983. Large-scale Quaternary detachments in Ventura Basin, southern California. J. Geophys. Res. 88, 569. https://doi.org/10.1029/JB088iB01p00569

Yeats, R.S., Huftile, G.J., Grigsby, F.B., 1988. Oak Ridge fault, Ventura fold belt, and the Sisar decollement, Ventura basin, California. Geology 16, 1112–1116. https://doi.org/10.1130/0091-7613(1988)016<1112:ORFVFB>2.3.CO;2

Yerkes, R.F., Lee, W.H.K., 1987. Late Quaternary deformation in the western Transverse Ranges, in: Recent Reverse Faulting in the Transverse Ranges, California. USGS Professional Paper 1339. pp. 71–82.

Chapter 4 Geological structure of the Sylmar basin: Implications for slip distribution along the Santa Susana fault system in the San Fernando Valley, California, U.S.A.

Levy, Y.[1, 2] and T.K. Rockwell[1]

[1]Department of Geological Sciences, San Diego State University, 5500 Campanile Dr. San Diego, CA 92182, USA

[2]Scripps Institution of Oceanography, University of California, San Diego, 9500 Gilman Drive, La Jolla, CA 92037 USA

Abstract

We developed a forward model using the Trishear module in MOVE to better understand the structure of the northwestern San Fernando Valley and the relationship between the Santa Susana, Mission Hills and Northridge Hills faults. This study was motivated by previous work that inferred a high slip rate on the Santa Susana fault, which is in apparent contrast to the lack of significant geomorphic expression of the fault in the Sylmar Basin region. Our work presents a structural analysis that demonstrates how the Santa Susana fault system evolved in time, with the frontal thrust progressively migrating southward to the Mission Hills fault, and now to the Northridge Hills blind thrust. We trenched the Mission Hills anticline from the crest to the base of slope and demonstrate that the Mission Hills anticline is an actively growing fault propagation fold. The associated thrust tip is either deeper than 15 m or sufficiently far to the south that the fault was not encountered in large diameter borings, but the minimum structural relief across the

Mission Hills fault since the late Pleistocene is on the order of 37 m, suggesting a minimum uplift rate of 0.5 mm/yr.

Introduction

Two of the most devastating earthquakes in southern California occurred in the San Fernando Valley: the 1971 Mw 6.7 San Fernando and 1994 Mw 6.7 Northridge earthquakes. Each of these events resulted in many millions of dollars in damaged infrastructure along with 60 causalities and thousands more wounded. Both earthquakes exhibited an oblique thrust focal mechanism, but indicated slip on fault planes with opposing dip (Whitcomb et al., 1973; Oakeshott, 1975; Hauksson et al., 1995). The 1971 San Fernando earthquake ruptured the ground surface around the Sylmar basin, which is located in the northern part of the San Fernando Valley (Figure 2) (Oakeshott, 1975). The Northridge earthquake originated on a 35-degrees south dipping thrust at a depth of 19 km on a fault which was unknown prior to the earthquake (Hauksson et al., 1995). No surface rupture was produced as a result of the Northridge earthquake, and the little ground deformation that was reported was located on a secondary structure or due to shaking effects (Woods and Seiple, 1995).

The Santa Susana fault in the northern San Fernando Valley has one of the highest reported average slip rates, although with very large uncertainties as currently used in earthquake risk assessments (Field et al., 2014). The estimated rate for the Santa Susana fault system is 0.5-10 mm/yr and it is based on structural analysis (Huftile and Yeats, 1996; Field et al., 2014). The calculation of the slip rate used magnetic stratigraphy of the fine-grained Saugus and Pacoima strata, with ages of 2.3 and 0.5 Ma for the base of the Saugus Formation and top of the Pacoima Formation, respectively (Levi and Yeats, 1993). Petersen and Wesnousky (1994) included the slip rate of the Santa Susana fault

(2-8 mm/yr) in their review of active faults in Southern California, and indicate the lack of reported Holocene movement on the fault. An exploratory trench study (Lung and Weick, 1987) speculated that no slip has occurred during the last 10,000 years, however Yeats (1987) reported movement on a small segment of the fault during the 1971 earthquake. These slip rates are much higher than the maximum measured erosion rates in the Transverse ranges of 0.002 mm/yr along the southern face of the San Gabriel Mountains (Scott and Williams, 1978).

Landscapes experiencing active base level fall, as occurs in virtually all onshore normal and thrust fault terrains, display a common set of landforms that relate to their type of faulting and level of activity (Bull and McFadden, 1978; Keller and Rockwell, 1984; Rockwell et al., 1985). Vertical displacements on reverse and thrust faults result in relative base level fall that invokes incision in the uplifted regions and deposition along the mountain front. Typical landforms along rapidly uplifting mountain fronts are alluvial fans with fan-head deposition, presence of fault scarps along the front, low range-front sinuosity, low valley and height/valley width (Vf) ratios because most of the stream power is devoted to incision (class I front) (Bull and McFadden, 1983). The fault generally produces alluvium from erosion of the hanging wall, and overrides the alluvium in the footwall. For mountain fronts with low uplift rates, stream power and critical power (Bull, 1979) is matched for significant periods of time such that a substantial amount of stream power is used for incision into the downthrown block, resulting in fan-head incision, more sinuous mountain fronts due to lateral cutting, higher Vf ratios and in many cases, the lack of young fault scarps along the range front (class 2 front). Stable tectonic environments (no base level fall) are typified by landforms that represent very low-energy environments where erosion is balanced with the lack of relative uplift. Stream power and critical power

are balanced over long time periods to transport the meager amount of sediment supplied from the drainage basins, with the formation of broad pediments (class 3 front).

The mountain front class assignment is dependent on a number of factors in addition to uplift rate. These include the hardness or erodibility of the hanging wall rock, local and regional climate, vegetation type and density (a byproduct of climate) and related factors. Class 1 thrust fronts are documented worldwide and generally require uplift rates in excess of 1 mm/yr (Keller and Pinter, 1996).

The Santa Susana thrust fault displays characteristics of a class 2 front. Strands of the fault crop out along the hillslope with no apparent alluvium in the footwall below the fault, which implies that the rate of erosion exceeds the rate of slip. The alluvial fans along the range front are old and all are incised (fan-head incision) and the younger alluvium is deposited to the south (Figure 2 and 3), indicating that the uplift front has migrated southward. There is an obvious lack of young scarps associated with the surface traces of the fault, leading previous workers to suggest a complete lack of Holocene activity. All of these characteristics indicate either a very low slip rate or that the fault has ceased activity altogether.

Southward propagation of the locus of deformation was observed in other parts of the Transverse Ranges: in the Western Transverse Ranges (Levy et al., 2019) west of the Santa Susana fault system, and the central Sierra Madre system to the east of it (Burgette et al., 2019). The Mission Hills and Northridge Hills faults, located south of the Santa Susana and Hospital faults (Figure 2), are estimated to be slipping at rates of 0.65-1 mm/yr and 0.35 mm/yr respectively (Tsutsumi and Yeats, 1999). The reverse slip on the Mission Hills and Northridge Hills faults post-dates the inception of reverse slip on the

Santa Susana fault (Tsutsumi and Yeats, 1999) and therefore could be the southern extension of the Santa Susana fault system (Fuis et al., 2003).

Our work presents new paleoseismic observations and a structural analysis that demonstrate how the structure of the Sylmar basin has evolved through time, and suggests an explanation for how the Santa Susana fault system propagated south and is producing uplift along the Mission Hills fault. Some slip has also propagated farther south, producing uplift associated with the Northridge Hills anticline, as discussed later in this paper.

Geological background

The San Fernando Valley is a Neogene basin in the Central Transverse Ranges of Southern California. The San Gabriel mountains that bound the basin in the north were formed by the compressional deformation regime attributed to the big bend of the San Andreas, located north of the San Gabriel Mountains and the San Gabriel fault zone (Dibblee, 1982b). A sedimentary and volcanic sequence of Cretaceous through Pleistocene rocks is present beneath extensive Quaternary alluvium in the San Fernando Valley (Shields, 1977). A stratigraphic column is presented in Figure 4. The Sylmar sub-basin is located at the northern end of the San Fernando Valley (Figure 2). It is bounded by the Mission Hills in the south and by the segments of the Santa Susana – Sierra Madre fault system in all other direction. In the north and east it is bounded by the Sierra Madre and Hospital faults, and in the west by the northeast step of the Santa Susana fault toward the Hospital fault. Gravity modeling suggests that the sediment thickness in the northern part of the basin is 5-8 km (Langenheim et al., 2011). In the next few paragraphs, we present a short summary based on previous studies (Shields, 1977; Tsutsumi and Yeats, 1999; Langenheim et al., 2011; Dibblee, 1991; Campbell et al., 2014) for the stratigraphy

of the San Fernando Valley. We follow the naming convention of Dibblee (1991) and specify additional names where the nomenclature in the literature can be confusing. We then present the relevant structures for our structural modeling and discuss the geological history.

Stratigraphy

The underlying basement of the San Fernando Valley is composed of Precambrian Gneiss, which is exposed in the mountains north of the basin. Late Cretaceous sedimentary rocks are exposed in the western boundary of the basin whose upper contact was encountered in a well (Figure 5) but the thickness of these units is unknown.

The Cretaceous rocks are predominantly marine sandstone with igneous and metamorphic cobbles (Langenheim et al., 2011; Shields, 1977). The Paleocene and Eocene marine clastic rocks overlay the Cretaceous units in angular unconformity.

The Paleocene and Eocene sequence is exposed or penetrated by wells only in the Simi Hills, Chatsworth Reservoir and Horse Meadows Reservoir, which is located west of our focus area (Langenheim et al., 2011; Shields, 1977). The Paleogene Simi Conglomerate of the Calabasas Formation is overlain by the Santa Susana Formation with an angular unconformity. The Santa Susana and Llajas Formations are both siltstone with layers of sandstone. The contact between the Santa Susana-Llajas sequence with the overlying Topanga Formation is an angular unconformity of less than 10° in the San Fernando Valley (Shields, 1977).

The Topanga Formation is of mid-Miocene age and consists of marine clasts and grades eastwards into non-marine beds at the base. The middle units include extrusive basalts and fragmental volcanic rocks interbedded with sandstone. The upper Topanga

Formation includes interbeds of marine sandstone and silt. The Topanga- Monterey contact in Aliso Canyon is conformable. The Monterey Formation (referred to as the Modelo in some studies) is exposed in Mission Hills (Figure 2) and was penetrated by wells in the subsurface throughout the region, with the exception of the northern part of the Sylmar basin. The Monterey Formation is thinly bedded diatomaceous marine shale with chert, siltstone, graded sandstone and laminated sandstone. Foraminifera indicate a middle- to late-Miocene age (Shields, 1977). Conformably overlying the Monterey Formation is the Towsley Formation which includes poorly sorted sandstones, interbedded with shales and siltstone. It is of late-Miocene to early-Pliocene age ranging from 6 to about 3 Ma, where the Miocene-Pliocene boundary is at about 5 Ma. (Boellstroff and Steineck, 1975). The contact with the overlying Pico Formation (referred to as Fernando in some studies) is generally conformable. The Towsley Formation is very thick along the Sylmar basin and it thins to the west and southwest. North of the Hospital fault, along its western portion, the early-Pliocene Towsley Formation unconformably overlies gneissic basal rocks.

The marine Pico Formation consists of sandstone and siltstone with layers of conglomerate. Wells in the Mission Hills area indicate two dominant facies within the Pico Formation: an upper coarse-grained facies and a lower silty facies that may represent a regressive sequence. The Saugus Formation is divided into a lower shallow-water Sunshine Ranch member and an upper non-marine member. The upper member is composed of a coarse-grained sandstone and conglomerate that contains cobbles derived from the San Gabriel Mountains. The upper 9-20 m of the Saugus Formation includes sandstone and shale cobbles derived from the Monterey and Towsley Formations. In the Sylmar Basin, a well penetrated over 3 kilometers of Saugus deposits. The Pacoima

Formation overlies the Saugus in several locations and consists of alluvial gravel and sand derived from adjacent mountains.

Figure 2 presents part of the map by Campbell et al. (2014). Quaternary alluvial fans are presented in stratigraphic order in this map, and show the deposition of young alluvial fans occurring south of the Mission Hills fault and that the Santa Susana fault is not producing young alluvium, as expected if the fault has mostly ceased motion and considering the estimated erosion rates of the region (Scott and Williams, 1978).

Structure

The structure of the subsurface in the San Fernando Valley has been studied extensively (e.g.: Shields, 1977; Davis and Namson, 1998; Tsutsumi and Yeats, 1999; Langenheim et al., 2011) but these structural models, with the exception of Davis and Namson (1998) do not present an actual fault model for the deeper underlying structure.

Tsutsumi and Yeats (1999) divided the late Cenozoic faults into three groups, inactive Miocene Normal faults, inactive reverse Pliocene faults (pre-Saugus) and Quaternary (post Saugus) active faults. We will focus our discussion to faults relevant to our study area.

The North Leadwell fault zone consists of a number of north dipping normal faults. Langenheim et al. (2011) interpreted a seismic reflection profile with well constraints that shows the Leadwell fault zone offsetting basement and the top of the Topanga Formation just south of the Northridge Hills anticline. They interpret the Miocene to Quaternary units to be offset in reverse sense under the Northridge Hills by the northern most fault in the system. The subsurface contacts north of the Mission Hills fault seem to be dipping and thickening north towards the fault (Langenheim et al., 2011). In their geological cross

section, Langenheim et al. (2011) did not include the reverse sense of slip for the north Leadwell fault zone.

The Hospital fault is located between the Sierra Madre fault system, and the northeastern step of the Santa Susana fault. The Hospital fault exhibits reverse sense of motion and places basement or Towsley and Pico Formations in the hanging wall over Quaternary sediments on the south, bounding the Sylmar basin on the North (Figure 2 and 5). The Hospital fault slipped a small amount (10-15 cm) during the 1971 earthquake, but this motion has been interpreted as the result of flexural slip as most of the surface deformation was located to the south (Lindvall and Rubin, 2008).

The Santa Susana fault is interpreted as an inverted normal fault (Huftile and Yeats, 1996) based on thickening of Towsley Formation towards the currently uplifted block and its absence from the other side, such a relation requires basin inversion. The Santa Susana fault is well up the hill side rather than at the topographic break, indicating deformation and uplift of the footwall block of a deeper fault (Huftile and Yeats, 1996). This is similar to the San Cayetano fault in the Fillmore basin of the Western Transverse Ranges, where a southward propagation of the thrust system has been interpreted (Levy et al., 2019).

The Mission Hills fault is a steep reverse fault penetrated by wells located at the edge of the Mission Hills and its associated narrow anticline (Figure 5). The Mission Hills fault continues west, where it parallels the Santa Susana fault for about 2.5 km to the south of it, along the foothills of the Santa Susana Mountain range. It offsets Miocene rocks in the hanging wall. An additional associated fault is the Mission Wells fault that ruptured to the surface during the 1971 earthquake (Dibblee, 1991; Oakeshott, 1975), and seems to be stepping north from the Mission Hills fault. There are additional smaller

backthrusts and splays associated with the Mission Hills fault. We expand more on the Mission Hills in the following section.

The Northridge Hills fault and its associated anticline are located south of the Mission Hills fault. Baldwin et al. (2000) observed folding of young surficial deposits across the Northridge Hills fault that was interpreted as an incremental fold growth caused by fault propagation. The surface expression is very minor, but the fault is observed in the subsurface (Langenheim et al., 2011; Shields, 1977; Baldwin et al., 2000). Shields (1977) and some of the later work (e.g.: Langenheim et al., 2011) interpret it as a high angle reverse fault in their text without assigning an actual dip to the fault. However, the cross sections presented in these papers (Shields, 1977; Tsutsumi and Yeats, 1999; Langenheim et al., 2011) show only the upper tip of the fault and it is dipping at about 30 degrees. In order for the Mission Hills fault to be structurally consistent with the observed fold geometry a flat is required to accommodate the shape of the anticline, therefore we incorporated a similar interpretation to the one made by Davis and Namson (1998). It has been suggested that the Northridge Hills fault and the Mission Hills fault merge at depth into a decollement (Tsutsumi and Yeats, 1999; Fuis et al., 2003), however this relationship has not been observed but nevertheless seems likely considering the dip of these faults.

A study (Fuis et al., 2003) that combined seismic imaging from the lower, middle and upper parts of the crust along with relocated aftershocks for the 1971 and 1994 earthquakes argues for a decollement dipping at ~25 degrees north from the Northridge Hills fault close to the surface to as far north as the San Andreas fault. This proposed decollement is a surface into which the north dipping faults such as the Santa Susana and Mission Hills fault may root.

Late Quaternary Activity of the Mission Hills Fault

In the introduction we explained why the Santa Susana fault does not seem to slip anywhere close to the average rate assigned to it in the literature (Huftile and Yeats, 1996; Field et al., 2014; Petersen and Wesnousky, 1994). To test the activity of the Mission Hills fault, which we interpret as one of the currently active surface traces of the Santa Susana fault system, we excavated a series of trenches from the crest of the fold to the base of the slope in the only undeveloped property in the area (Figure 2 – location of trench). The trenches, which are presented as a composite trench in Figure 6, exposed folded Miocene Monterey Formation shale near the fold crest, capped by fluvial terrace deposits that fold over the anticline to the base of slope. The fluvial deposits thicken at the base of slope, indicating alluvial fan deposition at the local range front. The trench was excavated close to the margin of the terrace, and in places cut the margin such that the terrace deposits were not continuously present on the western wall (Figure 6). Although not shown here, the terrace deposits were exposed continuously on the eastern wall of the trench as the alluvium thickens eastward into its paleo-channel. At the base of slope, the alluvium is buried by a progressively thickening wedge of colluvium to the southern end of the trench. The colluvium is interpreted to be entirely Holocene in age based on its dark color and high organic content, which will oxidize over time.

We bored two 60 cm-wide bucket auger holes at the southern boundary of the property to test the thickness of the colluvial deposits and to try and penetrate the Mission Hills fault. Instead, we encountered the fluvial alluvium beneath the colluvium, with the fluvial deposits cut across a strath surface on the folded Monterey Formation shale; this provides a marker from which to estimate the minimum structural relief since deposition of the alluvium, as discussed below.

Age of alluvial deposits – The alluvium exposed in the three trenches at the site fall into one of three broad categories: terrace deposits associated with the strath surface cut across the growing Mission Hills anticline; alluvial fill that thickens in the southern forelimb of the fold near the base of slope; and young colluvial deposits at the south side of the project site that represent recent colluvial deposition on the south limb of the fold. The soil description in Table 1 was described near the crest of the fold where deposits are thickest, and characterizes the minimum age of the terrace alluvium and the uppermost part of the thickened alluvial deposits on the forelimb, but not the young colluvial deposits at the south side of the project area, which are considered Holocene in age based on their lack of significant soil development, dark color and high organic content. The soil age estimate is considered a minimum because the trench was excavated near the top of slope but on a sloping surface, which implies some erosion from the site of the trench. Hence, the soil characteristics are considered minimum values in comparison to what they would have been on a completely stable surface. The deformed thickened alluvium in the forelimb is mapped as the Pacoima Formation, a Pleistocene alluvial deposit derived from Pacoima Wash that drains the San Gabriel Mountains.

Soil, in this context, is the weathering profile that develops at Earth's surface over time (Birkeland, 1984, Rockwell, 2000). The expression of a weathering profile is affected by many parameters, including the characteristics of the parent material, the climatic conditions that prevailed during the period of development along with the associated vegetation that was dominant, the amount of surface slope and aspect that may affect surface stability, and the length of time that a stable surface has been exposed to weathering (Rockwell, 2000).

In this study, the parent material for the terrace alluvium is mostly derived from the San Gabriel Mountains and likely began as a sandy gravel based on its clast-supported character; this is expected for a fluvial terrace environment. The thickened older alluvium on the forelimb contains clasts from the San Gabriel Mountains along with some clasts derived from the Monterey Formation and is likely derived principally from the Pacoima Wash drainage system as it is mapped as Pacoima Formation, although the Pacoima is a general term that includes all post-Saugus fluvial and alluvial fan deposits that are not associated with modern drainages. The young colluvium fronting the forelimb is a silty clay loam interpreted to have been derived from erosion off of the forelimb face.

Variations in the climate in the Mission Hills / Los Angeles basin region are well documented: climate was substantially cooler and wetter in the late Pleistocene than today, with conifer forests growing throughout the coastal and inland region until early Holocene time, whereas the climate during the last interglacial was warm and probably drier than today (Huesser, 1978; 2000; and many other studies by the same author). These changes in climate over time are important in understanding and correctly assessing the ages of the alluvial units exposed in the trenches.

Assessment of time is a critical component of this study: the strength of a soil profile increases with time such that the characteristics of a soil profile change in a predictable fashion over time, with strongly-developed soils requiring a longer period of formation than weakly-developed soils, assuming surface stability and little to no erosion. In the case of the terrace soil, based on the surface slope at the location of the trench, some erosion likely occurred so the soil age estimate is a minimum.

The soil profile described for this study is presented in Table 1. The trench excavated into the terrace deposits that cross the crest of the anticline varied in depth

from about 1.5 m to nearly 5 m, depending on the depth to Monterey Formation bedrock. The described pedon is in the deepest part of the trench near the anticlinal crest where the alluvium extended to the bottom of the trench; the alluvium was probably thicker to the east, which is now eroded out by the modern channel and adjoining hillslope, so the variations in alluvial thickness are interpreted to result primarily from distance to the paleo-channel wall. That said, we chose to describe the soil at the crest of the fold where erosion should be less than on the fold forelimb.

The terrace surface preserves a 30-40 cm-thick A horizon (37 cm at the description locale) overlying a 1.2-2 m thick, moderately well-developed argillic horizon exhibiting 7.5YR hues and a sandy clay loam texture. There is moderately well developed angular blocky structure, extremely hard dry consistence, and plastic and very sticky wet consistence. Clay film development is strongly expressed with continuous thick clay films on ped faces and in pores, and many moderately thick clay films bridging grains in the matrix. These are common characteristics of gravel-rich late Pleistocene soils in non-arid regions of southern California, as discuss further below.

The argillic horizon grades downward into a transitional horizon, the BC horizon, which grades downward into the Cox horizon below about 3 m depth. The BC horizon exhibits typical 10YR hues, which is likely the initial color of the parent material, and massive to weak subangular blocky structure. This is consistent with the loamy sand texture, soft dry consistence and weakly developed clay film frequency and thickness.

The Soil Development Index (SDI) (Harden, 1982) was applied to the soil description, and the SDI value was compared to dated gravelly, coarse-grained soils in southern California. The SDI compares the current characteristics of the soil to that of the parent material, which in this case is inferred to have been loose gravelly sand with an

initial color of 10YR x/2. The parent material for the A Horizon is assumed to be a loamy silt, as there appears to be a significant aeolian component to that horizon. Based on this, the SDI calculated for this profile is 123 at 380 cm depth, which is the depth used for comparison to the dated Ventura soil chronosequence because the SDI calculation is depth dependent. The Maximum Horizon Index (MHI) (Ponti, 1985; Rockwell, 2000) can also be used for comparison to dated soils, and for this profile, a maximum value of 0.76 was calculated.

The Mission Hills soil is most similar to the Q6 soils of Rockwell (1983), which suggests that the age falls in the 40,000 to 90,000 year range. Recalculated SDI values (Rockwell, 1983) for the Merced soil chronosequence of Harden (1982) suggest an older age that is comparable to the Riverbank series, which is correlated to the last interglacial period at about 120,000 years. For comparison, the oldest dated soil in the Cajon Pass chronosequence (McFadden and Weldon, 1985) yielded SDI values around 70-75 for the 55,000 year old terrace, supporting the older age range. However, in terms of parent material and proximity to the coast, the Ventura chronosequence is the closest match.

However, one factor that supports a late Pleistocene age of the terrace alluvium, rather than a last interglacial age, is the absence of a calcic horizon associated with the surface soil. Inland Los Angeles Basin region soils, and especially in the San Fernando Valley, experienced the extended dry period of the last interglacial period from about 130 to 115 ka, and perhaps as late as 80 ka, and typically exhibit a stage II to Stage II+ calcic horizon below the Bt and BC horizons. The absence of such a calcic horizon suggests that this soil is younger than 115-130 ka in age. It is possible that such a calcic horizon was leached out during the wetter late Pleistocene, but as a calcic horizon is preserved in last interglacial soils elsewhere in Los Angeles basin (Rockwell; unpublished catalogue of

dated soil profiles), this is not a satisfactory explanation. Consequently, we infer the likely age of the terrace deposits to be in the 60,000 to 80,000 year range, based on the soil profile characteristics. Considering that the upper part of the soil may be eroded or deflated, this soil age estimate should be considered a minimum, but again, there is no indication that the soil experienced the last interglacial dry period based on the lack of a calcic horizon, and the presence of a thick A horizon and a complete argillic horizon argue against a large amount of erosion.

Terrace deformation - The terrace is cut across Miocene Monterey Formation bedrock, which exhibits bedding dips up to ~65 degrees to the south. The maximum terrace gradient is about 15 degrees, based on trench observations, which implies that much of the folding occurred prior to formation of the strath terrace, and that there has been 12-14 degrees of additional tilting or folding in the past 60-80 thousand years. Continued late Quaternary folding of the terrace suggests that some slip on the Mission Hills fault is blind, although we cannot resolve whether the folding has continued into the Holocene.

As we intercepted the strath surface in the bucket auger holes at an elevation of about 300 m, and the terrace lies at about 337 m elevation over the fold crest, we estimate that there has been a minimum of 37 m of structural relief on the terrace deposit over the past 60-80 ka due to folding alone. This yields a long-term minimum uplift rate of about 0.5 mm/yr. However, as we did not encounter the fault in the auger borings, nor do we know how deep the late Quaternary alluvium is to the south of the frontal escarpment, this calculated rate is a gross minimum. Nevertheless, it demonstrates that at least some of the missing slip rate on the Santa Susana surface trace is accommodated by the Mission Hills fault. We point out that the range front along the Mission Hills is a class 1

front (Bull and McFadden, 1978; Keller and Rockwell, 1984) in that the modern drainages are incised only in the hanging wall, deposition is at the front, and topography to the north is rising. These characteristics are in marked contrast to that along the surface trace of the Santa Susana fault itself, which argues that the Mission Hills fault is considerably more active.

Geological History

Levy et al. (2019) demonstrated how a regional understanding of the evolution of geologic structure is important when constraining structural models. Therefore, a discussion of the geological history is warranted before presenting the forward structural model.

The Transverse Ranges accreted its basement rocks by subduction during the late-Jurassic and into the Cretaceous (Dibblee, 1982b). In the Mesozoic and early Cenozoic, the Transverse Ranges occupied the forearc region of a subduction zone collecting continental shelf sediments (Atwater, 1998). The Farallon plate was subducted under the North American plate since at least the Cretaceous and maybe earlier (Liu et al., 2008). The Cretaceous period in the San Fernando Valley appears to represent a period of northwestward flow of sediments from a granitic provenance (Shields, 1977). The Paleocene-Eocene aged units containing basal conglomerates overlies the Cretaceous with an angular unconformity, indicating a period of erosion close to the deposition of the Paleocene-Eocene formations (Shields, 1977). Deposition of the Paleocene-Eocene in the San Fernando Valley occurred in a shelf-environment with sediments flowing west (Shields, 1977).

During the Oligocene, the Pacific plate made contact with North America (Atwater, 1998), and the tectonic regime in the Western Transverse Ranges changed as the San Andreas transform plate boundary evolved over time (Crowell, 1979; Wright, 1991). Oligocene units, such as the exposed Sespe and Vaqueros Formations in the Western Transverse Ranges (Dibblee, 1982b, 1982a) are missing in the San Fernando Valley (Tsutsumi and Yeats, 1999). The Global lowering of the sea level (Miller et al., 2005) probably exposed the surface at the northern San Fernando Valley and unlike other nearby localities in Southern California, it did not accumulate sediments, or that these sediments have been removed (Nilsen, 1984).

Early in the Miocene, subsidence and extension with some form of rotation began along the Transverse Ranges (Nicholson et al., 1994; Schwartz, 2018). Either a spreading ridge associated with continued subduction (Tennyson, 1989) or the evolving transform plate boundary (Crowell, 1979) and the associated migration of the triple junction north (Furlong and Schwartz, 2004) caused this extensional tectonic regime. The presence of the volcanics in the early- to middle-Miocene Topanga Formation, the transition to deep marine sedimentation later in the Miocene, and normal faulting during that period support the model of a regional transtensional tectonic regime during the Miocene in the Transverse Ranges and other regions in Southern California (Atwater, 1998; Wright, 1991; Ingersoll, 2001a).

The angular unconformity between Eocene and Miocene rocks west of Mission Hills (Shields, 1977) might imply that tilting occurred during that time period. The observation of thickening of the Miocene formations northward suggests that the normal faulting continued during the deposition of these units. The Leadwell fault zone was active at least until the middle Monterey/Modelo and could have been reactivated as a reverse

fault during the late Pliocene (Langenheim et al., 2011). The Santa Susana fault was active as a normal fault during the Miocene and was reactivated a reverse fault in the Pliocene (Huftile and Yeats, 1995). Other normal faulting that extends north from the Leadwell system cannot be ruled out. Additionally, it is possible that either the Mission Hills fault or some other fault at depth was active during the Miocene and contributed to the formation of the Sylmar basin.

Analysis of the provenance of the Monterey/Modelo Formation and of the subsidence during the late Miocene suggests that the submarine fans depositing sediments during this period originated from the unroofing of the San Gabriel block. This implies that the San Gabriel Mountains were a topographic high during that time (Rumelhart and Ingersoll, 1997). This observation helps explain the unconformity between late-Miocene or early-Pliocene units and the basement that is located just north of the Hospital fault along its western portion (Figure 5).

During the Pliocene the tectonic regime changed to transpression as the big bend of the San Andreas plate boundary evolved (Crowell, 1979; Atwater, 1998; Ingersoll, 2001b; Wright, 1991). Reverse faulting initiated prior to the deposition of Saugus by a number of both south and north dipping faults, including the Santa Susana fault (Tsutsumi and Yeats, 1999). A new report on the seismic hazard in the Aliso Canyon gas storage facility (Numeric Solutions LLC, 2019) suggested that the slip on the Santa Susana fault might have started earlier than suggested by Tsutsumi and Yeats (1995). The initiation of the Mission Hills and Northridge faults was interpreted to be post-base of Saugus by Tsutsumi and Yeats (1999) based on the constant thickness of the Pico (Fernando) Formation on both sides of the fault. Well data indicates a relatively constant thickness of the Pico Formation across the Mission Hills fault (Langenheim et al., 2011). Tsutsumi and

Yeats (1999) estimated 1700-2300 meters of total slip on the Mission Hills fault based on dip separation of geological contacts.

South of Mission Hills, a number of low hills and folding of the subsurface mark the propagation anticline of the Northridge Hills fault (Shields, 1977; Tsutsumi and Yeats, 1999; Langenheim et al., 2011). The small size of the related folds and the small topographic expression suggest that the total amount of slip on this fault is not very large. The two faults are assumed to connect at depth (Tsutsumi and Yeats, 1999; Davis and Namson, 1998) despite the lack of direct observation (Langenheim et al., 2011).

The observations of thickening of Miocene strata southward and the observed offset through the Leadwell fault system suggest that the formation of the Sylmar basin initiated during the Miocene. In addition, it is likely the case that that the Mission Hills fault may represent an inverted normal fault as it bounds the Sylmar basin from the south with thickened Miocene in the hanging wall of the fault. Past interpretations explain the presence of the basin as a result of two thrusts on opposite sides, the north dipping Hospital fault from the north side and the south dipping Northridge fault at 12 km depth in the south of the basin. This interpretation will require the regional subsidence rate to be very high everywhere the San Fernando Valley with thrusts or reverse fault compensating for the vertical motion with the exception of Sylmar basin. However, the Sylmar basin itself is higher in topographic elevation than the San Fernando Valley south of Mission Hills, and streams incise the rising hanging wall block. These observations clearly indicate that the Sylmar basin is being uplifted at a faster rate than the San Fernando Valley, which contradicts the two opposing thrusts interpretation. In addition, these observations support the idea of connectivity of the north dipping faults at depth. The observed topographic relief in combination with the younger age of initiation for reverse slip on the Mission Hills

and Northridge faults support an interpretation of an evolving fault system that is propagating south.

Modeling Methods

In order to test our hypothesis of southward migration of the thrust front we used Trishear forward modeling (Erslev, 1991) in Move© (Petroleum Experts Ltd., 2018) and applied the same approach used by Levy et al. (2019) in the Western Transverse Ranges. The different stages of the model are presented in Figure 7.

A number of assumptions were made in order to simplify the initial conditions and justify kinematic elements of our model. First, we assume that the stratigraphy prior to the deposition of the Miocene was a layer cake stratigraphy. We know it was not entirely the case from the different unconformities described in the stratigraphy section. However, these units were deposited on a continental shelf so the assumption seems reasonable at first order. Further, the pre-Miocene sedimentary units in our cross section are mostly not directly observed as most wells do not penetrate deep enough. Therefore, trying to model the deformation of these units, or assess the exact stratigraphic model during the early Miocene would be pointless. Another assumption is that out of plane motion is negligible. There is a strike slip component, as was observed during the 1971 earthquakes (Whitcomb et al., 1973), but because the dominant sense of motion is dip slip and the stratigraphy doesn't dramatically vary laterally along the fault, our models will focus on the dip-slip deformation. An additional assumption is that we only model the main faults in the system, but it is important to remember that there may be additional faults, similar to the fault that moved in the Northridge earthquake (Hauksson et al., 1995).

We first tried to model a layer cake stratigraphy and south dipping stratigraphy for the sequence of reverse faults, however these attempts proved to be unsatisfactory. The depth of the sedimentary formations in the Sylmar basin is known to be deep both from wells and as implied by gravity and seismic data (Langenheim et al., 2011). South of Mission Hills, units dip to the south and thicken towards the Sylmar basin. Those observation and our lack of success with simpler models led us to add a period of normal faulting in our forward model. The first steps simulate the normal faulting that occurred during the Miocene. First, the faults are forced to slip from south to north for the normal faulting stage. The model does not allow separate faults to slip at the same time, and because the basin is south of the normal fault system, we chose this direction for the fault sequencing. After slipping the normal faults, we added another layer and repeated this step. This simulates the extension and normal faulting with continued deposition. This period of simulated extension is followed by compression represented by reverse sense of slip on some faults. For our case, we create a new fault that represents the Hospital fault. However, it is important to indicate that the Santa Susana fault west of the Hospital fault is interpreted as a reactivated normal fault (Huftile and Yeats, 1995). The next step in the model progression is to propagate slip to the Mission Hills fault, forming the anticline and topographic relief as observed in the southern boundary of Mission Hills. Finally, we slip the Northridge Hills fault which has a very small topographic expression that is related to folding observed in the subsurface, both the fold and the fault have been penetrated by wells.

Our model results appear to be structurally consistent to the first order with our interpreted cross section and other published cross sections. The depth of sedimentary units in the basin, folds and general relief are reproduced by the model. We do not try to

match exactly every observed dip, mainly due to the number of steps required for each simulation and the general lack of observations that will determine exact thickness of the formations in the subsurface of the Sylmar basin. The deep part of our cross section is based on our model results. Therefore the presented cross section includes both observations from the surface geology (Dibblee, 1991) a number of wells (appendix) and our interpretation of the deep structure as constrained by our model and geophysical data (Langenheim et al., 2011).

The model parameters we used are as follows. For each of the Leadwell normal faults we used 500 meters of Miocene dip slip, P/S ratio of 1, 1 Trishear zone, and no offset for the Trishear angle. We then offset the Mission Hills fault in a Normal sense by 1000 meters with a P/S ratio of 1, 1 Trishear zone, and no offset for the Trishear angle and sediment horizon after slipping this fault. We repeated this process 4 times. We then slip the reverse faults from north to south. The parameters we used for the different faults are: 7000 meters of slip for the Hospital fault, P/S ratio of 1, 1 Trishear zone, and no offset for the Trishear angle. We applied 3400 meters of slip on the Mission Hills fault, a P/S ratio of 1.2, 9 Trishear zones, and 0.6 offset on the Trishear angle. For the Northridge Hills fault, we applied 700 meters of slip, a P/S ratio of 1.2, 9 Trishear zones and 0.8 offset on the Trishear angle.

Discussion

Tsutsumi and Yeats (1999) suggested that the thick accumulation of Plio-Pleistocene sediments in the Sylmar basin is a result of a near-surface expression of the forelimb of the fault propagation fold related to the blind south dipping Northridge fault. Langenheim et al. (2011) proposed that the deeply buried Miocene Verdugo-Canyon fault played a role in the formation of the basin. Our model supports the hypothesis that the

Sylmar basin was formed during the Miocene due to normal faulting, and demonstrate how an inverted Mission Hills fault should also be considered as fault that was active in the Miocene.

The Monterey Formation was deposited north of the Santa Susana fault and west of the Sylmar basin, but the lithology north of the Hospital fault does not allow us to determine if the Hospital fault was active as a normal fault during the Miocene. Furthermore, the unconformity between the Towsley Formation and basement rocks makes it difficult to determine how much reverse slip the Hospital fault accommodated because this contact does not match the stratigraphy to the south. The depth of sediments in the Sylmar basin is between 5-8 km (Langenheim et al., 2011); such a thick sedimentary column requires either the Monterey Formation to be much thicker than it is south of Mission Hills or that there was preservation of old strata beneath the Miocene section. Therefore, our interpretation of normal faulting extending north of the Leadwell fault system at least to the edge of the basin or even into it seems very plausible. It is possible, as demonstrated by our model, that east of the northeastern step of the Santa Susana fault, that the Mission Hills fault was active as a normal fault during the Miocene.

The slip rate used for the Santa Susana fault system in earthquake modeling is based on calculation from structural cross sections and ages of the Saugus Formation (Field et al., 2014). Levi and Yeats (1993) dated the deposition of the Saugus Formation from about 2.3 to 0.5 Ma based on magnetic stratigraphy and an ash horizon. However, in the eastern Ventura basin, results of a study (Hughes, 2019) that applied cosmogonic dating methods seem to date the Saugus Formation at significantly older ages than Levi and Yeats's (1993) ages. Therefore, it is possible that the ages in the San Fernando Valley are older than previously estimated. This means that the long-term slip rate

estimates based on the structural cross sections for the Santa Susana fault will decrease. It is likely that the Santa Susana fault is no longer active, at least at a significant rate, considering the geomorphological observations we discussed above. In any case, if the fault is still active it clearly has a slip rate that is closer to the lower range of slip rates previously estimated for it (Huftile and Yeats, 1996; Field et al., 2014; Petersen and Wesnousky, 1994).

The total slip we applied to the Mission Hills fault in our model exceeds previous estimates (Tsutsumi and Yeats, 1999) and implies a higher rate on the fault. Using the same age of 2.3 Ma as Tsutsumi and Yeats, the minimum slip rate estimate will increase to 1.5 mm/yr. However, it is difficult to determine if our estimates in this model are close to the actual slip of this fault because we do not have a good marker horizon to make an accurate estimate of displacement. In addition, because of the lack of good age constraints for the Mission Hills fault, any structural estimate will be a minimum estimate because the displacement could have accrued in a much shorter time frame if the propagation of the fault occurred in the middle or late Quaternary. Our minimum estimate from the trench is 0.5 mm/yr, but this only accounts for folding and not surface slip, which is likely substantial.

Baldwin et al.'s (2000) observation of folding of young surficial deposits across the Northridge Hills fault led them to speculate that the fault undergoes a secondary deformation during a large magnitude earthquake. However, our structural analysis supports the idea that the north dipping faults are connected (Fuis et al., 2003; Langenheim et al., 2011) and that the shortening is distributing slip onto at least the two main faults, the Mission Hills and Northridge Hills faults, as was suggested for the Sierra

Madre fault farther east (Burgette et al., 2019). Therefore, both primary and secondary deformation should be considered for this fault system.

Summary

Our proposed model for the structural evolution of the Sylmar basin demonstrates the connectivity of the north dipping reverse and thrust faults in the subsurface, and helps explain how slip can be distributed along the Santa Susana fault system to the Mission Hills and Northridge Hills faults south of it. Additional investigation on the local age of the Saugus Formation may help constrain the wide range of estimated slip rates. However, the line of evidence we included in combination with our interpretation and forward model result supports the lower estimates (<< 1 mm/yr) for the Santa Susana fault system, particularly when considering the regional pattern of southward migration of the locus of deformation along the Western and Central Transverse Ranges.

Figures

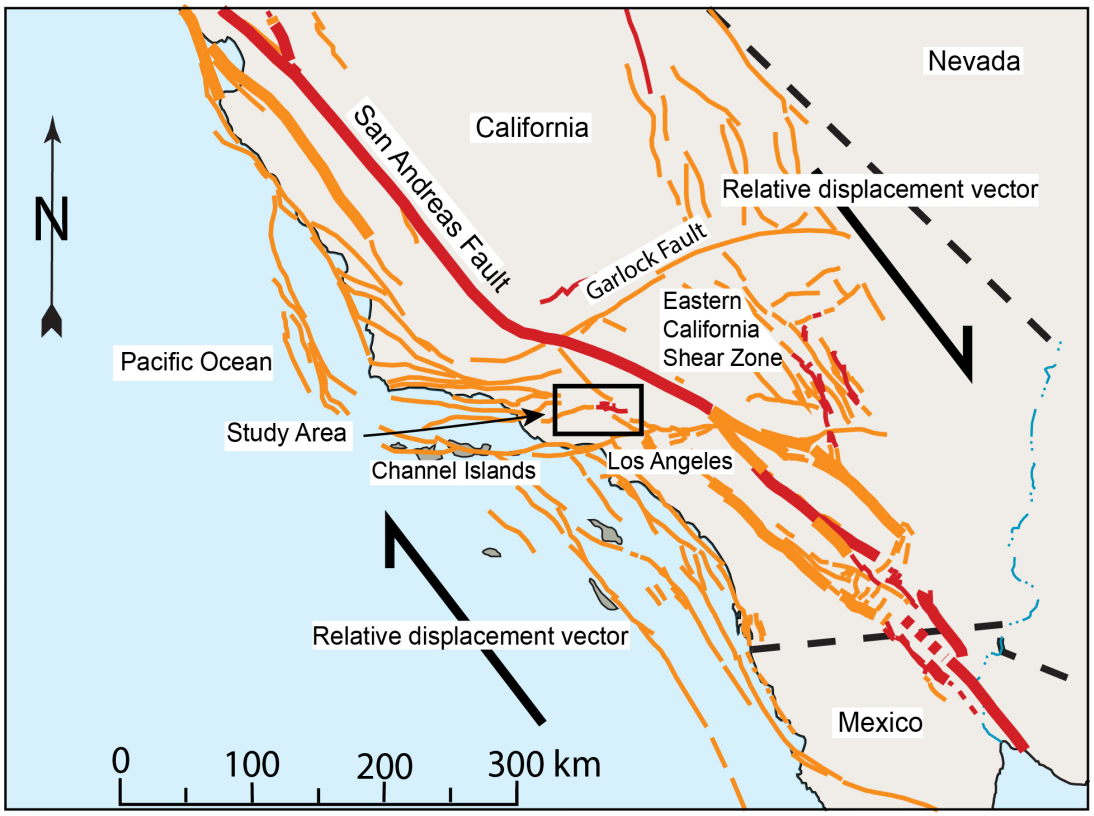

Figure 4.1. A regional fault map of California, USA. Location of our study area is marked by a black rectangle. The relative motion of the Pacific and North American plates is right lateral and is on the order of 45 mm/yr. The Transverse Ranges are located south of the big bend of the San Andreas Fault, accommodate the shortening resulting from the geometry of the big bend of the San Andreas.

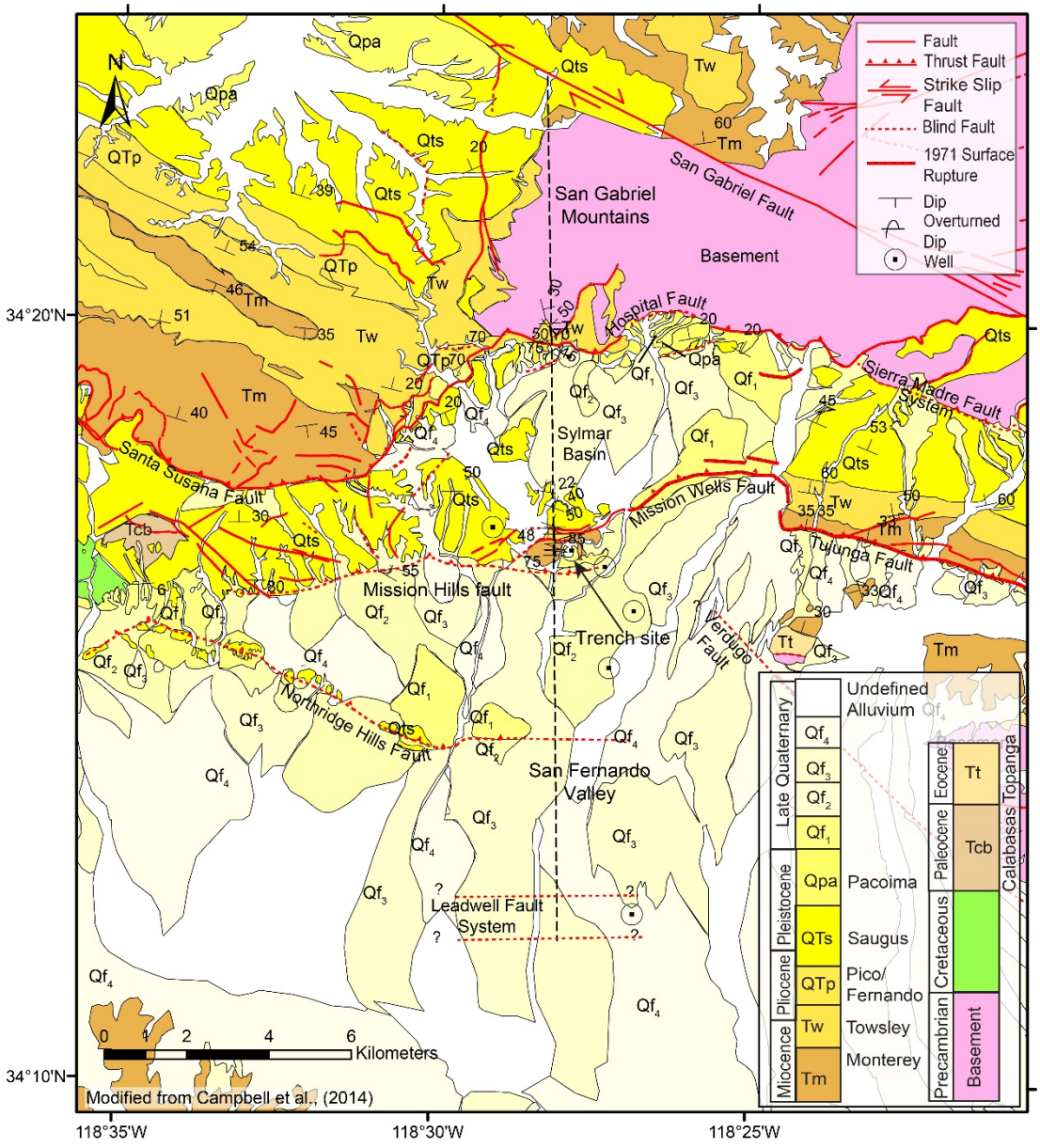

Figure 4.2. A geological map of the northern San Fernando Valley, modified from Campbell et al., (2014). The stratigraphic column is showing only the mapped units, for a descriptive stratigraphic column of the San Fernando Valley see Figure 4 The location of the cross section in Figure 5 is marked by the dashed black line. The location of the trench in Figure 6 is marked by a black arrow.

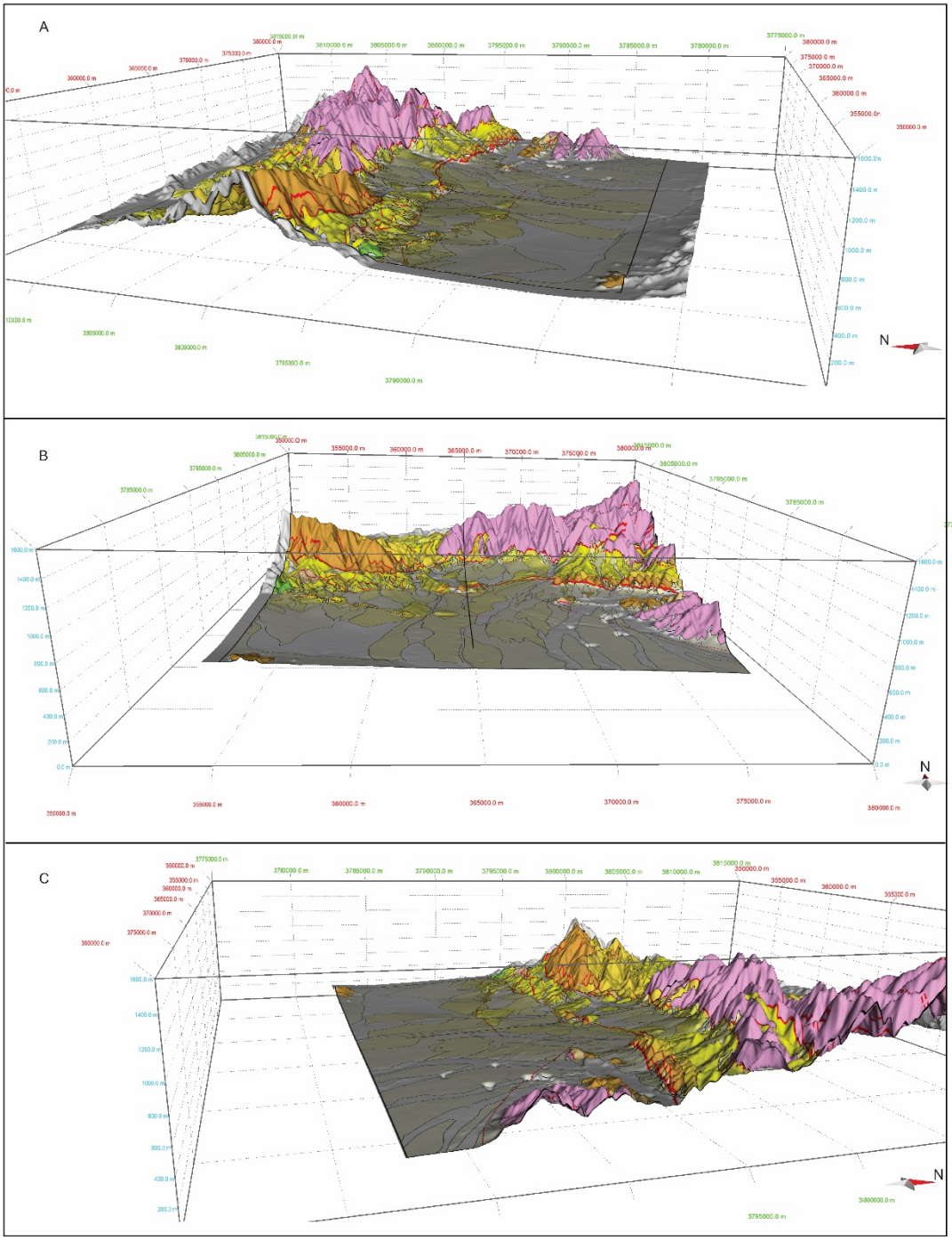

Figure 4.3. Oblique view from west south and east (A, B, C, respectably) of the geological map in figure 2 projected on a Digital Elevation Model (DEM) with a vertical exaggeration of 5. The young alluvium is almost entirely deposited south of the Mission Hills fault. The Sylmar Basin is higher in elevation than the San Fernando Valley, which suggests it is being uplifted by an underlying thrust.

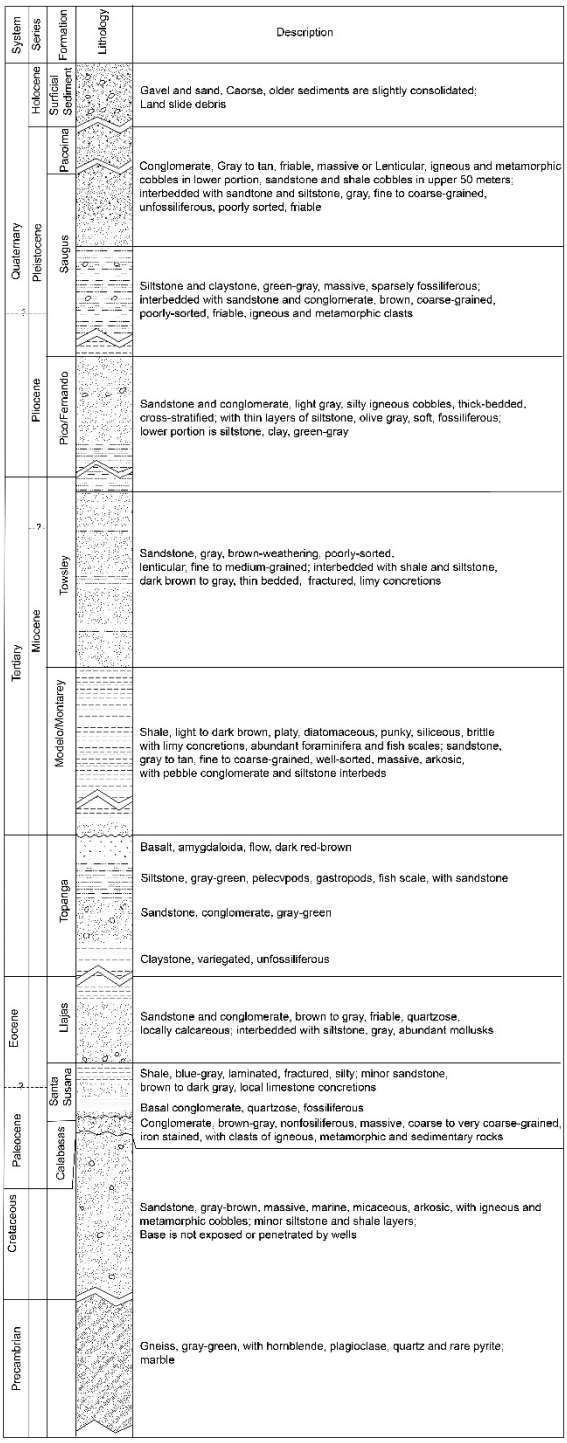

Figure 4.4. Stratigraphic column (Modified from Shields, 1977) of the geological formations in the northern San Fernando Valley.

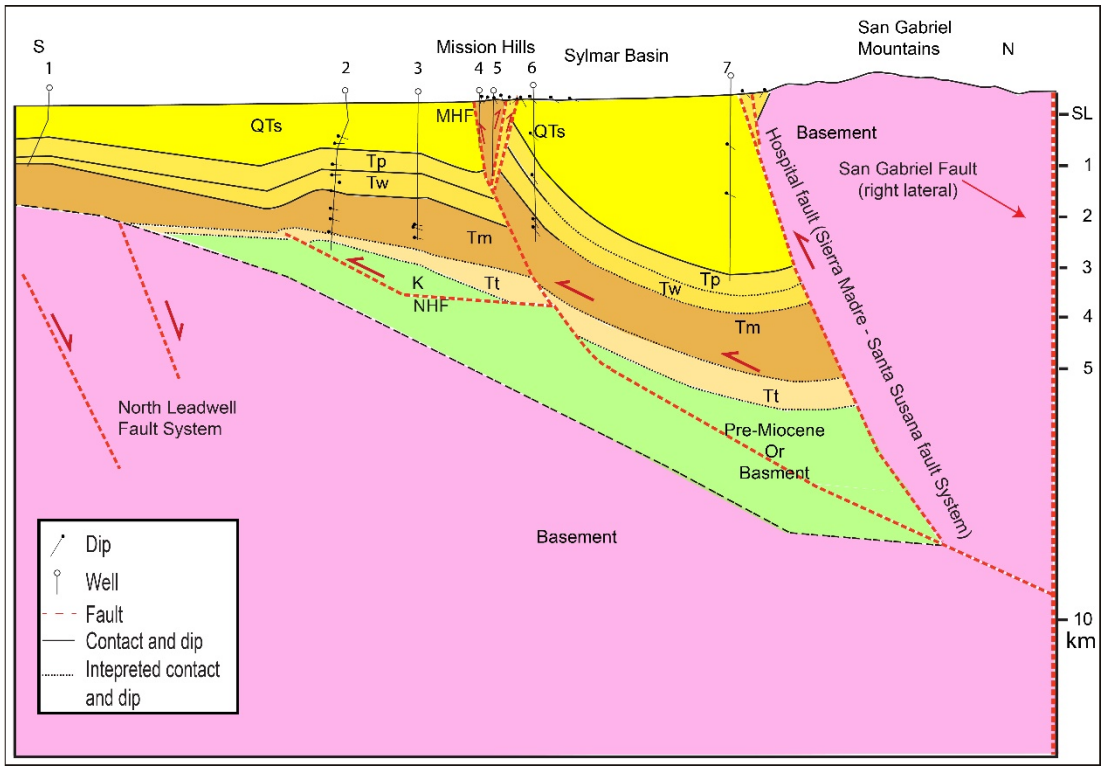

Figure 4.5. An interpretive geological cross section (location in Figure 2). Close to the surface the well the section contains observations. The deep part of the section is our interpretation based on the model in Figure 3.7 and geophysical observations (Langenheim et al., 2011).

Figure 4.6. Composite trench log across the front of the Mission Hills anticline. Bold line shows the base of trench, with the underlying geology inferred from the trench and boring exposures. The soil description in Table 1 was completed at the top of the trench where the alluvium was thickest near the fold crest.

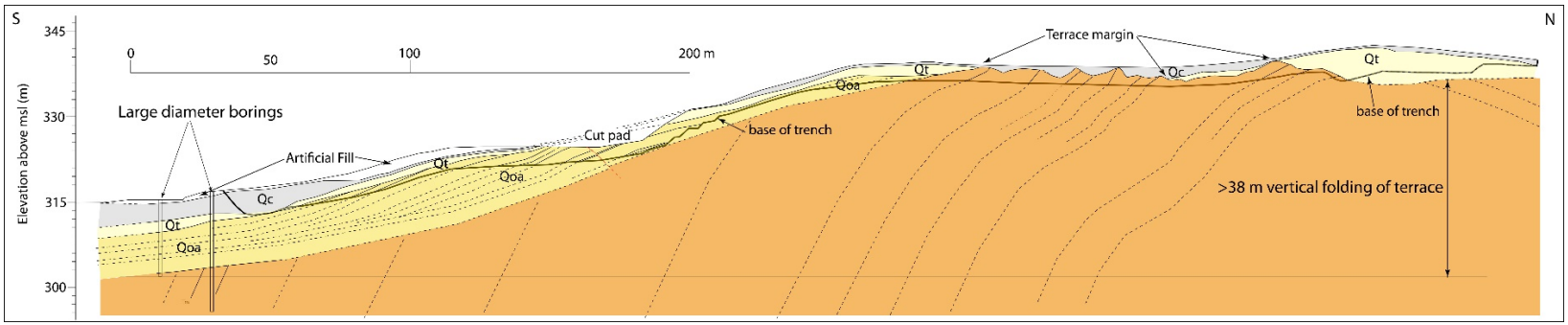
S
N
345
330
315
300
Elevation above msl (m)
0
50
100
200 m
Large diameter borings
Artificial Fill
Qc
Qt
Qoa
Cut pad
base of trench
Terrace margin
Qt
Qc
Qoa
Qt
base of trench
>38 m vertical folding of terrace

Figure 4.7. A Trishear forward model presenting the evolution of the Sylmar Basin since the Miocene. Pre-Miocene layer are horizontal. During the Miocene normal faults (Leadwell fault system and possibly the Mission Hills fault) are slipping due to the regional extension and subsidence. Later, early during the Quaternary, reverse fault (Hospital fault) uplifts the basement in the north. In the late quaternary the normal fault south of the basin is reactivated a reverse fault (Mission Hills fault), forming the Mission Hills anticline. Finally, small amount of slip is distributed farther south on a splay or a new thrust (Northridge Hills fault). The model illustrates how the observed dips of the pre-Miocene and early Miocene south of Mission Hills were formed, and how the thick sedimentary column in the Sylmar basin could have been formed.

Pre-Miocene
10 km
Miocene extention and subsidence
End of Miocene
Quaternary Shortening and thrusting
Legend
Pre-Miocene
Miocene
Post-Miocene
Fault
Direction of slip
Continued Miocene extention and subsidence
Quaternary Shortening and thrusting
Present

Appendices

In the Appendices we present the soil description (Table A4.1) and the wells we used for construction of the cross section (Table A4.2).

Table 4.1. Soil Description, Mission Hills anticline terrace soil

Horizon	Depth (cm)	Description
A	0-37	10YR3/3m, 4.5/3d; slightly gravelly Loam texture; moderate, coarse subangular blocky structure; soft to slightly hard dry consistence, slightly sticky and slightly plastic wet consistence; no clay films observed; abrupt, irregular boundary to:
Bt1	37-80	7.5-10YR4/4m, 7.5YR4/6d; very gravelly Sandy Clay Loam texture; strong, coarse angular block structure; extremely hard dry consistence, very sticky and plastic wet consistence; continuous thick clay films on ped faces and within pores, many moderately thick to thick clay films bridging grains (clay film colors range from 7.5YR 4/3 to 5/6m); clear, wavy boundary to:
Bt2	80-160	7.5-10YR4/4m, 4/6d; very gravelly Sandy Loam texture; weak to moderately developed coarse subangular blocky structure; slightly hard dry consistence, slightly sticky and non-plastic wet consistence; continuous, thick clay films lining pores, many thin to thick clay films bridging grains, few thick clay films on ped faces (clay film colors 7.5YR4/4 & 4/6m, 10YR 4/4m), boundary in bench:
Bench	160-230	Bt2 material exposed in the bench, so the Bt2 is inferred to extend to about 230 cm depth.
BC	230-280+	10YR4/6m, 5/6d; very gravelly Loamy Sand texture; massive breaking to weak, coarse subangular blocky structure; soft dry consistence, non-sticky and non-plastic wet consistence; common thin clay films bridging grains in lams, few thin to moderately thick clay films on clast-matric interfaces; boundary in bench;
Bench	280-335	BC in lower bench; gradual, irregular boundary to:
Cox	335-500+	10YR5/3m, 5/4d; very gravelly Sand texture; massive breaking to weak, medium subangular blocky and single grain structure; soft to loose dry consistence, non-sticky and non-plastic wet consistence; Fe2O3 and Mn2O3 banding (indicating a fluctuating groundwater level); boundary not exposed but expected to be abrupt and smooth over Tm bedrock.

Notes: Field conditions: soil is moist from previous nights' rain. Soil exposure is in a benched trench with 4-5 foot risers. Soil was described over a deep "pit" into Tm, where deposits are thickest. Alluvium is cobbly to boulder alluvium interpreted as fluvial deposits over a strath surface. Capping alluvium may be a debris flow deposit as it is more poorly sorted but contains well-rounded clasts. Clasts are rotted in Bt horizon: Most clasts in the upper part of the profile are easily cut with a scrapper although some show resistance but are cut with difficulty. Most clasts are of granitic composition, with some mafic-rich clasts (basalt? Or dark, fine-grained amphibolite) – interpreted as sourced out of the San Gabriel Mountains.

Table 4.2. The list of the wells used for constructing the cross section.

Well number	API	Longitude	Latitude	Source
1	3705974	-118.4479	34.2038	Tsutsumi and Yeats (1999)
2	3721802	-118.4549	34.2577	Tsutsumi and Yeats (1999)
3	3720519	-118.4485	34.2702	Tsutsumi and Yeats (1999)
4	3706330	-118.4563	34.2798	Tsutsumi and Yeats (1999)
5	3705892	-118.4652	34.2833	Davis and Namson (1998)
6	3705449	-118.486	34.2882	Tsutsumi and Yeats (1999)
7	3706034	-118.4666	34.3258	Davis and Namson (1998)

References

Atwater, T.M., 1998, Plate tectonic history of southern California with emphasis on the western Transverse Ranges and northern Channel Islands: Contributions to the geology of the northern Channel islands, southern California: American Association of Petroleum Geologists, Pacific Section, p. 1–8, doi: 10.1130/DNAG-GNA-N.21.

Baldwin, J.N., Kelson, K.I., and Randolph, C.E., 2000, Late Quaternary fold deformation along the Northridge Hills fault, Northridge, California: Deformation coincident with past Northridge Blind-Thrust Earthquakes and other nearby structures? Bulletin of the Seismological Society of America, v. 90, p. 629–642, doi: 10.1785/0119990056.

Birkeland, P.W., 1984, Soils and geomorphology.: Oxford University Press.

Boellstroff, J.D., and Steineck, P.L., 1975, Stratigraphic significance of fission-track ages on volcanic ashes in the marine late Cenozoic of Southern California: Earth and Planetary Science Letters, v. 27(2), p. 143–154.

Bull, W.B., 1978, Semi-Annual Technical report south front of the San Gabriel Mountains, California.:

Bull, W.B., 2008, Tectonic geomorphology of mountains: a new approach to paleoseismology: John Wiley & Sons.

Bull, W.B., 1979, Threshold of critical power in streams: Geological Society of America Bulletin, v. 90, p. 453–464, doi: https://doi.org/10.1130/0016-7606(1979)90<453:TOCPIS>2.0.CO;2.

Burgette, R.J., Hanson, A.M., Scharer, K.M., Rittenour, T.M., and Mcphillips, D., 2019, Late Quaternary slip rate of the Central Sierra Madre fault , southern California : Implications for slip partitioning and earthquake hazard: Earth and Planetary Science Letters, v. 1, p. 1–12, https://doi.org/10.1016/j.epsl.2019.115907.

Campbell, R.H., Wills, C.J., Irvine, P.J., and Swanson, B.J., 2014, Preliminary geologic map of the Los Angeles 30'x 60'quadrangle: California: Version 2,.

Crowell, J.C., 1979, The San Andreas fault system through time: Journal of the Geological Society, v. 136, p. 293–302.

Davis, T.L., and Namson, J.S., 1998, USGS Cross Section 10:, http://www.davisnamson.com/downloads/USGS Cross Section 10.pdf.

Dibblee, T.W.J., 1991, Geologic map of the San Fernando and Van Nuys (north half quadrangles, Los Angeles County, California): Dibblee Geological Foundation, v. Map DF-33, p. Scale 1:24,000.

Dibblee, T.W., 1982a, Geology of the Santa Ynez-Topatopa Mountains, Southern California, *in* Fife, D.L. and Minch, J.H. eds., Geology and Mineral Wealth of the California Transverse Ranges, Santa Ana, South Coast Geologcal Society, Inc., p. 41–56.

Dibblee, T.W., 1982b, Regional Geology of the Transverse Ranges Province of southern California, *in* Fife, D.L. and Minch, J.A. eds., Geology and Mineral Wealth of the California Transverse Ranges, Santa Ana, South Coast Geologcal Society, Inc., p. 7–26.

Erslev, E.A., 1991, Trishear fault-propagation folding: Geology, v. 19, p. 617–620.

Field, E.H., Arrowsmith, R.J., Biasi, G.P., Bird, P., Dawson, T.E., Felzer, K.R., Jackson, D.D., Johnson, K.M., Jordan, T.H., and Madden, C., 2014, Uniform California earthquake rupture forecast, version 3 (UCERF3)—The time-independent model: Bulletin of the Seismological Society of America, v. 104, p. 1122–1180.

Fuis, G.S., Clayton, R.W., Davis, P.M., Ryberg, T., Lutter, W.J., Okaya, D.A., Hauksson, E., Prodehl, C., Murphy, J.M., Benthien, M.L., Baher, S.A., Kohler, M.D., Thygesen, K., Simila, G., et al., 2003, Fault systems of the 1971 San Fernando and 1994 Northridge earthquakes, southern California: Relocated aftershocks and seismic images

from LARSE II: Geology, v. 31, p. 171–174, doi: 10.1130/0091-7613(2003)031<0171:FSOTSF>2.0.CO;2.

Furlong, K.P., and Schwartz, S.Y., 2004, Influence of the Mendocino Triple Junction on the Tectonics of Coastal California: Annual Review of Earth and Planetary Sciences, v. 32, p. 403–433, doi: 10.1146/annurev.earth.32.101802.120252.

Harden, J., 1982, A quantitative index of soil development from field descriptions: examples from a …: Geoderma, v. 28, p. 1–28, http://www.ncbi.nlm.nih.gov/entrez/query.fcgi?db=pubmed&cmd=Retrieve&dopt=AbstractPlus&list_uids=8683933844317967068related:3FqSnS4nDQwJ.

Hauksson, E., Jones, L.M., and Hutton, K., 1995, The 1994 Northridge earthquake sequence in California: seimological and tectonic aspects: Journal of Geophysical Research, v. 100, p. 12,335-12,355, doi: 10.1029/95jb00865.

Heusser, L., 1978, Pollen in Santa Barbara Basin, California: a 12,000-yr record: Geological Society of America Bulletin, v. 89, p. 673–678.

Heusser, L.E., 2000, Rapid oscillations in western North America vegetation and climate during oxygen isotope stage 5 inferred from pollen data from Santa Barbara Basin (Hole 893A): Palaeogeography, Palaeoclimatology, Palaeoecology, v. 161, p. 407–421.

Huftile, G.J., and Yeats, R.S., 1995, Convergence rates across a displacement transfer zone in the western Transverse Ranges, Ventura basin, California: Journal of Geophysical Research, v. 100, p. 2043–2067.

Huftile, G.J., and Yeats, R.S., 1996, Deformation rates across the Placerita (Northridge Mw = 6.7 Aftershock Zone) and Hopper Canyon segments of the western transverse ranges deformation belt: Bulletin of the Seismological Society of America, v. 86, p. s3–s18.

Hughes, A., 2019, Quaternary structural evolution and seismic hazards of the onshore Ventura basin, southern Calicornia, USA.: Imperial College London, 251 p.

Ingersoll, R. V, 2001a, Tectonostratigraphy of the Santa Monica Mountains, Southern California: AAPG Pacific Section, v. Geology an, p. 63–70, http://archives.datapages.com/data/pacific/data/101/101001/63_ps1010063.htm.

Ingersoll, R. V, 2001b, Tectonostratigraphy of the Santa Monica Mountains, Southern California: AAPG Pacific Section, v. Geology an, p. 63–70.

Keller, E.A., and Pinter, N., 1996, Active tectonics: Prentice Hall Upper Saddle River, NJ, v. 1338.

Keller, E.A., and Rockwell, T.K., 1984, Tectonic geomorphology, Quaternary chronology, and paleoseismicity, *in* Developments and Applications of Geomorphology, Springer, p. 203–239.

Langenheim, V.E., Wright, T.L., Okaya, D.A., Yeats, R.S., Fuis, G.S., Thygesen, K., and Thybo, H., 2011, Structure of the San Fernando Valley region, California: Implications for seismic hazard and tectonic history: Geosphere, v. 7, p. 528–572, doi: 10.1130/GES00597.1.

Levi, S., and Yeats, R.S., 1993, Paleomagnetic Constraints on Santa Susana fault , Western Transverse Ranges , California: Tectonics, v. 12, p. 688–702, https://doi.org/10.1029/93TC00133.

Levy, Y., Rockwell, T.K., Shaw, J.H., Plesch, A., Driscoll, N.W., and Perea, H., 2019, Structural modeling of the Western Transverse Ranges: An imbricated thrust ramp architecture: Lithosphere, v. 11, p. 868–883.

Lindvall, S.C., and Rubin, C.M., 2008, Slip Rate Studies along the Sierra Madre–Cucamonga Fault System Using Geomorphic and Cosmogenic Surface Exposure Age Constraints: Collaborative Research with Central Washington University and William Lettis & Associates, Inc.:

Liu, L., Spasojević, S., and Gurnis, M., 2008, Reconstructing Farallon plate subduction beneath North America back to the Late Cretaceous: Science, v. 322, p. 934–938.

LLC, N.S., 2019, Aliso Canyon Gas Storage Facility Geologic and Geomechanical Study:, https://www.conservation.ca.gov/dog/Pages/AlisoCanyon.aspx.

Lung, R., and Weick, R.J., 1987, Exploratory trenching of the Santa Susana fault in Los Angeles and Ventura counties: US Geol: Survey Prof. Paper, v. 1339, p. 65–70.

McFadden, L.D., and Weldon, R.J., 1987, Rates and processes of soil development on Quaternary terraces in Cajon Pass, California.: Geological Society of America Bulletin, v. 98, p. 280–293, doi: 10.1130/0016-7606(1987)98<280:RAPOSD>2.0.CO;2.

Miller, K.G., Kominz, A., Browning, J. V, Wright, J.D., and Mountain, G.S., 2005, The Phanerozoic record of sea level change: Science, v. 310, p. 1293–1298.

Nicholson, C., Sorlien, C.C., Tanya, A., C., C.J., and Luyendyk, B.P., 1994, Microplate capture, rotation of the western Transverse Ranges, and initiation of the San Andreas transform as a low-angle fault system: Geology, v. 22, p. 491–495.

Nilsen, T.H., 1984, Oligocene Tectonics and Sedimentation, California: Sedimentary Geology, v. 38, p. 305–336.

Oakeshott, G.B. (Ed.), 1975, San Fernando, California, Earthquake of 9 February 1971: California Division of Mines and Geology, v. Bulletin 1, 463 p.

Petersen, M.D., and Wesnousky, S.G., 1994, Fault slip rates and earthquake histories for active faults in southern California: Bulletin - Seismological Society of America, v. 84, p. 1608–1649.

Petroleum Experts Ltd. (MVE Ltd.), 2018, MOVE https://www.mve.com/:

Ponti, D.J., 1985, The Quaternary alluvial sequence of the Antelope Valley, California: Geol. Soc. Am. Spec. Pap, v. 203, p. 79–96.

Rockwell, T.K., 1983, Soil Chronology, Geology, and Neotectonics of the North Central Ventura Basin, California [P.hD Thesis]: University of California, Santa Barbara.

Rockwell, T.K., 2000, Use of Soil Geomorphology in Fault Studies: Quaternary Geochronology: Methods and Applications, v. 4, p. 273–292.

Rockwell, T.K., Keller, E.A., and Johnson Donald L., 1985, Tectonic geomorphology of alluvial fans and mountain fronts near Ventura, California, *in* Tectonic Geomorphology. Proceedings of the 15th Annual Geomorphology Symposium, Allen and Unwin Publishers, p. 183–207.

Rumelhart, P.E., and Ingersoll, R. V., 1997, Provenance of the upper Miocene Modelo Formation and subsidence analysis of the Los Angeles basin, southern California: Implications for paleotectonic and paleogeographic reconstructions: Bulletin of the Geological Society of America, v. 109, p. 885–899, doi: 10.1130/0016-7606(1997)109<0885:POTUMM>2.3.CO;2.

Schwartz, D., 2018, Large coherent block versus microplate rotaion of the Western Transverse Ranges: A fresh look at paleomagnetic constraints: University of California, San Diego, 35 p.

Scott, B.K.M., and Williams, R.P., 1978, Erosion and Sediment Yields in the Transverse Ranges, Southern California.:

Shields, K.E., 1977, Structure of the Northeastern Margin of the San Fernanado Valley, Los Angeles County, California: Ohio University, 82 p.

Tennyson, M.E., 1989, Pre-transform early Miocene extension in western California: Geology, v. 17, p. 792–796, doi: 10.1130/0091-7613(1989)017<0792:PTEMEI>2.3.CO;2.

Tsutsumi, H., and Yeats, R.S., 1999, Tectonic setting of the 1971 Sylmar and 1994 Northridge earthquakes in the San Fernando Valley, California: Bulletin of the Seismological Society of America, v. 89, p. 1232–1249.

Whitcomb, J.H., Allen, C.R., Garmany, J.D., and Hileman, J.A., 1973, San Fernando Earthquake series, 1971: Focal mechanisms and tectonics: Reviews of Geophysics, v. 11, p. 693–730, doi: 10.1029/RG011i003p00693.

Woods, M.C., and Seiple, W.R., 1995, The Northridge, California, Earthquake of 17 January 1994: California Department of Conservation, Division of Mines and Geology.

Wright, T.L., 1991, Structural geology and tectonic evolution of the Los Angeles Basin, California, *in* Biddle, K.T. ed., M 52: Active margin basins, AAPG Special Volumes, p. 35–134.

Yeats, R.S., 1987, Late Cenozoic structure of the Santa Susana fault zone: US Geol. Surv. Profess. Pap, v. 1339, p. 137–160.

Chapter 5 Summary

This dissertation presents the development of structural models for the western and central Transverse Ranges. In developing these models, I included the full range of available observations in order to make the proposed fault architecture more defendable than previous models for the region. In the chapter 2, I present a southward verging imbricate thrust model that evolved in time since the Pliocene. The fault model is based on seven forward models that explain well the observed surface geology and interpreted cross sections along the range. The proposed fault is dipping to the north and shoals from ~16-30˚ degrees at depth to ~45-60˚ near the surface. The potential surface area of a rupture in the seismogenic zone may be as large as ~6000 km2; such a scenario could yield an earthquake as large as M 7.8. In the third chapter, the range of plausible lower ramp dips was narrowed from 16-30˚ to 25-30˚ by comparing the predictions from forward kinematic dislocation models of the deep structure of the Western Transverse Ranges to GPS data.

In chapter 4, I developed a structural forward model in order to explain how a similar southward propagation has also occurred for the Santa Susana fault system in the central Transverse Ranges. In the chapter, we present new paleoseismic data from trenches that demonstrate the late Quaternary activity of the Mission Hills fault. Combined with the lack of accumulation of alluvium along the Santa Susana fault and deposition of new alluvium along the younger Mission Hills and Northridge Hills faults, I explain why the current slip rate assigned to the Santa Susana fault system is overestimated and how slip can be distributed along the system due to connectivity between these faults at depth. Hazard assessments along the Transverse Ranges should consider these fault systems I described in this work, rather than separate faults and individual seismic sources.